EXCITED STATE PROPERTIES OF ORGANIC AND ORGANOMETALLIC OLIGOMERS, POLYMERS, AND MATERIALS AND THEIR SOLID-STATE APPLICATIONS

By

RANDI SUE PRICE

A DISSERTATION PRESENTED TO THE GRADUATE SCHOOL
OF THE UNIVERSITY OF FLORIDA IN PARTIAL FULFILLMENT
OF THE REQUIREMENTS FOR THE DEGREE OF
DOCTOR OF PHILOSOPHY

UNIVERSITY OF FLORIDA

2013

To Zach

ACKNOWLEDGMENTS

Much gratitude goes to my advisor, Prof. Kirk Schanze, who has given me an amazing amount of support and guidance. He challenged me with designing and programming new instrumentation which gave me an intimate knowledge of the processes involved in chemical measurement and data acquisition. Most importantly, he encouraged me to become an independent scientist with the freedom to make my own discoveries. Also, I would like to thank my committee members Dr. Brucat, Dr. Hagen, Dr. Kleiman, and Dr. Omenetto for their time and support.

Everyone in the Schanze group, former and current, have been great colleagues and friends. For the better part of my two years of research, Dr. Abigail Shelton let me follow her around (asking many hundreds of questions), and she was so patient to teach answer them all. The past couple of years, it has been great fun working together with Dr. Galyna Dubinina on the nonlinear absorption project. We shared many laughs. Dr. Gyu Leem introduced me to the materials side of my research and helped me to better understand the Hg3 project by performing XRD and TEM experiments on my films. Thanks to Russ Winkel and his skills in NMR, I was able to get NMR data on MEH-PPV/Hg3 solutions even though they were difficult samples to run. The undergraduate research student who worked on the clay-oligomer project with me, Eduardo Acosta, did great work and helped me to become a better teacher of difficult concepts. A big thanks, also, to the guys in Sisler 420, who always laughed at my jokes and made being in lab a joy every day.

I was also given the amazing opportunity to spend ten weeks at Tokyo Metropolitan University in Japan with Dr. Haruo Inoue and his research group which was supported by Dr. Schanze, Dr. Inoue, and the graduate student research abroad

award from the International Center at UF. Dr. Inoue was a wonderful host, and he, Masae Asano, and the group members took great care of me. It was a fun experience, and I have great memories of everyone I met there. Many thanks particularly to Dr. Yu Nabetani and Satomi Onuki for guiding me through the Japanese lab and for helping to teach me new research experiments.

Finally, I have had nothing but the most heartfelt support from my friends and family even though they thought that maybe I was a little weird for being so in love with science. I owe a lot of my success to my Mom and Dad. They have always supported my education so that I could have the best chance to achieve my own success. So much gratitude goes to my husband, Zach, whose love and patience has kept me sane and who continues to laugh with me throughout this crazy adventure called life.

TABLE OF CONTENTS

page

LIST OF TABLES

Table page

LIST OF FIGURES

Figure page

Abstract of Dissertation Presented to the Graduate School
of the University of Florida in Partial Fulfillment of the
Requirements for the Degree of Doctor of Philosophy

EXCITED STATE PROPERTIES OF ORGANIC AND ORGANOMETALLIC OLIGOMERS, POLYMERS, AND MATERIALS AND THEIR SOLID-STATE APPLICATIONS

By

Randi Sue Price

August 2013

Chair: Kirk Schanze
Major: Chemistry

The goal of this research is to study the excited state dynamics of conjugated molecules, oligomers and polymers in the solid state and compare these photophysical properties to those found in solution. To study the triplet excited state dynamics of films a new nanosecond transient absorption instrumentation was developed. This instrument can detect transient absorption with ΔA as low as of 10^{-3}. Using this newly available instrumentation, it is possible to measure the triplet excited state dynamics so as to gain insight into several solid-state applications of photoactive molecules, oligomers, and polymers.

A series of *p*-phenylene vinylene platinum acetylide complexes are studied for optical power limiting applications, and they are incorporated into poly(methyl methacrylate) (PMMA) monoliths. The photophysical properties of the monoliths and Triplet-triplet annihilation in conjugated co-polymers containing phenylene and *p*-phenylene vinylene platinum acetylide units is observed and compared against representative “monomer” complexes using transient absorption spectroscopy as a function of increasing laser fluence of the excitation pulse. The interaction between

conjugated polymer, MEH-PPV, and a trimeric perfluoro-*ortho*-phenylene mercury complex, Hg3 is investigated in solution and in films. Finally cationic oligomers are intercalated into a clay host, and the photophysical properties of the clay-oligomer hybrid are investigated in disperse solutions and in films.

CHAPTER 1
INTRODUCTION

The Interaction of Light with Matter

The nature of light and its interaction with matter has an interesting history, ranging from the discovery of fire, which provided portable “lamps” in the form of a bundle of sticks set ablaze to aid early man in sight, to the evolution of laser technology for controlling chemical reactions, and even the harvesting of light for conversion to energy. Light is categorized into three regions of the electromagnetic spectrum: the ultra-violet (200 – 400 nm), the visible (400-700 nm), and the near-infrared (700-1000 nm).

In the wave model, light is treated as a wave propagating from a source characterized by Equation 1-1.

$$\lambda = \frac{c}{\nu} \qquad (1\text{-}1)$$

where λ is the wavelength of light, v the frequency and c the velocity of light (2.998 x 10^8 $m \cdot s^{-1}$ in vacuum). The wave-theory of light was supported by the observation of refraction in different media by Huygens and Fresnel and also by the wave-like interference pattern observed by Thomas Young during his double-slit experiment.[1-3] The most convincing evidence was when Maxwell combined four simple equations previously developed by Coulomb, Faraday, Ampere, and Gauss to describe the propagation of oscillating electric and magnetic fields and found that light waves propagate at 3 x 10^8 $m \cdot s^{-1}$.[4,5]

In the particle model of light, light is quantized. Planck developed the particle model of light during his blackbody experiment in the early 20th century, where he found that blackbody radiation is limited to discrete values.[6] Shortly after, Einstein further

developed the idea of quantized photons in 1905 when he discovered the photoelectric effect for which he was recognized with the Nobel Prize in 1921.[7] Photons are massless particles which are localized energy in a small volume of space and radiate from the source with a velocity *c*. The energy of a given photon is given by

$$E = h\nu = \frac{hc}{\lambda} \qquad (1\text{-}2)$$

where *h* is Planck's constant (6.62 x 10^{-34} J·s), *v* is the frequency of the wave associated with the photon, *c* is the speed of light, and λ is the wavelength.

Originally, the wave-particle duality of light was troubling to many scientists. In many circumstances, such as when observing interference and diffraction phenomena, it seemed that light behaved as a wave that could generally be described by Maxwell's wave equations. In others, such as the quantized energies detected by blackbody radiation or the photoelectric effect, light acts like discrete particles with discrete energies. This duality was extended to other particles, such as electrons when de Broglie theorized that all particles can also act as waves.[8] This theory was confirmed with the observation of electron diffraction patterns by independent research done by Thomson and by Germer.[9,10]

Owing to the development of quantum mechanics, the wave-particle duality of light and other particles can be described in a single theory.[11] A particle can be described by its wavefunction, which describes the amplitude of a wave at each point in space. The evolution of the wave can be described by a differential equation, known generally as the Schrodinger equation developed in 1928. The propagation of this wave causes the observed effects such as interference and diffraction.

Excited State Dynamics

The Grotthuss-Draper law, proposed in the early 1800s, asserts that only light that is absorbed can cause photochemical changes.[12] Only the photons with energy equal to the energy gap of that transition will be absorbed, promoting valence to a higher energy level. The result is an electronically excited state. The Beer-Lambert law shown in Equation 1-3 gives a quantitative relation describing the absorption of light through a material.

$$A = \varepsilon l c \tag{1-3}$$

where A is the absorbance, ε is the molar absorptivity (M^{-1} cm^{-1}), l is the pathlength in cm, and c is the molar concentration of the absorbing molecule. An excited molecule can relax radiatively or nonradiatively. Radiative decay is accompanied by emission of a photon, either by fluorescence from the singlet excited state or by phosphorescence from the triplet excited state. Nonradiative decay is a relaxation process that does not involve emitting photons. Generally, photophysical characterization involves the measurement of the quantum yield and lifetime of the produced excited states.

The quantum yield describes the efficiency of a photophysical process. For example, the quantum yield of emission is the ratio of the number of photons emitted to the number of photons absorbed. A quantum yield of 1 indicates that 100% of the photons absorbed by a molecule produce emitted photons. Quantum yield measurements can be used to quantify both photophysical processes (fluorescence, phosphorescence and intersystem crossing) and photochemical reactions (where the absorption of a photon converts a reactant, R, to a product, P).

Unimolecular Excited State Dynamics

The excited state dynamics of an optically excited molecule can be described with a Jablonski diagram as shown in Figure 1-1.

Most molecules exist as ground state singlets, where all electrons are paired with another of opposite spin. (The most notable exception is molecular oxygen, O_2, which exists as a ground state triplet.) Upon absorption of a photon of appropriate energy, the molecule becomes excited, and an electron is promoted to a higher energy orbital and produces a singlet excited state, S_1.

$$A + h\nu \rightarrow A^* \qquad (1\text{-}4)$$

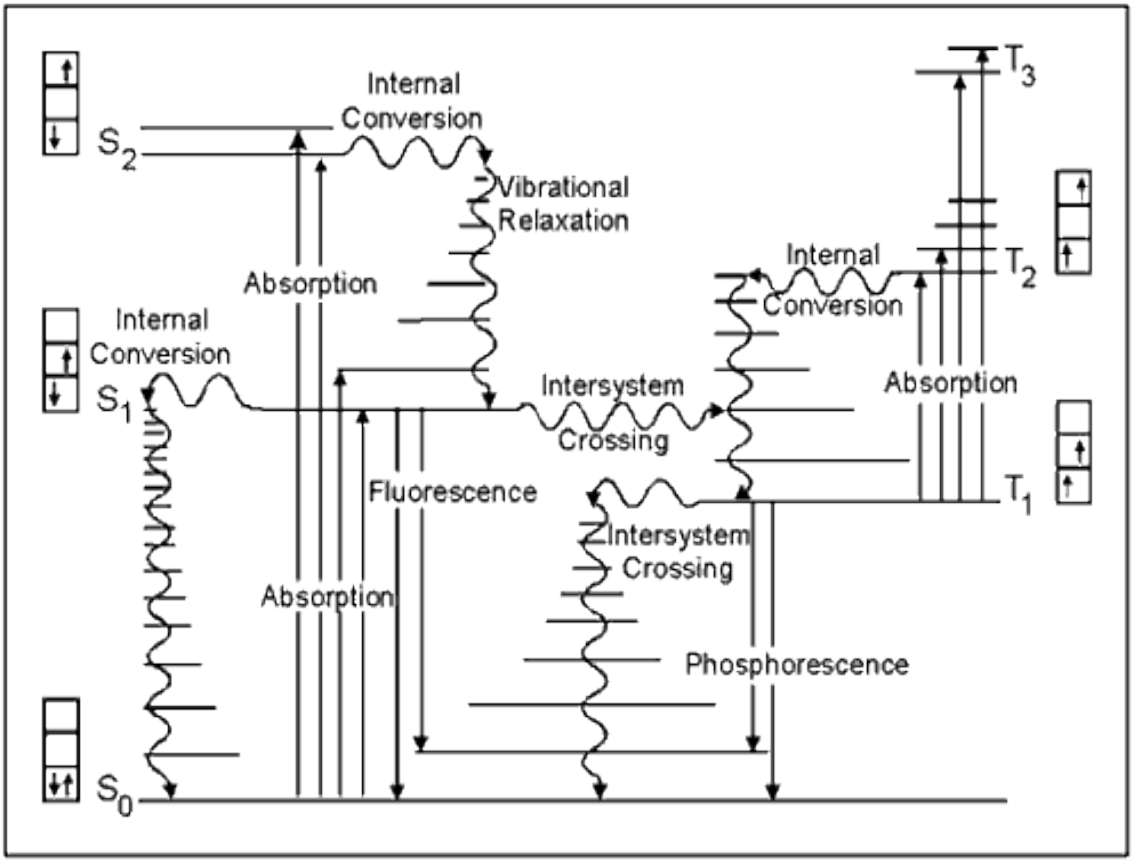

Figure 1-1. Jablonski diagram demonstrating intramolecular photophysical pathways.[13]

From the S_1 state, the system can lose energy by fluorescence or nonradiative decay, IC, returning back to the ground state. Fluorescence is a spin-allowed radiative transition, so it is a very fast process (~10^9 s). Internal conversion, IC, is nonradiative decay between states with the same multiplicity, $S_1 \rightarrow S_0$ or $T_2 \rightarrow T_1$, seen as energy loss due to collisions or less of heat. IC occurs when there is significant orbital overlap between the excited vibrational levels between electronic states. Due to the loss of energy during vibrational relaxation of the initially excited S_1* state to a relaxed S_1 state from which fluorescence occurs, the emitted photons will be of slightly lower energy than those absorbed. This red-shift of the fluorescence spectrum compared to the absorption spectrum is called the Stokes shift.

Intersystem crossing (ISC) can also occur from the S_1 state. Intersystem crossing is a radiationless transition between two states of different multiplicity, such as a singlet to a triplet excited state or vice versa. Formally, this process is spin-forbidden by the law of conservation of angular momentum. For organic molecules, the yield of ISC is typically very low. However, when heavy atoms are present, spin-orbit coupling occurs between the orbital and spin angular momenta, and the singlet-triplet transition becomes more allowed.[14] The total angular momentum in the system is conserved even though the individual electron's spin momentum and the orbital momentum are changed.[15]

The triplet excited state, T_1, produced by intersystem crossing from the S_1 state, can be deactivated by phosphorescence or nonradiative decay. The lowest triplet excited state, T_1, is always lower in energy than S_1 because of decreased Coulombic repulsion between electrons due to Hund's Rule. Phosphorescence is a radiative decay

process between states of different spin. For this reason, the observation of phosphorescence from T_1 always occurs at longer wavelengths than the fluorescence observed from S_1.

Although the gaps between electronic energy levels have discrete values, the absorption and emission spectra always appear as broad bands. Light absorption is a very fast process (fs), and occurs much faster than nuclear motion, as described by the Franck-Condon Principle. Immediately upon absorption of light, an electronic excited state is produced that initially is also vibrationally excited. Vibrational relaxation, occurs quickly after excitation, typically involving molecular collisions which dissipate small amounts of energy to the environment in each collision.

Bimolecular Excited State Dynamics

It is possible that an excited molecule may encounter another molecule during its excited state lifetime. There are several processes that can occur including the enhancement of intersystem crossing, electronic energy transfer, and complex formation. An important feature of bimolecular excited state dynamics is that these processes are dependent on the concentration of the excited molecules and "quenchers" and is also a diffusion-controlled process.

The enhancement of nonradiative decay by intersystem crossing occurs if a molecule, M_1, in the excited state comes across a heavy metal –containing complex, M_2, which is capable of inducing spin-orbit coupling. This can be seen as a quenching of the fluorescence of M_1. Phosphorescence may also be observed.

Intermolecular energy transfer can occur between colliding molecules which is a form of nonradiative decay. An excited state is quenched if it is lost by energy transfer to another molecule, or an excited state can be sensitized if it is created by energy

transfer from another molecule. This quenching process involves transfer from an energy donor (*D*) to suitable acceptor (*A*).

$$D^* + A \rightarrow A^* + D \quad (1\text{-}5)$$

The kinetics of energy transfer are more complicated than for unimolecular decay. First, there is a dependence on the concentration of the species involved. Second, in order for Dexter energy transfer or photochemical reaction to occur, the excited donor must "collide" with the acceptor. This collision may involve actual overlap between the orbitals of the two species, or the two molecules can come together within a specified reaction radius. After collision, either energy can be transferred between donor and acceptor or they can separate without further interaction. Energy transfer between donor and acceptor can occur by either Förster energy transfer or Dexter exchange.

Förster resonance energy transfer (FRET) is a Coulombic interaction by dipole-dipole coupling.[16] FRET requires spectral overlap between the emission of the donor and the absorption of the acceptor as shown in Figure 1-2. Energy transfer by FRET is related to the transition dipoles of the acceptor and the donor and the distance between them.

$$k_{et}(Coulombic) \sim \frac{\mu_D^2 \mu_A^2}{R_{DA}^3} \quad (1\text{-}6)$$

FRET is most favored if: (1) the emission $D^* \rightarrow D$ and the absorption $A \rightarrow A^*$ spectrally coincide (2) the radiative rate constant, k_r, of D is very large, (3) A has a high molar extinction coefficient, ε, and (4) A and D are within close proximity.

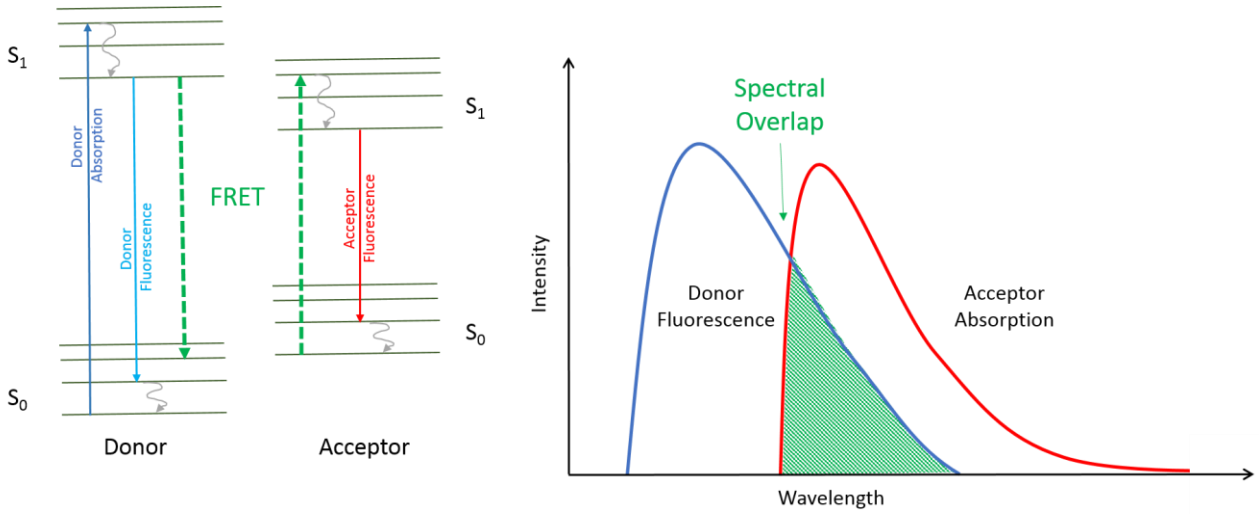

Figure 1-2. Energy diagrams of a donor and acceptor demonstrating FRET when the emission of the donor overlaps with the absorption of the acceptor.

The FRET efficiency, E, describes the fraction of energy transfer occurring per donor excitation.

$$E = \frac{k_{ET}}{k_f + k_{ET} + \sum k_i} = \frac{1}{1+(\frac{r}{R_0})^6} \quad (1\text{-}7)$$

where k_{ET} is the rate of energy transfer, k_f is the radiative decay rate of the donor, k_i are other decay pathways of D^*, and R_0 is the Forster distance which is defined as the energy transfer between donor and acceptor has 50% efficiency. When FRET occurs, fluorescence may occur from the acceptor.

Dexter exchange involves energy transfer by an electron exchange mechanism. Electron exchange requires an overlap of the wavefunctions of the excited donor, D^*, and the acceptor, A. D. L. Dexter worked out the rate constant of energy transfer by electron exchange.[17]

$$k_{ET}(Exchange) = KJe^{\frac{-2R_{DA}}{L}} \quad (1\text{-}8)$$

where K is related to the specific orbital interactions, J is a spectral overlap integral, R_{DA} is the donor-acceptor separation, and L is the sum of their van der Waals radii. J is

normalized such that the absorption and emission spectra are on the same scale. So k_{ET} of Dexter energy transfer is independent of the absorption characteristics of the acceptor, in contrast to the k_{ET} of FRET which is dependent on ε_A. The rate of electron exchange decreases exponentially as the distance between D^* and A increases.

Complex formation between an excited molecule and a molecule in the ground state can precede or enhance the bimolecular decay processes discussed earlier. In the case where a complex forms between an excited molecule and another of the same molecule in the ground state, it is called an excimer, whereas if the complex forms between two different molecules in the ground and excited state, it is termed an exciplex.[15,18,19] Excimers can be formed with either locally excited or charge-transfer character. In an excimer, resonance interactions involving either intermolecular exchange of the excitation energy and/or charge causes weak intermolecular forces that hold the two molecules together. Most commonly, excimers occur between aromatic molecules.

A key feature of excimers and exciplexes is that they are associative when one of the molecules is in the excited state but are dissociative in the ground state.[15,20] In both excimers and exciplexes, the new emission will be highly concentration dependent and typically has a broad, featureless, red-shifted emission compared to the component molecules. This loss in vibrational structure of the emission is due to the repulsive nature of the component molecules in the ground state that leads to rapid separation of the complex after loss of the excited state.[15] Excimers can be used as fluorescent labels yielding information about macromolecular conformation due to the contact required for excimer formation between label pairs. A classic example of an excimer is

that formed by pyrene which has been studied in detail in systems ranging from pyrene-labelled polymers to pyrenes in crystals and other matrices.[21-26]

Photophysics of Conjugated Polymers

Conjugated polymers are molecules that consist of many repeating monomer units having contiguous conjugation along the polymer backbone. These polymers are known as conductive polymers due to their semi-conductive properties. Polymers interact with light in much the same way as their small-molecule analogues. After the absorption of light, an electron from the highest occupied molecular orbital (HOMO) gets promoted to the lowest unoccupied molecular orbital (LUMO). This absorption takes place without a change in the spin angular momentum of the electron, thus transitioning between the singlet ground state, S_0, and the first singlet excited state, S_1. Deactivation from S_1 involves either fluorescence or nonradiative decay back to the ground state, S_0; or if there is sufficient spin-orbit coupling, intersystem crossing to the triplet state, T_1, can occur followed by phosphorescence or nonradiative decay. It is known that upon excitation of a polymer, the excited state tends to be delocalized over a few repeat units. This delocalized quantum of excited energy in a polymer is called a Frenkel exciton.

There are several fundamental differences in the photophysical processes of polymers compared to discrete molecules.[27,28] First, the large size and weight of a polymer may slow down diffusional motions of the polymer, such as translation or rotational movement in a solvent, or speed up restricted relative motions, such as vibration of side groups or segmental motion along the polymer chain. Second, polymers tend towards heterogeneity. For example, a sample of polymer will typically contain a distribution of molecular weights, stereoregularity, etc. Third, in polymers

where the chromophore is a repeating unit, the local concentration of chromophores is always high, even when the number of polymer chains in a solution or media are very low. This means that bimolecular processes such as energy transfer, concentration quenching, and excimer formation will be more prevalent in polymers compared to free molecules.

Energy transfer in polymers can be divided into three main types: (1) Intramolecular energy transfer along a single polymer chain usually by hopping of the exciton between overlapped orbitals in a conjugated polymer backbone, (2) Intramolecular energy transfer between two regions of the polymer when the polymer is coiled or aggregated, and (3) Intermolecular energy transfer between two separate polymer chains that are in proximity due to collision or interchain aggregation. In dilute solutions, it is rare that a polymer chain will diffuse and collide with another polymer chain before the excited state decays, so (1) and (2) are the main mechanism of energy transfer. In thin films or solids, where the polymer is aggregated or organized into a small volume with other polymer chains, all three types of energy transfer occur. Singlet excitons can diffuse in a polymer by Förster transfer, whereas triplet excitons diffuse by Dexter exchange.

Photophysical Characterization Methods

Absorption and Emission

An absorption spectrum measures the light absorbed by a substance as a function of wavelength. The absorption spectrum can be measured using a spectrophotometer. Spectrophotometers quantitatively measure the transmission of light through a sample, comparing it to a reference, usually a sample of solvent. The transmission is then converted to absorbance by Beer's Law in Equation 1-4.

Spectrophotometers can either be single-beam or double-beam. A single-beam spectrophotometer compares the light intensity of a single beam before and after a sample is inserted into the path. A double-beam spectrophotometer compares the light intensity between two light paths: one which passes through the sample and one that does not.

The modern spectrophotometer typically consists of a broad-spectrum white light source, a monochromator containing a diffraction grating, and a single-wavelength detector such as a photomultiplier tube or photodiode. The broad-spectrum white light source must have a continuous emission spectrum and be temporally stable in regards to emission intensity. The monochromator allows discrete wavelengths of the light source to pass through the sample, and the transmission is measured by the detector. The grating can be scanned step-wise so that transmission of light through the sample can be measured at each wavelength. On the other hand, detectors such as charge coupled devices (CCD) or photodiode arrays (PDA) can be coupled with a fixed grating to capture the transmittance of every wavelength of light at the same time.

The molar absorptivity, or molar extinction coefficient, is a measurement of how strongly a chemical species absorbs light at a given wavelength and is an intrinsic property of the molecule that relates the absorbance to the concentration. The units of molar absorptivity are M^{-1} cm^{-1}. The molar absorptivity can be calculated by taking the absorption of a species at varied concentrations. Rearranging the Beer-Lambert law shown in Equation 1-3, the slope of absorbance vs. concentration will be the molar absorptivity value.

$$\varepsilon = \frac{A}{C}\, l \qquad (1\text{-}9)$$

where *A* is the absorbance measured by the spectrophotometer, *C* is the concentration of the solution in M, and *l* is the pathlength of the cuvette in cm (usually 1).

The experimental absorption intensity provides a measure of the theoretical quantity of oscillator strength. These values are related by the following equation:

$$f \equiv 4.32x10^{-9} \int_{\tilde{\nu}_2}^{\tilde{\nu}_1} \varepsilon \; d\tilde{\nu} \qquad (1\text{-}10)$$

where $\tilde{\nu}_1$ and $\tilde{\nu}_2$ are the limits of the transition measurement in wave numbers (cm^{-1}) and the molar extinction values, ε, are in $M^{-1}\ cm^{-1}$. Thus, the integrated absorption band is the transition probability. Values of *f* are normalized so that a highly probable transition has an *f* value of close to 1, whereas a forbidden transition will have a value approaching zero.

There are some experimental considerations to be aware of when measuring absorption spectra.[29] The environment around the absorbing species can play a large role in the observed absorption spectrum. The absorption spectrum of a gas at low pressure will have sharp lines with rotational and vibrational fine structure. If absorbing molecules are allowed to interact with each other (such as in high pressure gas) or with a solvent, the band width of the absorption bands will become more diffuse as intermolecular interactions cause small changes in the electronic energy states, eventually becoming a nearly infinite smearing of energy levels.

At very low temperatures in rigid media, collisions with other molecules are minimized, and the spectrum becomes more structured. Also, low temperatures will eliminate the absorption transitions from the higher energy states, as the Boltzmann distribution mandates that only the lowest vibrational level in the ground state will be populated. Conversely, at higher temperatures there exists more population of

molecules in higher vibrational states in the ground state which again introduces a different absorption spectrum.

Solvent polarity also has a consequence because molecules in the ground state versus an excited state may exhibit a change in polarity. A change in polarity leads to different stabilization of the ground and excited states causing a difference in the energy gap. This introduces significant shifts in the absorption spectra and is termed solvatochromism. Solvatochromism is a complex phenomenon dependent on many factors such as polarity, solubility, and hydrogen-bonding capability of the solvent.[30] Generally, if the excited state is more polarizable than the ground state, then a red-shift (bathochromic shift) will occur in more polar solvent. If the excited state is less polarizable, then the spectrum will exhibit a blue-shift (hypsochromic shift) in more polar solvent. Charge-transfer states, either MLCT or LMCT, which involve intramolecular charge transfer between donor and acceptor chromophores, give the largest shifts. This is because charge-transfer states typically have a large change in dipole moment upon excitation which is very sensitive to small changes in the environment such as solvent polarity or hydrogen-bonding capability.

Emission spectra can be measured with a spectrofluorimeter which consists of an excitation light source, a grating monochromator, and a detector. The excitation light source is typically a white light source such as a xenon arc lamp which passes through a monochromator to single out the excitation wavelengths of interest before hitting the sample. The luminescence from the sample is collected at 90° to the excitation beam with condensing optics and passed through a second monochromator with a grating which can be scanned stepwise through the detection region of interest. Detection is

usually with a photomultiplier tube which produces an amplified signal upon detection of photons. Spectrofluorimeters can also be double beam to correct for fluctuations in lamp intensity during the experiment.

Both fluorescence and phosphorescence can be detected by spectrofluorimeters assuming that the solution has been sufficiently deoxygenated. Molecular oxygen is a ground state triplet and efficiently quenches other triplet excited states with a second order quenching constant in the range of the diffusional quenching constant, typically on the order of 10^9 L mol^{-1} s^{-1}.[15] A solution can be deoxygenated by substitution with an inert gas like N_2 or Ar achieved by a gentle flow of the inert gas into the solution for about 15 minutes for every 3 mL while stirring. This purging process works rather well for solutions where the triplet excited lifetime of interest is on the order of a few microseconds. For solutions containing chromophores with substantially long lifetimes, > 100 μs, a more complicated deoxygenation procedure is needed.

One method of removing oxygen from a solution is by freeze-pump-thaw. Freeze-pump-thaw cycling is when a solution in a borosilicate tube is flash frozen with liquid nitrogen, and the gas present in the headspace is removed by applying vacuum for 10-30 minutes. The tube is then sealed off from the vacuum and the solution is allowed to thaw. During thawing, gas trapped in solution will bubble out and escape. This freeze-pump-thaw process is repeated a minimum of three times.

For compounds with relatively low phosphorescence quantum yields, the emission spectrum can be collected with the sample in a glass forming solvent, such as 2-methyltetrahydrofuran (MeTHF), at very low temperatures. At low temperatures, phosphorescence is promoted by slowing the rate of radiationless decay. Typically, a

cryostat or cold-finger containing liquid nitrogen is used to cool a sample to 77 K. Sometimes this involves modification of the sample holder to mount the cryostat securely in the optical path.

The fluorescence (or phosphorescence) quantum yield is the ratio of photons emitted by fluorescence or phosphorescence to photons absorbed. A comparative method by Williams et al. is the most commonly used method for determining quantum yields.[31] The fluorescence intensity of a standard sample with a known quantum yield, Φ_F, is compared to that of a test sample prepared to the same optical density at the same excitation wavelength. A range of concentrations of the standard and sample solutions are prepared in a clean, optical quality cuvette such that the optical density at the excitation wavelength is < 0.1. Higher absorbances can introduce reabsorption effects.[32] The integrated fluorescence intensity of the solutions are acquired and plotted against the absorbance at the excitation wavelength. The absolute quantum yield of the sample can be calculated with the following equation:

$$\Phi_X = \Phi_{std}\left(\frac{slope_x}{slope_{std}}\right)\left(\frac{\eta_x^2}{\eta_{std}^2}\right) \qquad (1\text{-}11)$$

where the subscripts *x* and *std* denote standard and unknown sample, respectively, Φ is the quantum yield, *slope* is the slope of emission intensity vs. absorbance, and η is the refractive indices of the solvents used.

Some considerations are important in order to get the most accurate results. First, two standard samples should be cross-calibrated to confirm good technique and that the standard Φ_f value can be used confidently. Second, the same instrumental parameters should be used for both sample and standard, including slit width, excitation wavelength, number of averages, etc. They should absorb in the same region such that

the same excitation wavelength can be used, and it is best if they share a similar range of emission wavelengths.

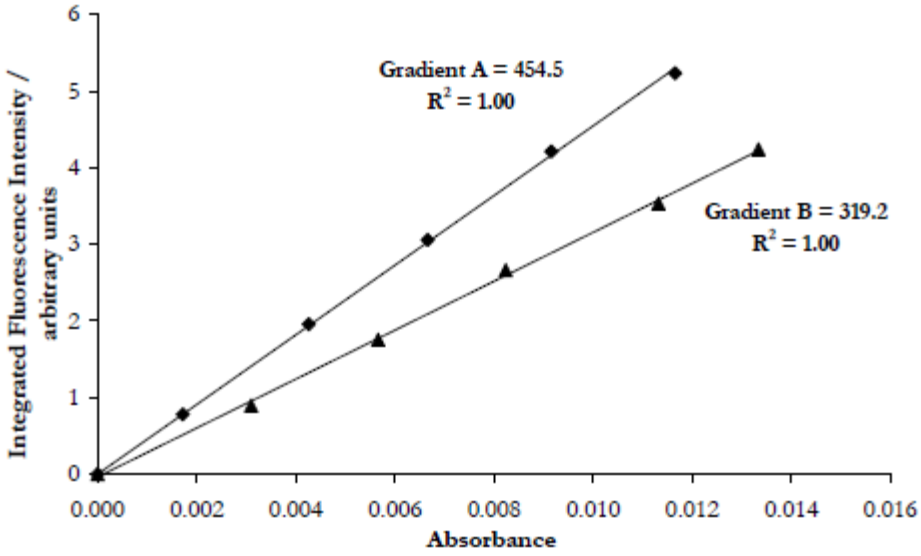

Figure 1-3. Absorbance vs. integrated fluorescence intensities for two samples measured at 5 different concentrations for quantum yield determination.[33] The gradients or slopes from this plot for each sample can be used with Equation 1-11 to calculate the fluorescence quantum yield.

Time-resolved fluorescence allows measurement of the emitting singlet excited state lifetime, S_1, and can be acquired using the Time Correlated Single Photon Counting (TCSPC) method. The fluorescence of a sample is monitored at a wavelength as a function of time after photoexcitation. TCSPC works by detecting emission from individual molecules in a sample and totaling the outcomes, resulting in an intensity vs. time plot that represents the exponential decay of the process. The excitation pulse is split into a reference beam and a sample beam. The reference beam travels directly to the detector (PMT) while the sample beam excites the sample. When the reference beam is detected by the PMT, it starts an internal clock. The sample beam excites the sample promoting a molecule to a higher energy state. After some time, the molecule

relaxes back to the ground state and a photon is emitted. This photon is detected by the PMT and the clock stops, marking the time from excitation to emission. The probability that a photon is emitted decreases over time. After many repeated acquisitions, the exponential decay of the emission process is generated and the fluorescence lifetime can be obtained.

Phosphorescence lifetimes can be obtained by less sensitive methods due to the long lifetime natural to the triplet excited state. Because of the longer lifetime, a larger population of the emitting state, T_1, can be produced over a sustained laser pulse, and single-photon detection becomes unnecessary. As such, emission from a large ensemble of molecules can be detected in a single shot using a PMT.

Transient Absorption Spectroscopy

Transient absorption (TA) spectroscopy, also known as “pump-probe” spectroscopy and flash photolysis, is a powerful technique which allows the study of short-lived transient species. These transient species can involve photoreaction intermediates as well as higher excited states of a molecule accessed by the absorption of photons. Spectral and dynamic information are acquired which provide information about the evolution of excited states that are populated upon excitation with light. The absorption spectra acquired by TA depends on the energy gap of the excited states involved in the transition. Using TA spectroscopy alongside the other spectroscopic techniques described above, it is possible to complete a photophysical profile of the most important electronic transitions of a molecule.

Norrish and Porter first developed flash photolysis to study reactive intermediates by excitation with a flashlamp in 1949,[34] which later was recognized when they shared the Nobel Prize in 1967 for their development of the flash photolysis method. The time

resolution for transient absorption spectroscopy was significantly improved with the introduction of laser technology. As shown in Figure 1-4, modern instrumentation typically uses laser light for quickly creating large populations of reactive chemical species in a variation of the laser flash photolysis system reported by Lindqvist in 1966.[35]

Transient absorption instrumentation works by using a pump source (laser) to create a detectable population of the transient species. A probe source (lamp) with a detector such as a photomultiplier tube (PMT) is used to detect differences in the transmitted light through the sample as the population of the transient species changes through time.

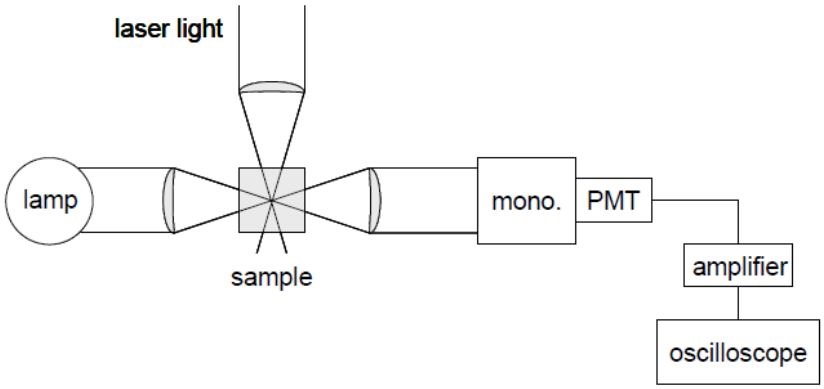

Figure 1-4. Laser flash photolysis system first reported by Lindqvist.[35] Laser light is used as the pump source and a broad spectrum white-light source is used as the probe source. Single wavelength detection is achieved with a monochromator and photomultiplier tube. The signal is amplified and collected on an oscilloscope.

One of the difficulties in acquiring transient absorption is that the excited state population of interest is relatively small leading to only tiny changes in the measured absorbance of the sample. To achieve the highest signal possible, an intense laser pulse and high power lamp are used as the pump and probe beams, respectively.

Computer control and data processing has certainly streamlined this process since starting in the 1970s,[36] making transient absorption a more routine experiment for even less-experienced users.

Depending on the instrumentation that is used, different transient species can be detected. The development of femtosecond-picosecond lasers has pushed the detection of transient absorption to shorter-lived species, allowing the investigation of the dynamics of singlet excited states whose lifetimes are typically on the order of 10^{-9} seconds. Nanosecond instrumentation, typically with the use of Nd:YAG Q-Switched lasers, allows the routine study of triplet excited states which have >ns lifetimes. Further discussion about nanosecond transient absorption instrumentation is given in Chapter 2.

Nonlinear Absorption

In the early development of the interaction between matter and light, only one-photon processes were considered. Two-photon absorption (2PA), by which a transition between a lower and higher energy level occurs by absorption of two identical photons through an intermediate (virtual) state, was first proposed in 1931 in a doctoral dissertation by M. Göppert-Mayer under the supervision of Max Born.[37] The probability of this transition was too small to be measured, however, without the use of laser technology developed in the 1960s. The first reports of nonlinear optical phenomena that were observed to prove her theory were in 1961. Kaiser and Garrett irradiated a $CaF_2:Eu^{2+}$ crystal with a ruby laser (694.3 nm) and observed the characteristic bright blue fluorescence of the crystal at 425 nm.[38] Also reported around the same time was the observation of the second harmonic generation of a quartz crystal irradiated with a

ruby laser.[39] Since then, the field of nonlinear optics and nonlinear absorption has been growing steadily.[40]

Nonlinear absorption can be experimentally determined by the nonlinear transmission method (NLT) where the transmittance of light through a sample is measured as the intensity of the light increases. An open-aperture z-scan instrument can be used to measure the nonlinear absorption of a sample to nanosecond laser pulses. A schematic of the open-aperture z-scan system used in the studies reported in Chapter 3 is shown in Figure 1-5. A laser beam produced by an optical parametric oscillator (OPO) pumped by the third harmonic of a Nd:YAG laser (355 nm, Continuum Surelite II-10, 5 ns fwhm) passes through an iris and using a 50:50 beamsplitter, is split into a sample beam and a reference beam which are focused onto two matched detectors. A neutral density filter can be used to attenuate the energy/pulse. The sample beam is brought into a very tight focus by a plano-convex focusing lens. The sample in a 1-mm pathlength cuvette is mounted on a translational stage and moved along the z-axis through the focus of the laser. The transmitted beam is collected by a detector and the transmittance relative to that of the reference beam is recorded by computer software.

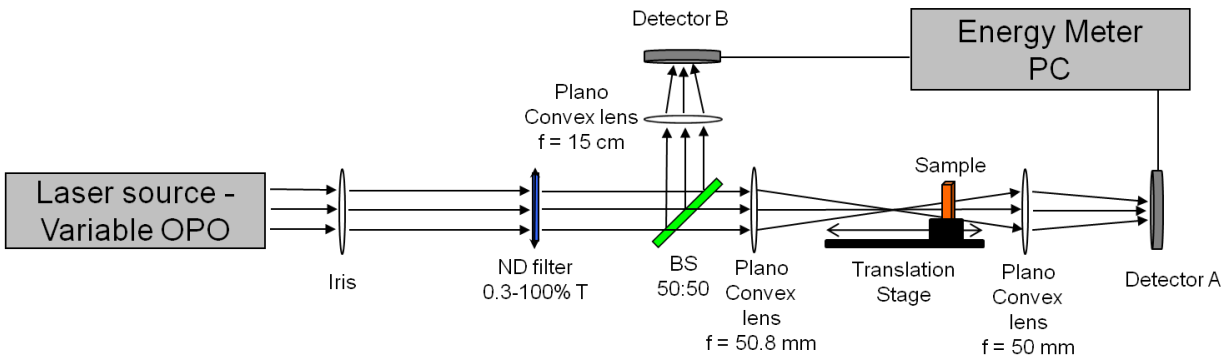

Figure 1-5. Schematic of an open-aperture Z-scan system.

Nonlinear absorption is observed as a dip in the relative transmittance of the laser beam through the sample with the lowest transmittance at the focus of the beam as shown in Figure 1-6. At the focus of the laser beam, the intensity of the light is the highest.

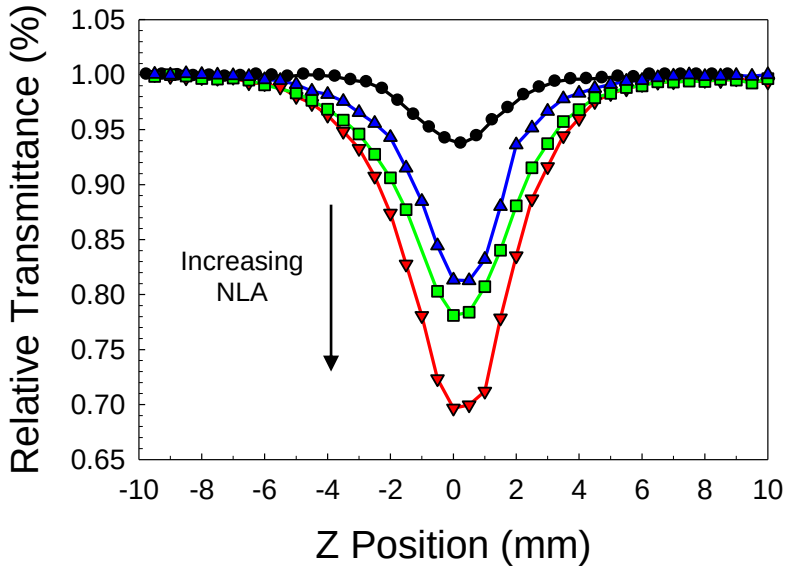

Figure 1-6. Representative data demonstrating the nonlinear absorption of samples with increasing NLA measured by the open-aperture Z-scan apparatus.

If no nonlinear absorption is present, the relative transmittance will be the same at all sample intensities, whereas a sample with strong nonlinear absorption will show a large dip in the transmittance at z=0.

The attenuation of light through a medium can be expressed by the following general equations[40]:

$$\frac{dI(z)}{dz} = -\alpha I(z) - \beta I^2(z) - \gamma I^3(z) - \cdots \quad (1\text{-}12)$$

The function *I(z)* is the intensity of the incident beam propagating along the z-axis and *α*, *β*, and *γ* are the one-, two-, and three-photon absorption coefficients of the transmitting medium under the assumption that the light has a uniform transverse intensity distribution and that the initial intensity is independent of time. If only 2PA is

present, the change in intensity of the propagating light beam through the absorbing medium is dependent on the square of the intensity of the light and the two-photon absorption coefficient of the medium, β.

$$\frac{dI(z)}{dz} = -\beta I^2(z) \quad (1\text{-}13)$$

Assuming a top hat pulse shape, a solution for Equation 1-13 can be calculated for a given position, z, where $I_0(\lambda)$ is the incident light intensity, z is the propagation length in the medium, and $\beta(\lambda)$ is the two-photon absorption coefficient of the medium .

$$I(z,\lambda) = \frac{I_0(\lambda)}{1+\beta(\lambda)I_0(\lambda)z} \quad (1\text{-}14)$$

The value $\beta(\lambda)$ can be expressed as a macroscopic constant for a medium at a given wavelength where σ'^2 is the 2PA cross-section, N_A is Avogadro's number, and d_0 is the molar concentration of the absorbing species.

$$\beta(\lambda) = \sigma'_2(\lambda)N_A d_0 x10^{-3} \quad (1\text{-}15)$$

The units of σ'_2 are cm^4/GM and the units of d_o are mol/L giving units to $\beta(\lambda)$ of cm/GW. This equation is valid only when the population of the ground state is much larger than the population of the excited state promoted by 2PA. The 2PA cross section σ'_2 is also expressed as a factor of the energy of a photon in the incident light beam which has units of cm^{4}s. For simplicity an informal unit, GM (for Göppert-Mayer) is sometimes used which is equal to 10^{-50} cm^{4}s.

$$\sigma_2(\lambda) = \sigma'_2(\lambda) \times h\nu \quad (1\text{-}16)$$

Converting Equation 1-14 to describe the nonlinear transmission through a medium with optical path length l, the equation becomes as written below.

$$T(I_0,\lambda) = \frac{I(l,\lambda)}{I_0(\lambda)} = \frac{1}{1+\beta(\lambda)I_0(\lambda)l} \quad (1\text{-}17)$$

Excited state absorption (ESA) has an enhancing effect on the observed two-photon absorption of a medium. The population of an excited state can be significantly increased by 2PA, resulting in further ESA via a two-step process involving the absorption of three photons.[41] In fact, at higher intensities of incoming light, it has been shown that ESA becomes the dominant source of reduced transmission.[42] In part because of this magnifying effect, the combination of 2PA and ESA have been studied extensively in recent years for nonlinear absorption applications such as optical power limiting.[40,43] It is difficult to separate the contribution of 2PA from that of ESA, so an effective 2PA cross-section value β_{eff} has been used in the literature to describe the nonlinear absorption of chromophores under specific conditions.

Several models for describing experimental NLT to nanosecond laser pulses have been proposed.[40,42,44] Sutherland et al. successfully modeled the nonlinear absorption of alkyl fluorenyl (AFX) chromophores accounting for 2PA and ESA from both the first singlet excited state and triplet excited state with good agreement.[42] They used a five-level system and a simple three-photon absorption model where two of the photons are absorbed simultaneously through a virtual intermediate state as shown in Figure 1-7. The attenuation of the light intensity, I, through a sample along the z axis can be described by a modified equation of Equation 1-12.

$$\frac{\partial I}{\partial z} = -\sigma_2 N_{S0} I^2 - \sigma_S N_{S1} I - -\sigma_T N_{T1} I \qquad (1\text{-}18)$$

where N_{S0}, N_{S1}, and N_{T1} are the number densities (in 1/cm^3) of molecules in S_0, S_1, and T_1 states, respectively, and σ_2, σ_S, and σ_T are the absorption cross sections. The absorption cross sections can be experimentally determined by picosecond and nanosecond photophysical techniques. The difficulty of this calculation is in determining

the number densities. Equation 1-18 must be solved simultaneously with kinetic equations which describe the population of each state N_{S0}, N_{S1}, and N_{T1} based on the excited state lifetimes and quantum yields.

$$\frac{\partial N_{S1}}{\partial t} = \frac{\sigma_2 I^2}{2\hbar\omega} N_{S0} - \frac{N_{S1}}{\tau_S} \quad (1\text{-}19)$$

$$\frac{\partial N_{T1}}{\partial t} = \frac{\varphi_T}{\tau_S} N_{S1} - \frac{N_{T1}}{\tau_T} \quad (1\text{-}20)$$

$$N_{S0} = N - N_{S1} - N_{T1} \quad (1\text{-}21)$$

Using several approximations, Sutherland et al. also derived an analytical expression which gives good agreement with experimental results for AFX chromophores.[42] However, both methods involve challenging calculations and require accurate determination of experimental values such as lifetimes and quantum yields. Assumptions about the laser beam profile, both spatially and temporally, are also necessary to calculate the intensity, *I*.

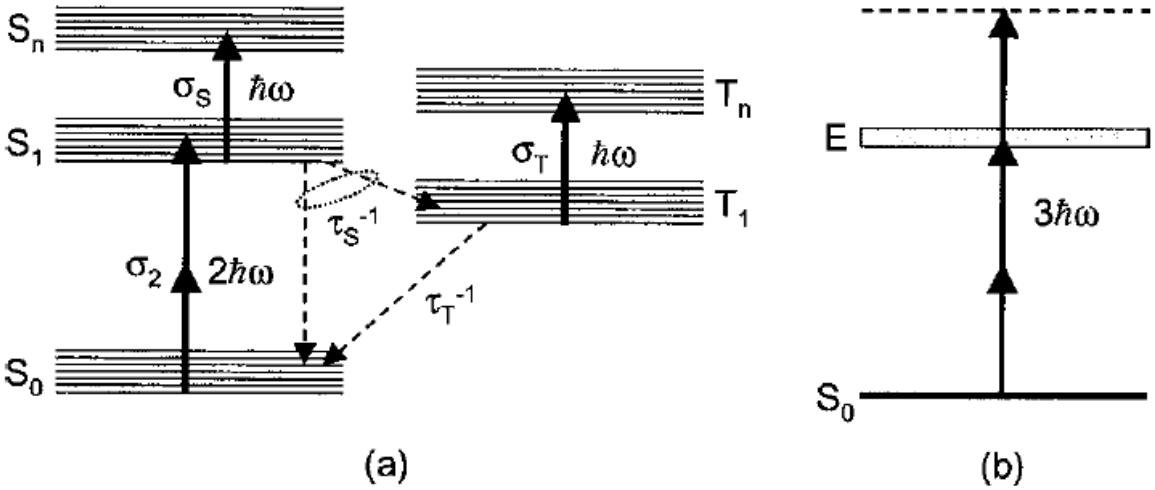

Figure 1-7. Five level energy diagram (a) and the three-photon absorption model (b) used by Sutherland et al to describe the nonlinear absorption of AFX chromophores.[42]

An easier way to quantify the nonlinear absorption experiment is to define an *effective* nonlinear absorption coefficient which describes the overall nonlinear absorption without separating 2PA and ESA. Equations 1-13 to 1-17 describe a purely 2PA process. A parallel equation can be realized to relate the transmittance to an effective nonlinear absorption coefficient, β_{eff}:[40]

$$T(I_0, \lambda) = \frac{I(l,\lambda)}{I_0(\lambda)} = \frac{1}{1+\beta_{eff}(\lambda)I_0(\lambda)l} \quad (1\text{-}22)$$

To calculate I_0, it is necessary to know the parameters of the excitation laser beam. The peak power of the laser pulse can be calculated from the energy per pulse and the pulse duration. For Gaussian-shaped pulses, the constant 0.94 is used.[45]

$$P_p \approx 0.94 \frac{E_p}{\tau_p} \quad (1\text{-}23)$$

In the case of a Gaussian beam, as is depicted in Figure 1-8, the beam is radially symmetrical. The beam waist or radius, w_0, is the radius at which the intensity decreases to $1/e^2$ of its peak value. The Rayleigh length, z_R, is defined as the distance from w_0 where the cross-sectional area of the beam doubles.

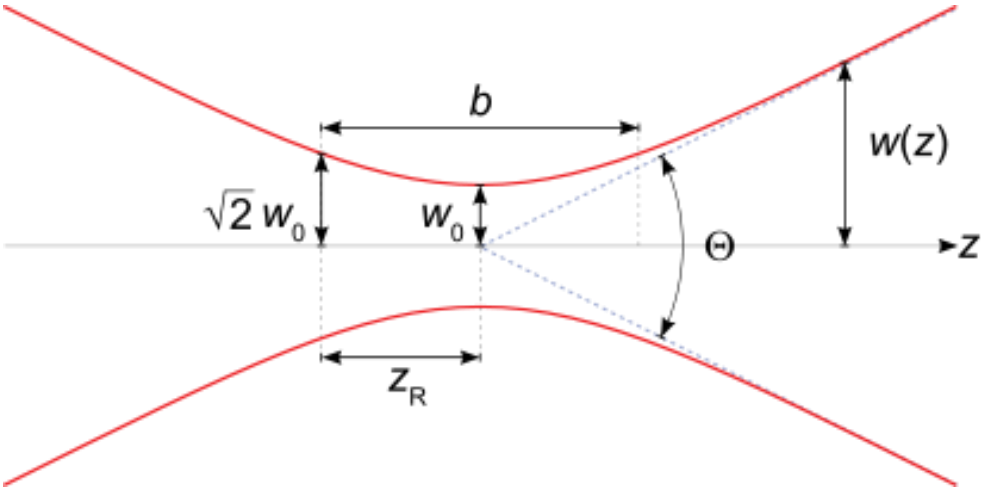

Figure 1-8. Properties of a Gaussian beam: w_0 is the beam waist, Z_R is the Rayleigh range, b is the depth of focus, and θ is the beam divergence.[46]

The diameter of the beam waist, $2w_0$, can be calculated by Equation 1-24.

$$2w_0 = \frac{4\lambda}{\pi\theta} \quad (1\text{-}24)$$

Using the small angle approximation ($\tan\theta \approx \theta$), θ can be approximated as the inverse of the f-number of the focusing lens. The f-number is the focal length, F, of the lens divided by the diameter, D, illuminated onto the lens. Thus the diameter of the beam waist is approximately equal to Equation 1-25.

$$2w_0 = \left(\frac{4\lambda}{\pi}\right)\left(\frac{F}{D}\right) \quad (1\text{-}25)$$

In the open-aperture Z-scan apparatus shown in Figure 1-4, the focal length of the focusing lens is F = 50.8 mm. If the excitation wavelength is λ = 600 nm and the diameter of the beam illuminated onto the lens is D = 2 cm, then the beam diameter is 3.2 μm. This is an unreasonably small value for our beam diameter. A necessary assumption in Equation 1-24 is that the beam is collimated; however the beam output from the OPO is slightly divergent. There are ways of accurately measuring the beam waist, but they are expensive, upwards of several thousand dollars. A reasonable estimate for the beam waist would be 30-50 μm.

As 2PA only occurs in the focused region of the beam, it is necessary to check the assumption that the beam stays focused throughout the entire cuvette. The Rayleigh length, z_R, gives an approximate value for the length over which the beam stays focused. The Rayleigh length can be calculated by equation (1-26).

$$z_R = \frac{\pi w_0^2}{\lambda} \quad (1\text{-}26)$$

The wavelength λ is the vacuum wavelength divided by the refractive index *n* of the material. For a beam waist of 30 μm, the Rayleigh length is approximately 6 mm. Interestingly, the dip in the transmittance of the z-scans obtained using the described

instrumental setup, as shown in Figure 1-4 and Figure 1-5, begins about 6 mm away from z=0. This supports that a 30 μm beam waist is a good approximation.

Typical open-aperture Z-scan experimental paramaters, as are used in Chapter 3, are as follows: Excitation is with a λ_{exc} = 600 nm laser beam through an OPO with a pulse energy of 600 μJ/pulse (10 Hz repetition rate, 5 ns fwhm). Samples are prepared at 1 mM concentration in THF in a 1-mm pathlength quartz cuvette. To calculate the effective nonlinear absorption coefficient, β_{eff}, for a sample with a transmittance at the focus (z=0) of 0.9, the following calculations would be used:

1. The peak power of the laser pulse is 1.13 x 10^5 W. If a 30 μm beam waist is assumed, the intensity of the beam is:

   $I_0 = \frac{1.13x10^5\ W}{\pi(30x10^{-4}\ cm)^2}$ = 4.00 x 10^9 W/cm^2

2. The pathlength, *l*, is 1 mm. The refractive index of THF is 1.40 at 25°C.

   $l = 1.0\ mm$ = 0.10 cm

3. Equation 1-22 can be rearranged to solve for β_{eff}.

   $\beta_{eff} = \frac{(1-T)}{T\ x\ I_0\ x\ l} = \frac{(1-0.90)}{0.90\ x\left(4.00\frac{GW}{cm^2}\right) x\ 0.10\ cm}$ = 0.28 cm/GW

This effective nonlinear absorption coefficient, β_{eff}, allows an easy comparison between the nonlinear absorption of different compounds at the same excitation wavelength λ_{exc}. In Chapter 3, these calculations will be applied to assign quantitative values to the overall nonlinear absorption of a series of platinum acetylide complexes for the purpose of evaluating their use in optical power limiting applications.

This Study

The goal of this research is to study the excited state dynamics of conjugated molecules, oligomers and polymers and compare the properties in solution and in the

solid-state. Instrumentation was developed to study the triplet excited state dynamics of solid state films and materials by transient absorption. This new transient absorption system was used to study photoactive materials ranging in applications from nonlinear absorbing PMMA monoliths, trimeric mercury-containing polymer films, and conjugated cationic oligomers absorbed onto clay scaffolds.

Chapter 2 introduces the development of new transient absorption instrumentation specifically optimized for use with thin films and solids is described. The instrumental components and optical layout is discussed. A custom Labview program was made to make the transient absorption experiment a user-friendly routine experiment. Further, the instrument was validated and optimized using platinum acetylide polymer films to examine the capabilities of the instrument. Sensitive detection of as low as 10^{-3} ΔA was achieved which is over 10x the sensitivity of previously available instrumentation for solution measurements.

In Chapter 3, the photophysical properties and nonlinear absorption of series of *p*-phenylene vinylene platinum acetylide complexes are investigated. The photophysical properties of the series are investigated in THF. The triplet molar extinction coefficients of a series of *p*-phenylene vinylene platinum acetylide complexes are measured with transient absorption by relative actinometry against benzophenone as the actinometer. The complexes are incorporated into PMMA monoliths with high transparency, stability, and optical quality for optical power limiting application. Properties of the PMMA monoliths are studied, and the photostability of the complexes in the polymer glasses is discussed. Triplet-triplet annihilation in conjugated co-polymers containing the phenylene and *p*-phenylene vinylene platinum acetylide units is

observed and compared against representative “monomer” complexes using transient absorption spectroscopy as a function of increasing laser fluence of the excitation pulse. The nonlinear absorption of the complexes in solution and in monolith is measured with open-aperture z-scan and the effective nonlinear absorption coefficient, β_{eff}, is calculated.

Chapter 4 details the interaction between conjugated polymer, MEH-PPV, and a trimeric perfluoro-*p*-phenylene mercury complex, Hg3 in solution and in films. The addition of Hg3 to MEH-PPV templates aggregation of the polymer leading to interesting effects on the photophysical properties. Nanosecond transient absorption is employed to study the excited state dynamics of the polymer. Additionally, the changes in structure and morphology of MEH-PPV in films upon addition of Hg3 are observed using ^{1}H NMR, powder XRD, and TEM. The interaction of Hg3 with another conjugated polymer, P3HT, is briefly discussed.

Chapter 5 reports the intercalation of cationic oligomers into a synthetic saponite clay matrix and the study of the photophysical properties of clay-oligomer hybrid in dispersed solutions and in films is reported. The absorption and emission measurements reveal ordering of the oligomers once they are incorporated into the clay. An increase in interlayer spacing of the clay observed by XRD confirms the intercalation of the oligomer. Thermogravimetric analysis and fluorescence titration studies are performed to determine the quantity of oligomer integrated into the clay.

CHAPTER 2
TRANSIENT ABSORPTION INSTRUMENTATION FOR THIN FILMS

Background

Transient absorption can be measured using two modes of detection. The first acquires a whole transient absorption spectrum at a given time *t* with very precise wavelength detection. To get decay information, many spectra need to be collected at varied *t* and then imported into a spectral kinetics program such as SpecFit. An alternative way to collect transient absorption data is by single wavelength detection, such as is described in the introduction. Single-wavelength detection gives more precise transient decay lifetime information at a single wavelength, but to acquire a spectrum, many transient decays at different wavelengths are collected and then collated using a custom executable Matlab program. Depending on which system is used, there is a trade-off between time and wavelength resolution.

The pump beam used in these transient absorption experiments comes from a Nd:YAG Q-Switched laser with excitation possible at 355 nm or 532 nm by use of harmonic generation of the 1064 nm fundamental. For single wavelength detection, the probe source is a xenon arclamp. Detection is with a PMT which provides detection up to 800 nm or with a Si Photodiode for detection into the near-IR. A Triax 180 Monochromator is used for single wavelength detection. This transient absorption system has been used for many years, however the electronic components and programming was beginning to become incompatible with upgraded computer hardware necessitating a considerable upgrade of components. The system was updated with new electronic components and Labview programming including a Berkely Nucleonics Corporation Model 575 and a Tektronix 4032B Phosphor oscilloscope. Labview

programming offers complete automation and data collection for the transient absorption system and replaced the old Visual Basic programming that controlled the old electronic components that were replaced in the latest upgrade of this system.

Instrumentation of a Transient Absorption System for Thin Films and Solids

Here we describe the instrumentation and optimization of a nanosecond transient absorption system for thin films. There are some considerations for optical instrumentation for films compared to solution samples. Solutions placed into a standard cuvette can easily be prepared to a set concentration, and the sample will be the same size (1 cm pathlength) and shape making placement of the sample into the instrument very straightforward. Thin films may require more preparation time than solutions and, for many analyses, are more sensitive to decomposition under pulsed laser irradiation due to the fact that molecules in solid films cannot dissipate heat as effectively as molecules in solutions. Typically, films also produce weaker signals with an increased signal to noise ratio due to the shorter pathlength (nm – μm thickness). Nonetheless, many real-world applications involve the incorporation of chromophores into solid state materials, so measuring the properties of these compounds in thin films or polymer monoliths is particularly important.

A typical TA instrumentation setup for solution measurements involves an excitation path perpendicular to that of the probe beam and the detector in order to minimize laser reflection and scattered light into the detector. For a thin film, the laser must hit either the front or the back face of the sample film. In the instrumentation described here, a nearly antiparallel laser path was chosen. For protection against thermal degradation of the films, low laser energies of 300-800 μJ/pulse are used for excitation and longpass filters in a manual filter wheel are incorporated to block

unwanted wavelength regions of the probe lamp. This decreases the overall intensity of the light without any information loss in detection. Maybe the most significant feature of the newly developed TA system is that sensitive detection for thin films is acquired by using a very intense, stable light source and a low-light, sensitive detector. Polymer thin films typically give TA intensities of 10^{-3}-10^{-4} ΔA, whereas a solution sample under optimal conditions will have a transient absorption intensity on the order of $10^{-1}\Delta$A.

Instrument Description

A transient absorption system for thin film analysis was constructed. The optical schematic is shown in Figure 2-1. A Surelite I-10 Nd:YAG laser with second and third harmonic generators delivers nanosecond pulses for excitation at 532 or 355 nm, respectively. A 250 watt quartz tungsten halogen lamp and power supply (Newport catalog #6334NS lamp and #69931 radiometric power supply) is used as the probe source. Light exposure of the sample is controlled by a series of mechanical shutters and a manual filter wheel is placed between lens **6** and the sample to protect from heat damage caused by the intense light. A Cornerstone 130 motorized monochromator is used to isolate a single wavelength using one of two available gratings: one for UV-Vis analysis (1200 l/mm blaze 500) and one for nIR analysis (800 l/mm blaze 1000) and detection is by either a photomultiplier tube (Hamamatsu R928 PMT, 400 – 800 nm) or an avalanche photodiode (APD, 750 – 1000 nm) to observe the TA signal decay versus time. For UV-VIS detection, a Hamamatsu R928 PMT powered by 730 volts is mounted to the monochromator in a custom base modified in-house using 5 of the 9 PMT stages for signal amplification. For nIR detection, the PMT is removed, lens **9** is slid into place to collect the output light from the monochromator, and concave mirror **10** focuses the light onto a Si avalanche photodiode (Thorlabs #APD110A).The signal from the

detector is collected with a Tektronics 3032B Oscilloscope and sent to a computer. Laser flashlamp, Q-switch, slow shutter, fast shutter, and oscilloscope timings are controlled by a BNC Model 575 8-channel pulse generator.

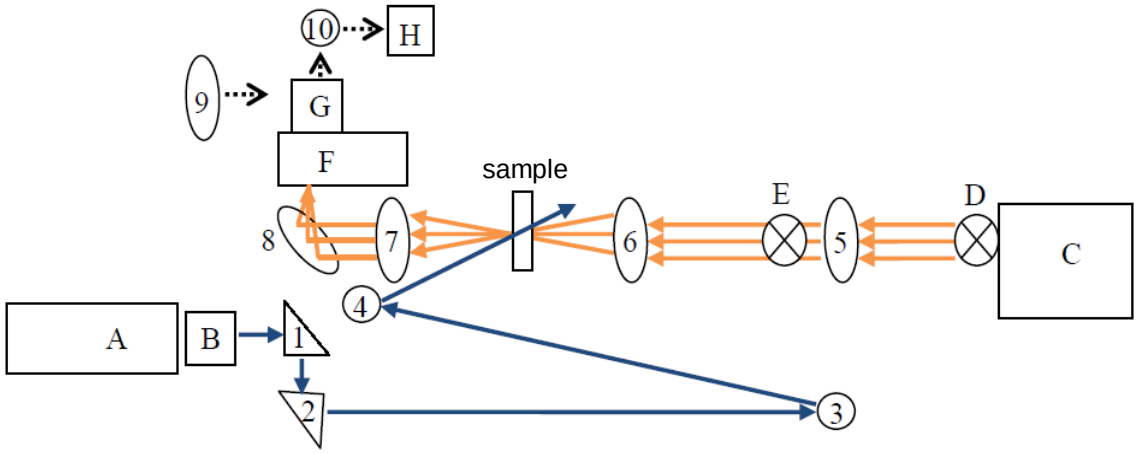

Components: **A**: Surelite I-10 Nd:YAG laser, **B**: Second and Third Harmonic Generator, **C**: 250 W QTH Lamp, **D**: Slow Shutter, **E**: Fast Shutter, F: Cornerstone 130 Monochromator, **G**: PMT, **H**: APD. *Optics*: **1/2**: 1" prisms, **3/4/10**: 1" mirrors, **5**: 10 cm f.l. plano convex 2" lens, **6**: 10 cm f.l. plano convex 2" lens, **7**: 10 cm f.l. plano convex 2" lens, **8**: 10 cm f.l. concave mirror, **9**: 5 cm f.l. plano convex 2" lens, **10**: 5 cm f.l. concave mirror

Figure 2-1. Transient absorption system for films.

Computational Considerations

A custom executable for this system was written in Labview 8.0 and saved as executable file "TA.vi" (Figure 2-2). The TA.vi program enables live control of all instrumental components in the TA system via GPIB communications so that the optimum settings for transient absorption measurement such as the oscilloscope time/div, number of waveforms to average, etc, can be obtained before the acquisition begins. The Izero.vi subvi performs a routine to calculate Izero at a given wavelength as follows: The slow and fast shutters are activated so that the probe beam passes through the sample and the oscilloscope collects an average of 16 waveforms. The

average value in mV of the collected waveform is Izero. The laser Q-switch is not enabled so Izero essentially measures the baseline transmittance of the probe beam through the sample. This Izero is then saved on the scope as the vertical offset. This allows the oscilloscope to zoom in on the TA signal when viewed live on the TA.vi window or on the oscilloscope screen itself when the appropriate instrument controls are enabled.

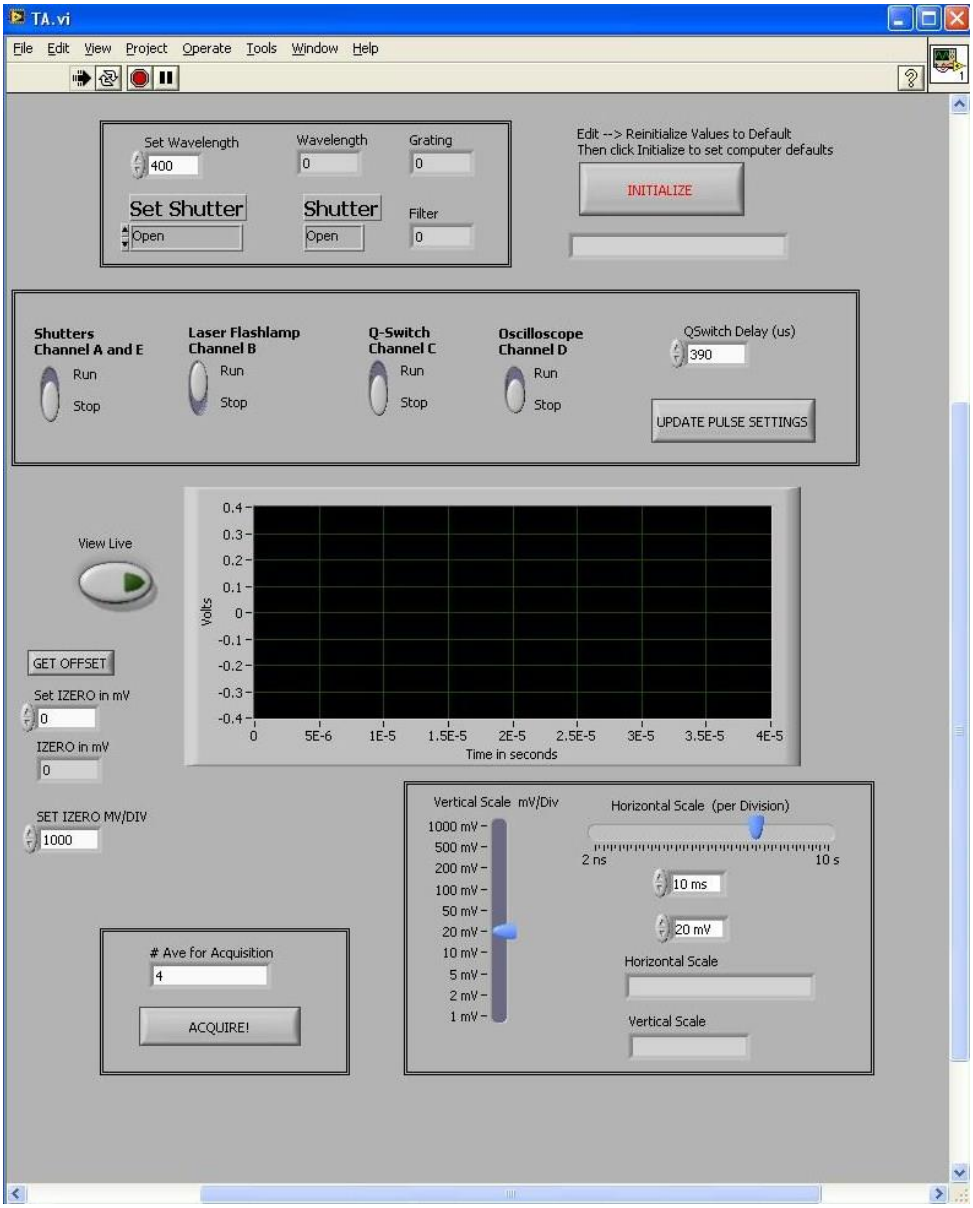

Figure 2-2: Screenshot of the TA.vi program.

After the transient absorption settings have been optimized for acquisition, the acquisition window is opened by clicking the “Acquire!” button in the TA.vi window (Figure 2-2) to open the Acquire.vi subvi. In the Acquisition window shown in Figure 2-3, parameters for a full acquisition scanning many wavelengths can be set. On the top left-hand part of the screen, the start, stop, and interval wavelengths are input by the user and the progress indicator on the right is updated with the correct number of iterations. A smoothing parameter is selected to reduce the number of data points collected for each run from the 10,000 sent by the oscilloscope to a more manageable number for manipulation in post-acquisition processing in Matlab or other plotting programs. Typically a smooth factor of 10 is used, which decreases the number of data points to 1,000. The acquisitions for the wavelength series indicated by the user are saved to temporary files with consecutive numeric filenames.

When the acquisition program is run, the monochromator is set to the starting wavelength. At that wavelength, Izero is calculated. The oscilloscope is set to the horizontal scale the user defined in the TA.vi program for transient absorption data acquisition and the vertical scale defined by the user for the Izero computation. The shutters and oscilloscope trigger are activated, and sixteen waveforms are averaged on the scope. The Q-switch is not enabled for Izero calculation. The resulting waveform is transmitted to the computer where the software takes the mean value of the 10,000 data points. The waveform data sent from the scope is in mV vs. data point (1 to 10,000). The time parameter is not important for the Izero computation.

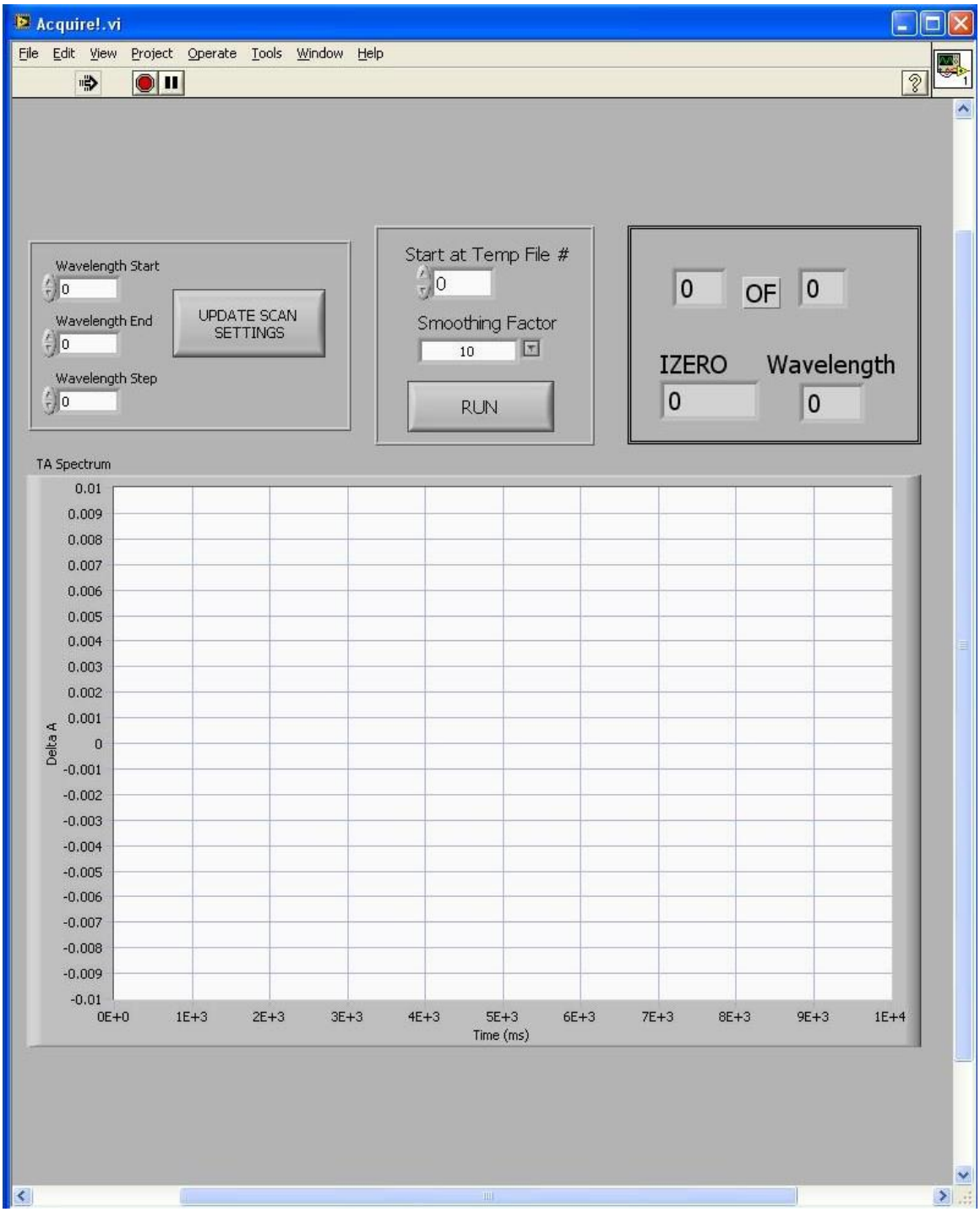

Figure 2-3. Screenshot of the Acquire.vi program.

For the TA data acquisition at each defined wavelength, the scope offset is set to the Izero computed by the software. The oscilloscope is set to the horizontal and vertical scales the user defined in the TA.vi program for data acquisition. The shutters,

oscilloscope, laser flashlamps and laser Q-Switch are enabled. A user-chosen number of waveforms are averaged on the scope, and the resulting waveform is transmitted to the computer. The waveform data off the scope is in mV vs. data record. The time parameter is computed externally and added to the waveform data by taking the ms/div user defined setting and multiplying by the total number of divisions (10) and dividing by the number of data points (10,000) to get the ms/data point. The "TA.vi" software, at this time, is not able to perform computations with scale settings of 200 ns/div and lower. In post-processing Matlab software, time zero, t_0, is selected manually by the user.

The raw mV data is converted to ΔA as demonstrated by Figure 2-4 and Equations 2-9 and 2-10, where *ΔI(t)* is the change in transmittance intensity observed due to transient absorption.

$$\Delta A = log\left[\frac{I_0}{I_0 - \Delta I(t)}\right] \quad (2\text{-}9)$$

Δ Absorbance = log (1/Δ Transmittance) (2-10)

The mean of the first 50 data points of the acquisition (for a 4 μs/div timescale, 50 data points is 20 ns) is taken and this is designated as I_0. I_0 is computed similarly to the Izero previously computed but with more precision due to the expanded y-axis scale. Each raw data point is subtracted from I_0 to get ΔI(t). The signal $\Delta I(t) = (I_0 - I(t))$ divided by the background (I_0) is the change in transmittance. The output from a PMT is negative current, so the Izero appears as a negative mV value. Other detectors, such as the APD, output positive so the schematic shown in Figure 2-4 will appear upside-down.

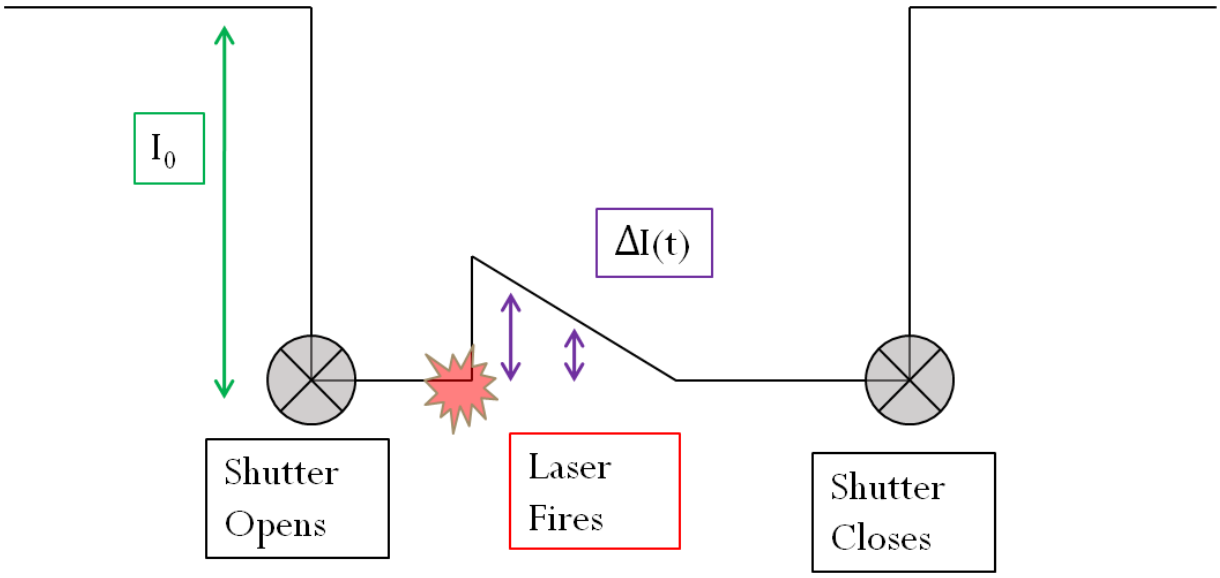

Figure 2-4. Schematic of TA data acquisition and processing for a PMT signal.

The software averages a user-defined (smoothing factor) number of sequential points to create a "smoothed" waveform. Smoothing serves to reduce random noise, increasing the signal/noise ratio of the signal, but most importantly, it reduces the number of data points which provides more manageable file sizes. A smoothing factor of 2 reduces the 10,000 data points to 5,000 data points and a smoothing factor of 10 reduces the 10,000 data points to 1,000 data points.

The described system acquires transient absorption decays with low signal-to-noise with intensities on the order of 10^{-3} ΔA and can even resolve decays on the order of 10^{-4} ΔA. Analysis between 400 and 1000 nm is possible on timescales of 4 μs or longer with the available instrumentation and software. As triplets in solid state typically have longer lifetimes than those found in solution, shorter timescales are rare. A sample decay profile is shown in Figure 2-5.

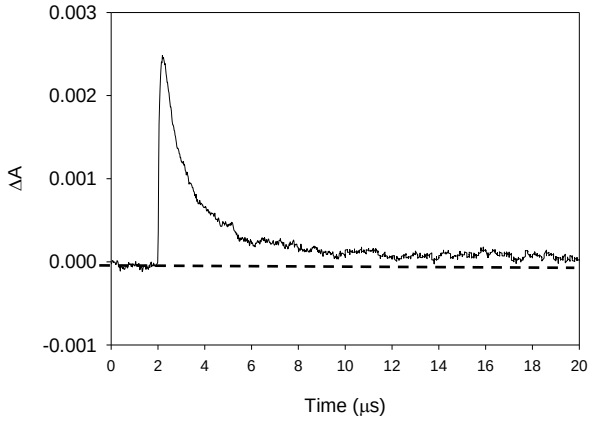

Figure 2-5. Transient decay signal of a platinum acetylide polymer film (pPtPh) from the described film TA.

Further processing can be performed to produce ΔA vs. wavelength transient absorption spectra from the ΔA vs. time raw data using an in-house written Matlab program "TAS.m". The "TAS.m" program allows the user to graphically select time zero (t_0). Time zero is taken to be end of the laser pulse, indicated on the raw decay by the peak maximum of the transient absorption. Using t_0, a transient absorption spectrum (ΔA vs. wavelength) is generated for the wavelength range of the "TA.vi" acquisition run. Several spectra at regular time intervals can also be generated and overlaid onto the t_0 spectrum to visualize the spectral decay.

Instrument Validation and Optimization with pPtPh Polymer Films

The platinum acetylide polymer pPtPh shown in Figure 2-6 was used in the validation of the transient absorption system. The properties of this polymer have been well studied in the literature.[47-50] It is a model platinum acetylide and has a maximum ground state absorption at 370 nm with fluorescence at 390 nm and phosphorescence at 515 nm.

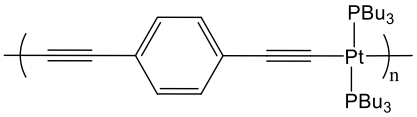

Figure 2-6. Structure of the platinum acetylide polymer pPtPh.

To prepare thin films of pPtPh, glass slides were cut into 1 cm wide pieces with a glass scribe and were thoroughly cleaned with sonication in a SDS/water solution, isopropanol, and acetone followed by plasma cleaning. Three solutions of varying concentration of pPtPh were prepared in toluene: 5 mg/mL, 10 mg/mL and 20 mg/mL.

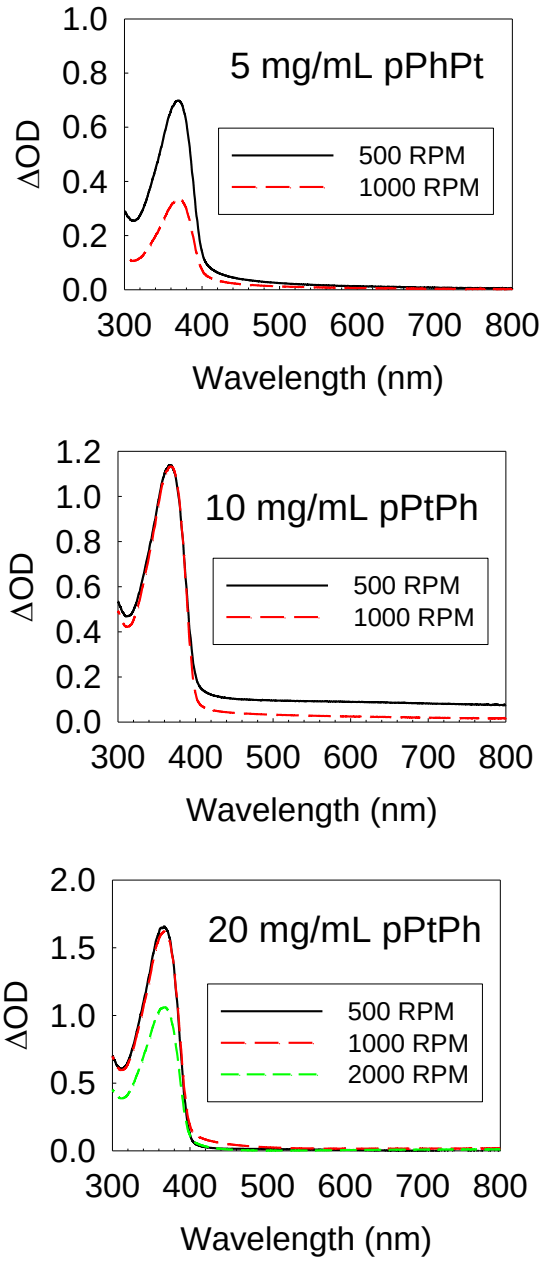

Figure 2-7. Absorption spectra of pPtPh spin-coated films prepared from various solution concentrations in toluene and spin speeds.

The solutions were stirred for 4 hours before films were spin-coated at varying spin-speeds at each concentration level: 500 RPM, 1000 RPM, and 2000 RPM producing films of different thicknesses. The spin-coating process has been described in the literature.[51-53] Although the film thicknesses were never directly measured, films of pPtPh made under similar conditions had thicknesses on the order of 50 nm.[54] The ground state absorption spectra of the films are shown in Figure 2-7.

Thin film transient absorption spectra were taken with the thin film transient absorption system described previously and the transient absorption of a pPtPh film is shown in Figure 2-8. Transient absorption decays were collected from 550-800 nm and processed in Matlab to produce the transient absorption spectra.

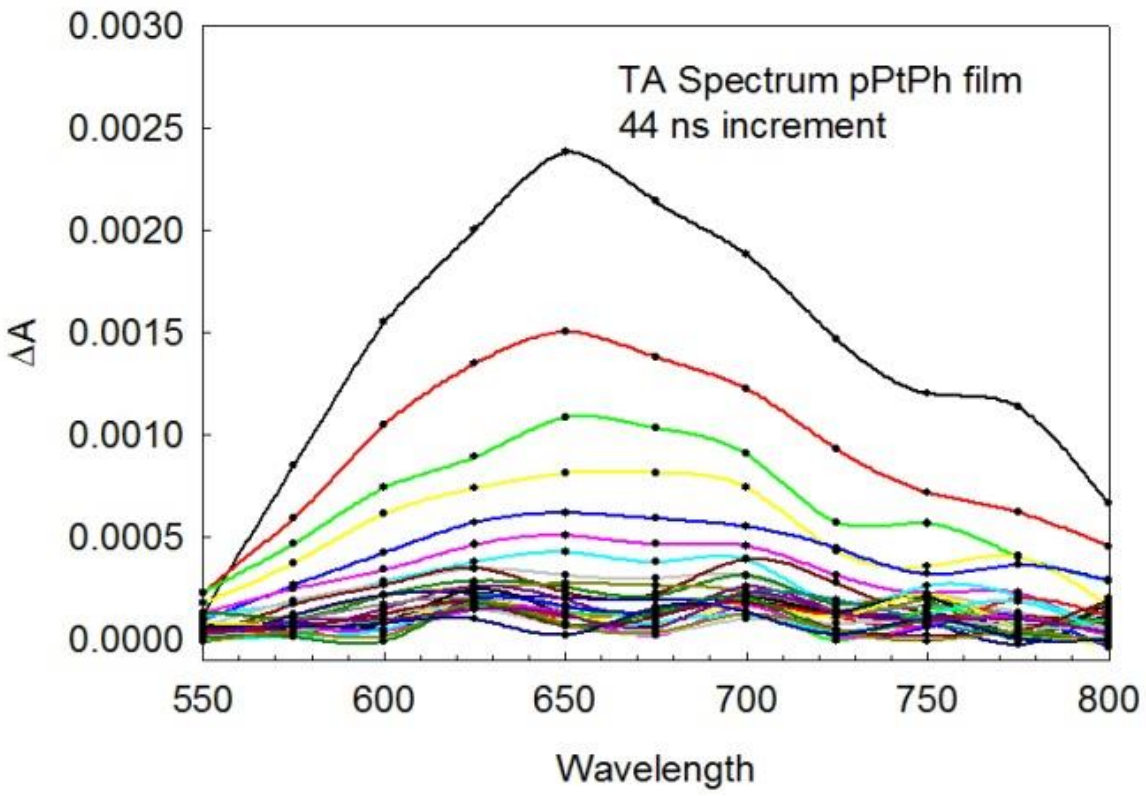

Figure 2-8. Transient absorption spectrum of pPtPh film (20 mg/mL, 500 RPM) with nanosecond excitation at λ_{exc} = 355 nm, 500 μJ/pulse (1 kΩ termination, 128 averages, slits 0.7 mm, smoothing factor of 10).

The transient absorption decay of a pPtPh film (prepared from a 10 mg/mL solution and spin-coated at 1000 RPM) at TA_{max} = 650 nm was fit to a single exponential decay of the form $y=ae^{-kt}$ with an R^2=0.9247, a=0.001298, b=0.446 (units in μs^{-1}). This corresponds to a triplet lifetime of pPtPh in thin films of 2.2 μs, which is on the same order as the 0.996 μs reported by Jarrett Vella by a time correlated single photon counting technique (TCSPC).[54]

The transient absorption of pPtPh in tetrahydrofuran (THF) was performed for comparison to the film TA measurements. A solution of pPtPh in THF was prepared to an optical density of 0.7 at 355 nm and purged with argon. The transient absorption excitation source was the 355 nm third harmonic of a Continuum Surelite II-10 Nd:YAG laser. The probe source was a Xe arc flashlamp, and detection was with a PI-Max intensified CCD camera mounted onto a spectrograph. Data processing was done with an in-house Matlab program. The excitation energy was about 5 mJ. The TA spectrum was collected from 350 nm to 850 nm with a 20 ns initial camera delay and 750 ns increments. One hundred averages were taken at each time. The solution showed a broad transient absorption peak over the wavelength range 410 nm to acquisition end, with ΔA_{max} at approximately 650 nm (Figure 2-9). The spectra between the solution and thin film are similar with little shift in the absorption maximum. Instrument optimization was performed using pPtPh films. The optimal settings for slit width, number of waveforms to average, and smoothing of the acquired data were determined. These are the default settings that will be used for routine sample analysis, although optimization should be performed for each individual sample.

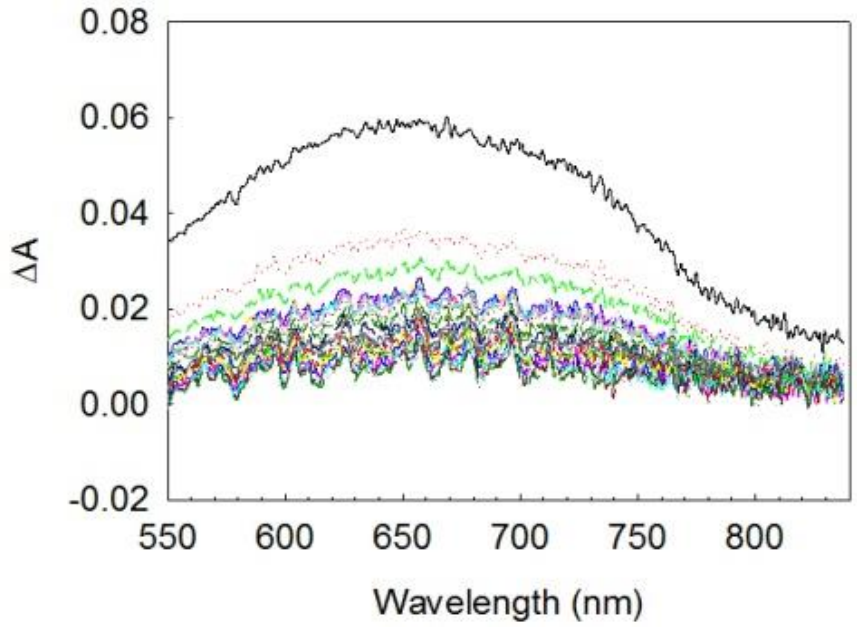

Figure 2-9. Nanosecond transient absorption spectrum of pPtPh in THF solution (λ_{exc} = 355 nm, 5 mJ/pulse, initial camera delay 20 ns, camera delay increment 750 ns, 25 transients, 100 averages).

The wavelength resolution at the detector is dependent on the slit width of the monochromator and the bandpass of the grating used. The grating used in for the film TA is a 500 nm blaze grating with 1200 lines/mm which has a bandpass of about 7 nm/mm. Generally, a smaller slit width gives higher wavelength resolution. Using larger slits, more light hits the detector which normally decreases the noise in the acquired data; however, a slit that is too large will also allow stray and scattered light to affect the signal. The optimal slit width for this instrument was determined by observing the signal intensity vs. the signal-to-noise ratio of TA decays acquired under the same conditions varying only the slit width as shown in Figure 2-10. The optimal slit width was determined to be 0.70 mm. This gives a bandpass of about 5 nm, which is an acceptable value for the broad spectral features detected with transient absorption spectroscopy.

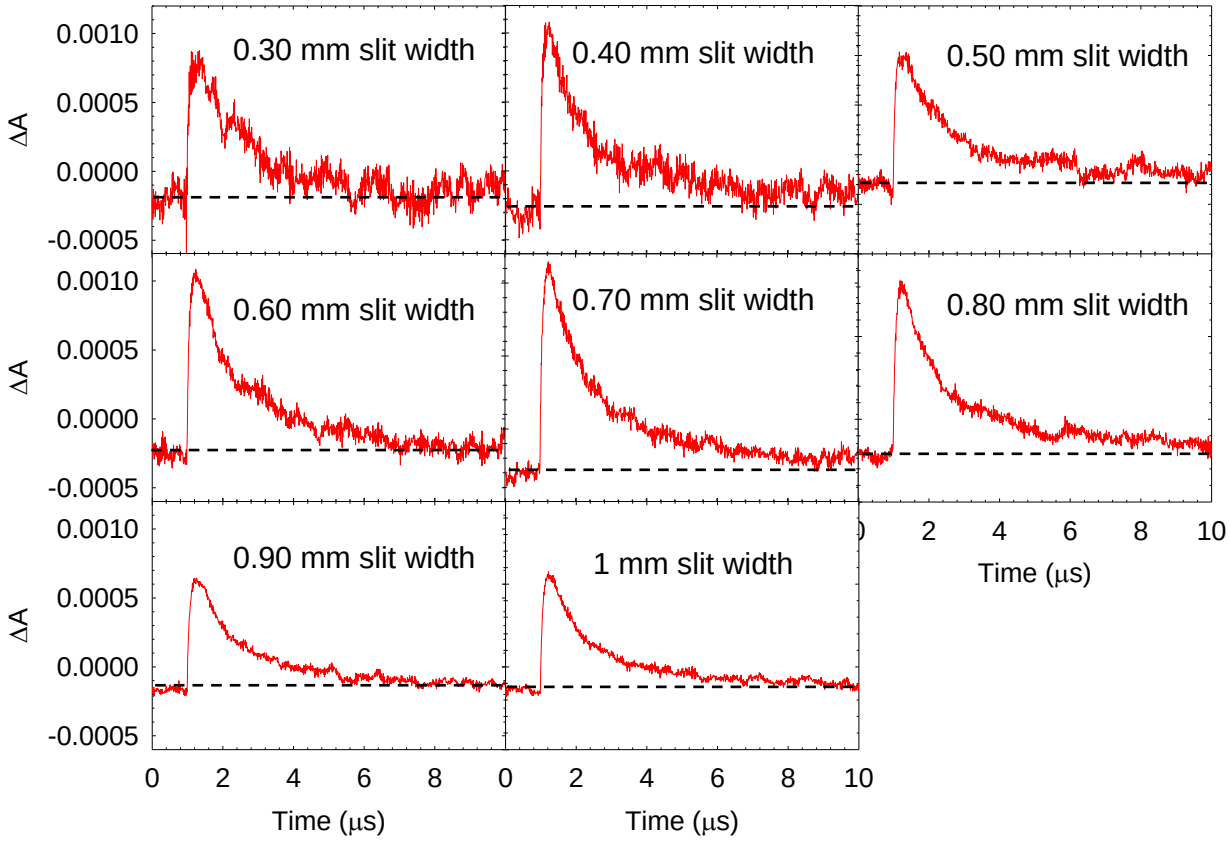

Figure 2-10. Transient decays collected of a pPtPh film (prepared from a 20 mg/mL solution in toluene spun at 2000 RPM) with increasing slit width on the monochromator. Detection was with a PMT at λ_{max} = 650 nm (λ_{exc} = 355 nm, 600 μJ/pulse, 1 kΩ termination, 128 avgs, smooth 10).

The number of waveforms to average was also optimized (Figure 2-11). With the weak TA signals produced by thin films whose thicknesses (aka pathlengths) are on the order of nanometers, a significant amount of averaging in the signal is necessary to get meaningful data. The more a signal is averaged, the less noisy it becomes. Films, however, are very sensitive to the heat produced by intense light sources and cannot dissipate heat as easily as solutions can. Thus, it is necessary to find a balance between the number of times the sample film is shot with the relatively intense lamp and laser beams and the quality of the data acquired. It was found that 128 averages was sufficient to produce a quality transient decay.

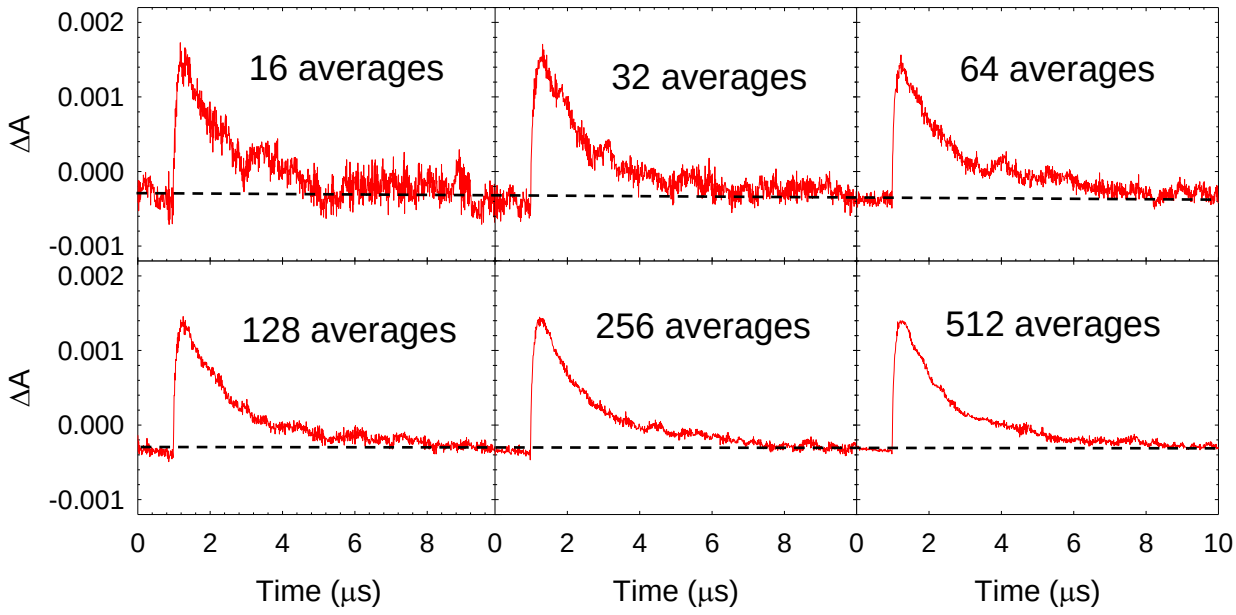

Figure 2-11. Transient decays of a pPtPh film (prepared from a 20 mg/mL solution in toluene spun at 2000 RPM) with an increasing number of averaged waveforms. Detection was with a PMT at λ_{max} = 650 nm (λ_{exc} = 355 nm, 600 μJ/pulse, 1 kΩ termination, slits 0.5 mm, smooth 10).

The oscilloscope outputs 10,000 data points which is a burden for plotting programs such as Excel or Origin to handle. Smoothing was introduced to reduce the number of data points output by the scope, and it also decreases the signal-to-noise ratio of the acquired transient. Smoothing does affect the time resolution of the decay, but after smoothing, the transients still display a sharp rise indicating that the time resolution is still acceptable. Based on the decays collected with varying smooth factors as shown in Figure 2-12, a smooth factor of 10 was shown to satisfactorily decrease the noise of the signal while keeping a workable amount of data points (1,000). The smooth factor of 10 takes an average of each 10 data points.

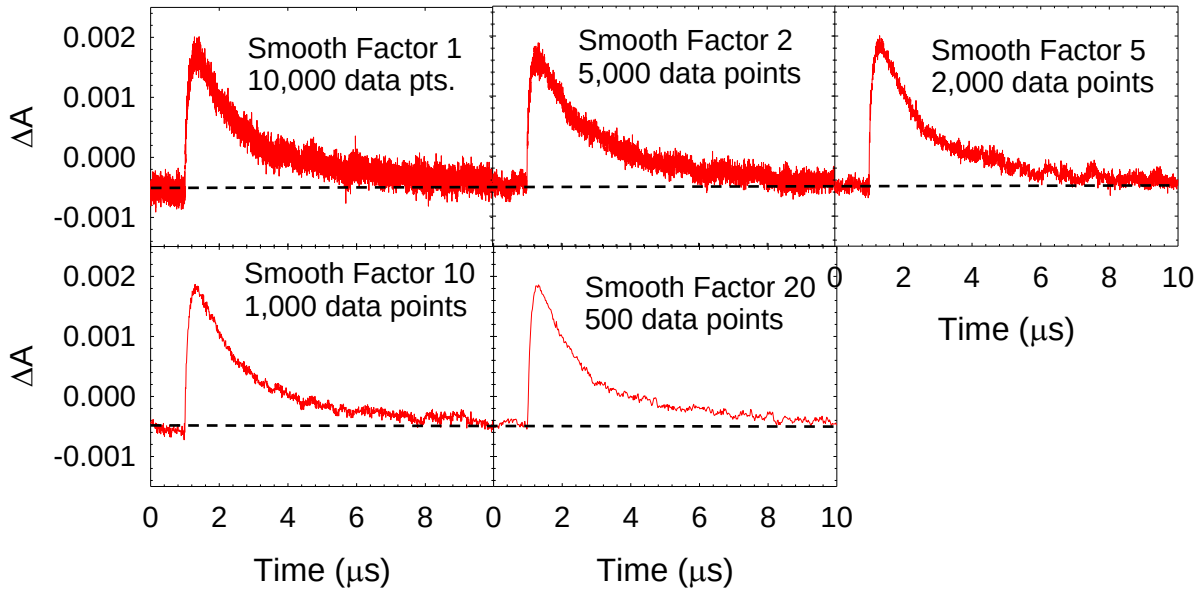

Figure 2-12. Transient decays of a pPtPh film (prepared from a 20 mg/mL solution in toluene spun at 2000 RPM) with varying smooth factors. Detection was with a PMT at λ_{max} = 650 nm (λ_{exc} = 355 nm, 600 μJ/pulse, 1 kΩ termination, slits 0.5 mm, 128 averages).

This new instrumentation was developed to measure the transient absorption of thin films and solids. The experimental parameters that were found to be optimal for routine use of this instrument are as follows: 1 kΩ termination at the oscilloscope, entrance and exit slits of 0.70 mm on the monochromator, 128 waveforms to average, and a smoothing factor of 10. Altering these parameters may be necessary depending on unique experimental factors, however these settings should ensure optimal transient absorption data for most analyses.

CHAPTER 3
SOLID STATE MATERIALS FOR OPTICAL POWER LIMITING

Optical Power Limiting by Nonlinear Absorption

Due to the rapid development of lasers, there has been significant research focused on materials that can provide defense to some of the threats, accidental and hostile, involved with laser technology.[41,55-58] Optical power limiting (OPL) materials are materials that allow the transmission of low intensity light while strongly attenuating high intensity light. These materials are used in applications for the protection of sensitive optical sensors, such as the human eye, from being harmed by exposure to laser light.[59,60] After the input fluence reaches an initial threshold, these materials strongly attenuate the transmitted light to a safe clamping energy. The key property in OPL activity of these materials is their strong nonlinear absorption.[60-63]

Platinum(II) acetylide complexes exhibit nonlinear absorption via a dual-mechanism pathway, and their nonlinear absorption and optical power limiting properties have been studied extensively in the past decade or so.[43,64-67] When the two-photon absorption (2PA) spectrum and the triplet-triplet excited state absorption (ESA) spectrum have significant overlap, particularly efficient nonlinear absorption is achieved.[42,67-69] Initially, instantaneous two-photon absorption occurs which populates the singlet excited state S_1. Spin-orbit coupling due to the heavy platinum atom promotes intersystem crossing from the first singlet excited state with efficient yield to form the triplet state T_1. The triplet state, T_1, which in platinum acetylides typically has a particularly large molar extinction coefficient, readily absorbs additional photons after a significant triplet population is achieved. [65,70] Nonlinear absorption by two-photon absorption allows for the production of transparent materials because no ground state

absorption is required at the active wavelength. Dual-mode nonlinear absorption utilizing 2PA and ESA has broad temporal response, offering protection from both short pulses (fs – ps) and longer pulses (ns – μs). [41,65,69,70]

The majority of research on platinum acetylides for OPL properties has been reported in solution experiments, but, recently, attention has shifted to the incorporation of these complexes into solid-state materials that are more useful to real-world applications. Inorganic sol-gel glasses offer high stability and excellent optical quality. [62] Platinum acetylides incorporated into sol-gels have demonstrated good optical power limiting abilities; [71,72] however the sol-gel method is time-consuming, requires careful attention to pH and temperature, and typically requires additional functionalization of the active chromophores in order to reach adequately high concentrations for effective optical power limiting. On the other hand, polymer glasses, such as those made with poly(methyl methacrylate) (PMMA), make good solid-state hosts due to their simple preparation, high optical transparency, and ability to be cut and polished with good optical quality.

In 2008, Westlund and coworkers prepared platinum(II) acetylides containing phenylene ethynylenes units into PMMA polymer glasses with high doping concentrations (up to 100 mM) as both blended and covalently bonded materials.[73] They found that these materials exhibited nonlinear absorption as shown by strong attenuation of transmitted laser energy to nanosecond pulses. Their results demonstrated that platinum(II) acetylides could be incorporated into PMMA glasses for optical power limiting applications and found that the blended glasses actually

performed better than those prepared by covalent attachment of the chromophore to the polymer backbone.[73]

The work discussed here involves the incorporation of highly two-photon absorbing platinum acetylide chromophores into PMMA polymer monoliths and the evaluation of the photophysical properties in the monoliths compared to the properties measured in solution. One goal is to establish whether the photophysical properties important to optical power limiting are retained in the solid state. Also proposed here is a quantitative analysis of nonlinear absorption to nanosecond pulses and this quantitative method is applied to the open-aperture z-scan results of these platinum acetylide complexes in solution and in PMMA monolith.

Linear and Cross-Conjugated Pt(II) OPV Series

Previous research on π-conjugated chromophores containing triphenylamine groups at the ends of *p*-(phenylene vinylene) units have found that these types of complexes have very large 2PA cross-section values in the visible to near-infrared region.[40,74-76] Linking these types of chromophores to a heavy metal atom such as platinum, the triplet-triplet absorption can be enhanced and optical power limiting by dual-mode nonlinear absorption can be achieved. In this study, highly two-photon absorbing oligomeric p-(phenylene vinylene) π-conjugated chromophores (OPV) are connected to platinum(II) centers and the one- and two-photon photophysical properties are examined in solution and in solid state PMMA monoliths with a focus on optical power limiting.

Two series of oligo (*p*-phenylene vinylene) platinum(II) acetylides were studied to elucidate the structure-property relationship for optical power limiting (Fig. 3-1). A linear series TPVn has two OPV chromophores linked to a platinum center through a

triphenylamino- group with an increasing number of OPV units (n=0 to 2, where n is the number of phenylenes between the terminal triphenylamine groups). The complex TPV2-T2 has two OPV chromophores each connected to a platinum atom that is connected through a dithiophene center. The cross-conjugated series crossTPVn has two OPV chromophores attached to a center phenyl unit that is conjugated through platinum phenyl ethynylenes (n=1 and 3, where n is the number of phenylenes between the terminal triphenylamine groups and the center phenyl ring). The complex crossTPV1-DPAF has diphenylaminofluorene (DPAF) groups instead of the terminal triphenylamines.

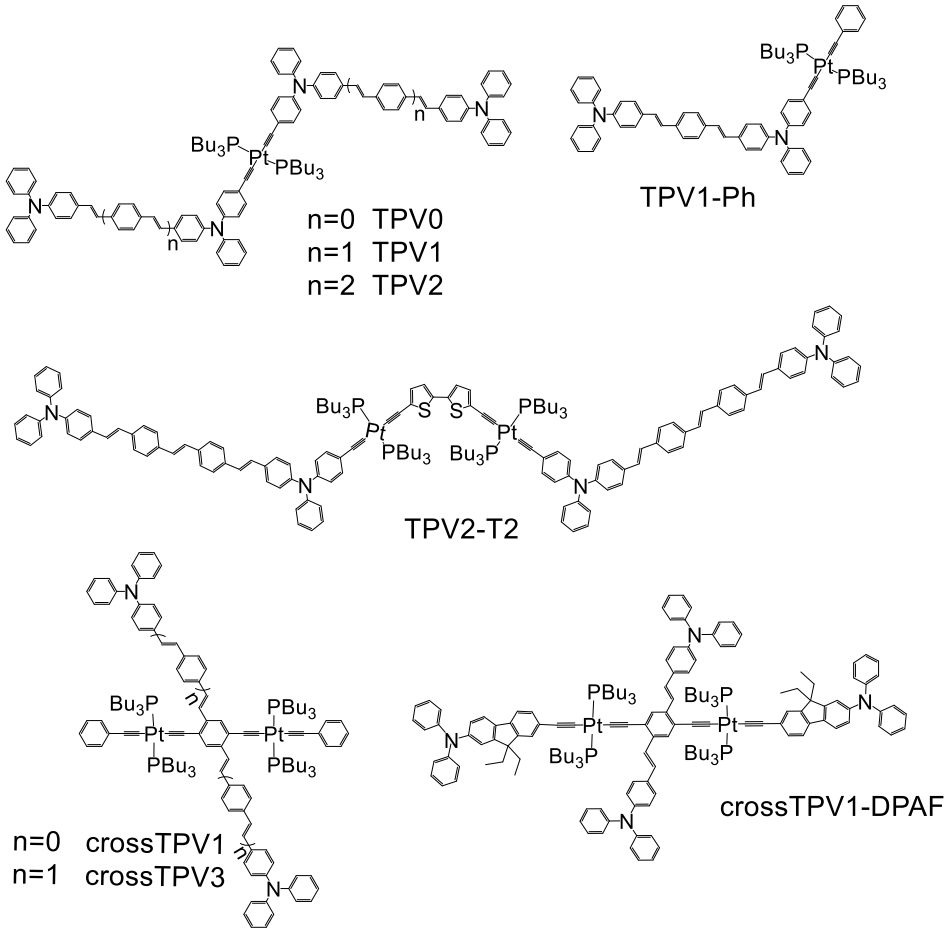

Figure 3-1. Structures and acronyms for *p*-(phenylene vinylene) platinum(II) acetylide chromophores synthesized by Galyna Dubinina.

Solution Photophysical Studies

The one-photon photophysical properties in solution were measured for each complex to investigate the structure-property relationship of increasing OPV chain length and the linear or cross-conjugated geometry. The results in THF are summarized in Table 3-1.

Table 3-1. One Photon Photophysical Properties in THF Solution.

Name	λ_{abs}[a]	ε_S ($x10^4$)	λ_{fl}[a]	Φ_{fl}[b]	$\langle\tau_f\rangle$, ns	$\lambda_{T\text{-}T}$[a]	ε_T[c] ($x10^4$)	τ_{TA}, μs	Φ $^1O_2$[d]
TPV0	395	13.5	459	0.10	0.18	585	7.4	0.3	0.13
TPV1	415	20.9	502	0.30	0.78	678	11.0	1.19	0.73
TPV2	424	29.5	525	0.52	1.15	687	10.0	67.9	0.51
TPV2-T2	423	24.5	522	0.28	0.66	683	39.3	0.79	0.79
TPV1-Ph	415	9.33	502	0.46	1.44	671	18.1	0.59	0.35
crossTPV1	355 405	11.2 7.6	476 507	0.01	<0.1[e]	662	7.7	0.85	0.83
crossTPV3	343 415	9.5 10.7	501 537	0.04	<0.1[e]	719	8.1	0.43	0.98
crossTPV1-DPAF	301 381	8.7 21.4	478 511	0.005	<0.1[e]	660	11.8	0.96	NA

[a]Wavelengths of ground state absorption (λ_{abs}), triplet-triplet absorption ($\lambda_{T\text{-}T}$), and fluorescence (λ_f) maxima are in nm.
[b]Measured at rt using 9,10-diphenylanthracene in cyclohexane as a std, (Φ_{fl}=0.75).[77]
[c]Determined by relative actinometry with benzophenone as the actinometer (Φ_T=1.00, ε_T=7870 mol^{-1} cm^{-1}).[78,79]
[d]Measured in $CDCl_3$ using terthiophene as a std, (Φ^1_{O2}=0.75).[80]
[e]Lifetime is less than the instrument time resolution which is ~100 ps.

The normalized absorption and emission spectra of the complexes are shown in Figure 3-2. For the linear (TPVn) series, the peak molar absorptivity values increase with OPV length, and the ground state absorption and fluorescence maxima red-shift. The cross-conjugated chromophores (crossTPVn) have very broad absorption peaks with two maxima. As the length of the OPV unit increases from crossTPV1 to crossTPV3, the fluorescence maxima red-shift and the longer wavelength absorption

band becomes more pronounced. This suggests that the shorter wavelength transition is due to the platinum phenylene ethynylene unit,[81] while the longer wavelength band can be assigned to the OPV chromophore axis. Although the crossTPVn series absorbs more broadly in the blue, all complexes are optically transparent in the visible region λ>525 nm, which is important for OPL applications.

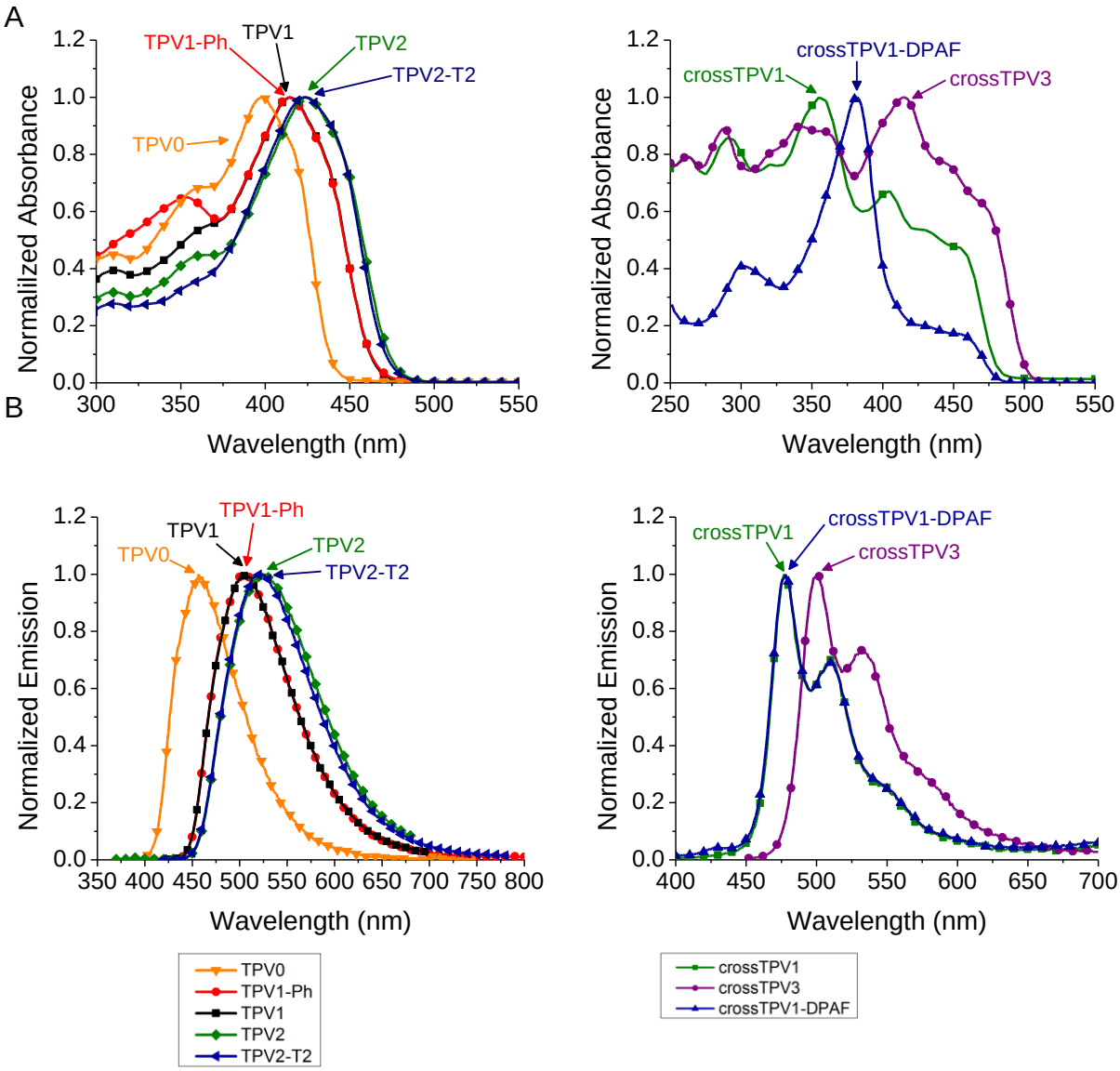

Figure 3-2. Normalized (A) absorption and (B) emission spectra of the linear and cross-conjugated *p*-(phenylene vinylene) platinum(II) acetylide chromophores in THF.

The fluorescence quantum yields and lifetimes shown in Table 3-1 demonstrate several interesting trends. For the TPVn series, the fluorescence quantum yield and fluorescence lifetimes are increased with longer OPV chain which suggests that the competing nonradiative decay, ISC, is significantly less efficient when the conjugated OPV chromophore is lengthened. The mixing of the platinum-centered orbitals with the frontier orbitals decreases with increasing OPV length resulting in decreasing spin-orbit coupling and intersystem crossing which explains the decreased Φ_f and τ_f. TPV2-T2 had significantly lower Φ_f and faster τ_f, indicating that ISC is particularly efficient, likely due to the presence of thiophene units which are known to increase the rate of ISC in conjugated organic molecules. The crossTPVn complexes had low fluorescence quantum yields (<5%) and short fluorescence lifetimes (<instrument response, ~100 ps) indicative of especially efficient ISC.

Nanosecond transient absorption was used to investigate the triplet state properties of these complexes. The triplet-triplet absorption spectra are shown in Figure 3-3. Each of the chromophores exhibits strong, broad triplet-triplet absorption throughout the visible and near-IR regions, with bleaching <500 nm corresponding to ground state absorption. The chromophores are prepared to matched optical density at λ_{exc} = 355 nm in THF. The Pt-complexes containing the longer conjugated ligands, TPV2-T2 and crossTPV3, have the largest T-T absorption which is supported by the triplet molar extinction coefficients shown in Table 3-1. The T-T absorption bands for the cross-conjugated series are distinctly sharper and more intense than for the linear series because the triplet chromophore is more influenced by the Pt centers. Comparing the crossTPV1, crossTPV3, and crossTPV1-DPAF complexes, there is a

red-shift in the TA with increasing conjugation length of the OPV axis indicating that the triplet excited state is primarily localized along the OPV axis and not the phenylethynl-axis. This is further supported by the fact that in crossTPV1-DPAF, the triplet-triplet absorption spectrum aligns with that of crossTPV1 (λ_{max} of T_1-T_n = 660 nm), so the axis containing the two DPAF units does not contribute significantly to the triplet excited state.

In order to be effective optical power limiters, two-photon absorption is a necessary process. To quantify the two-photon absorption properties of these complexes, the femtosecond 2PA cross-sections across the wavelength range of 570-1070 nm was measured by two methods, two-photon excited fluorescence (2PEF) and a newly developed intensity-dependent nonlinear transmission (NLT) method by collaboration with Dr. Aleks Rebane at Montana State University.[82] Similar results were obtained using the wavelength tunable output of an amplified Ti-sapphire source (80-120 fs) by both the NLT and 2PEF methods as shown in Figure 3-4 (pulse repetition rates 100 Hz and 1 kHz, respectively).

Several features are significant with respect to the 2PA spectra of each complex shown in Figure 3-4. Specifically, each system exhibits strong 2PA with σ_2 greater than 500 GM over a large range of the visible to near-IR region, 600 nm-900 nm. Also, the longest linear OPV-containing complexes have peak σ_2 values larger than 10,000 GM, which is one of the largest 2PA values reported.[82,83] The cross-conjugated chromophores have particularly broad and intense spectra, over a 200-300 nm window. In all cases, there is exceptional spectral overlap between the 2PA spectra and the

triplet-triplet absorption spectra which is the most important property in dual-mode nonlinear absorption for optical power limiting applications.

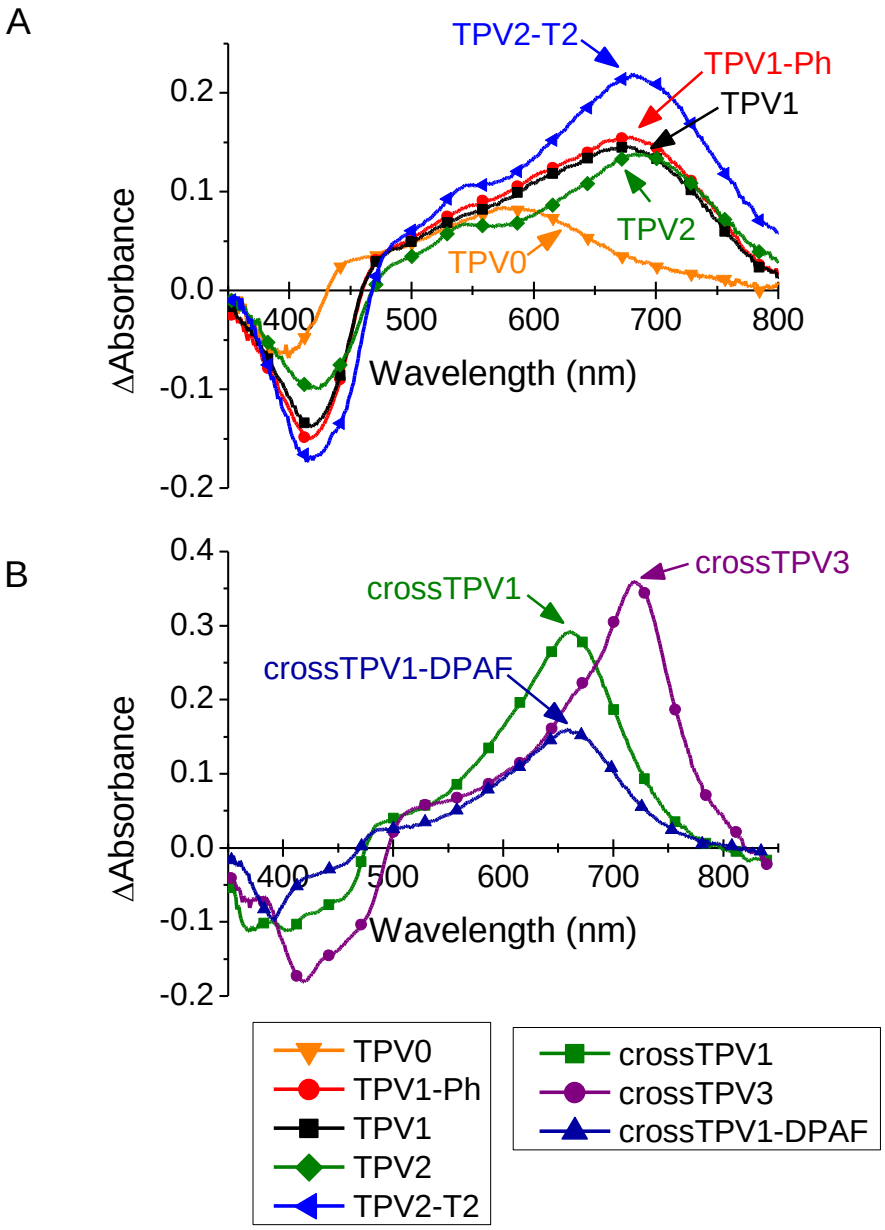

Figure 3-3. Transient triplet-triplet absorption spectra of the linear (A) and cross-conjugated (B) *p*-(phenylene vinylene) platinum(II) acetylide chromophores in argon-purged THF using nanosecond-pulsed excitation at 355 nm (energy = 5 mJ/pulse). The solutions were prepared to the same optical density at 355 nm (OD = 0.4) and the spectra shown here were collected after a camera delay of 50 ns after the laser pulse.

To examine the effect of the platinum on the nonlinear absorption, the two photon absorption properties of the ligands (TPV0-L, TPV1-L, TPV2-L) were investigated and compared to the properties of the linear and cross-conjugated platinum acetylides. The ligands consist of oligomeric OPVs with terminal triphenylamine groups that are not attached to a platinum acetylide. Generally, the peak values of the ligands correspond to approximately one-half of the peak values in the platinum acetylide complex. This is reasonable since there are two OPV ligands present in each linear and cross-conjugated platinum acetylide complex. The discrepancy in the NLT peak values for the TPV0-L and TPV0 compounds are likely due to photobleaching of the high concentration samples used in the NLT experiment.

The peak in the 2PA absorption spectra of the complexes is different than the S_0-S_1 transition in the ground state (1PA) absorption spectrum. This is explained by the selection rules for 1PA and 2PA transitions, which require alternative parity in the 1PA and 2PA transitions for centrosymmetric molecules.[74] Analogous to the ground state absorption spectra shown in Figure 3-2, the 2PA peaks red-shift with increasing conjugation length. Both the 2PA spectra and T-T absorption spectra red-shift with lengthened OPV unit, so the spectral overlap of these two processes remain well-maintained. The large discrepancy in the 2PA cross-sections at shorter wavelengths seen in the NLT compared to the 2PEF measurement for TPV2-T2 and crossTPV3 may be due to a large contribution in the NLT from excited state absorption in the singlet state (S_1-S_n) during the laser pulse duration. Singlet excited state absorption is not measured by the 2PEF method.

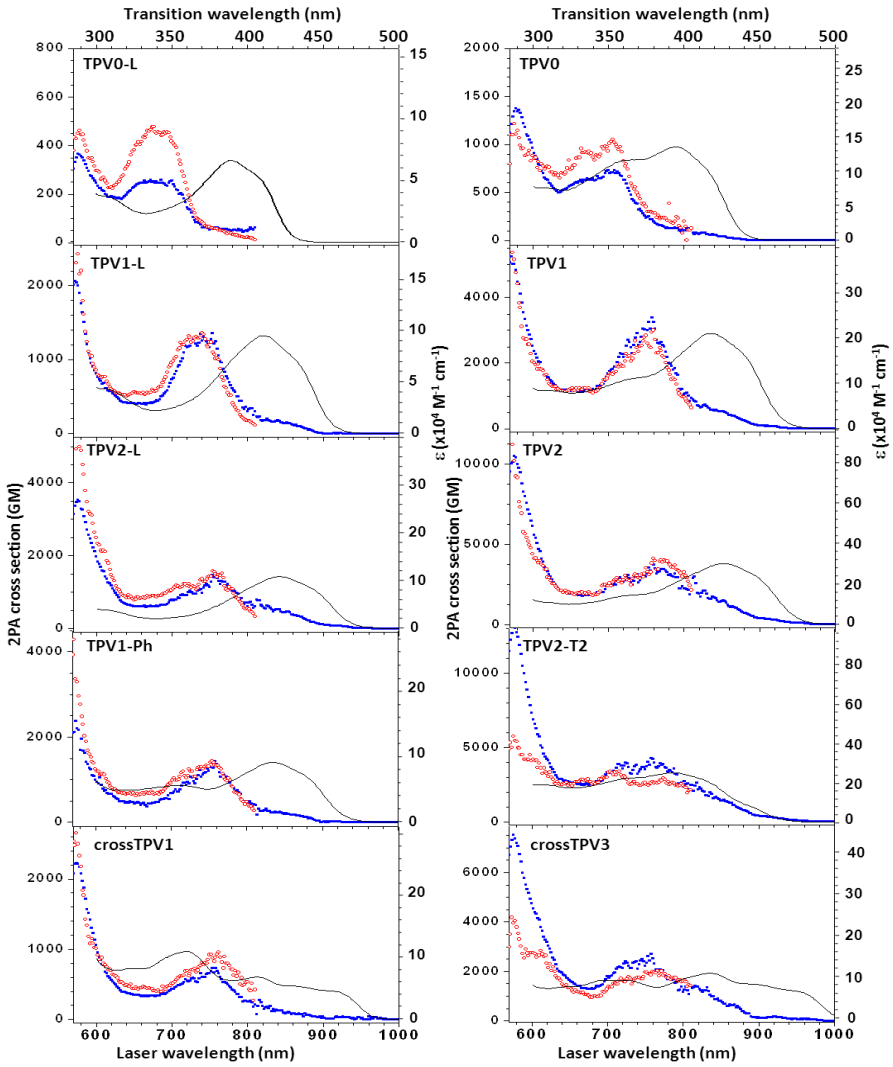

Figure 3-4. Two-photon absorption (2PA) spectra and values of the linear and cross-conjugated OPV Pt-acetylides and ligands measured by 2PEF (open red symbols) and NLT (filled blue symbols) methods by Dr. Rebane and his research group at Montana State University. The one-photon absorption spectra are shown in black for comparison.

The nonlinear absorption of each complex and ligand to nanosecond pulses (680 nm, 800 μJ/pulse) was measured by open-aperture z-scan. Well-known nonlinear absorbing platinum acetylide Pt-DPAF[67] was used as a reference compound in each scan as a means of comparing Z-scan measurements performed on separate occasions.

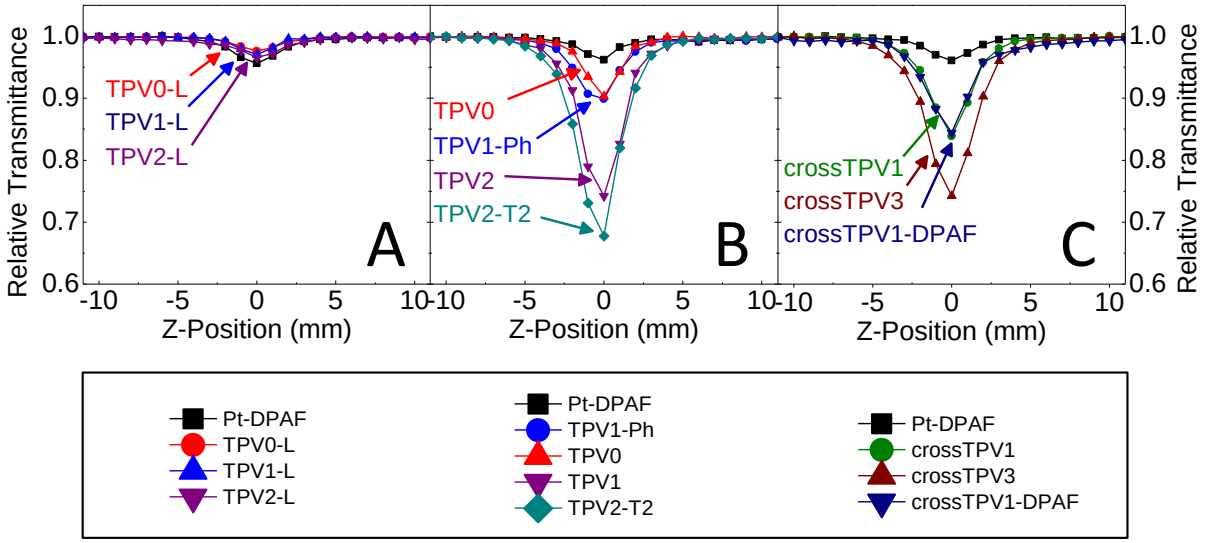

Figure 3-5. Open-aperture Z-scan measurement showing nonlinear absorption to nanosecond laser pulses at 680 nm (800 μJ/pulse) for the (A) ligands, (B) linear series, and (C) cross-conjugated series in THF. Pt-DPAF, a well-known nonlinear absorbing platinum acetylide, was used as a reference compound for purposes of comparison between different scans.

As shown by the z-scans in Figure 3-5, all complexes and ligands exhibit nonlinear absorption under these conditions. The nonlinear absorption of the ligands in plot A is only due to simultaneous two-photon absorption because the ligands have near zero ISC yields, whereas the nonlinear absorption of the complexes is due to the dual-mode mechanism of 2PA and ESA. By comparing the nonlinear absorption of the ligands (Figure 3-5, A) to that of the platinum acetylide complexes (Figure 3-5, B and C), it is clear that the nonlinear absorption to nanosecond pulses is considerably enhanced when both 2PA and ESA are present. Sustaining the trends in 2PA cross-section values and triplet-triplet absorption molar extinction coefficients, the longer conjugated OPVs display stronger attenuation of the transmittance at the focus.

PMMA Monoliths for OPL Applications

PMMA monoliths were prepared by a procedure adapted from Westlund and coworkers.[73] The monoliths are highly transparent and could potentially be made to any size and shape with the appropriate mold (Figure 1). For measurement of their photophysical properties, the monoliths were cut and polished to approximately 1 mm to high optical quality. Varying concentrations of chromophore were attempted, but monoliths containing higher initial concentrations (>2 mM) of chromophore were not transparent due to phase separation. Table 3-2 lists the final thickness and calculated concentration of each monolith.

The absorption spectra could not be measured for the monoliths due to saturated optical density. The photoluminescence spectra of the monoliths were measured in front-face alignment and compared to the spectra in THF solution in Figure 3-6. The linear TPV complexes display a slight blue-shift in the PMMA monolith; however the peak shape and broadness is similar to solution measurements. The cross-conjugated complexes do not exhibit a shifted spectrum in the monoliths.

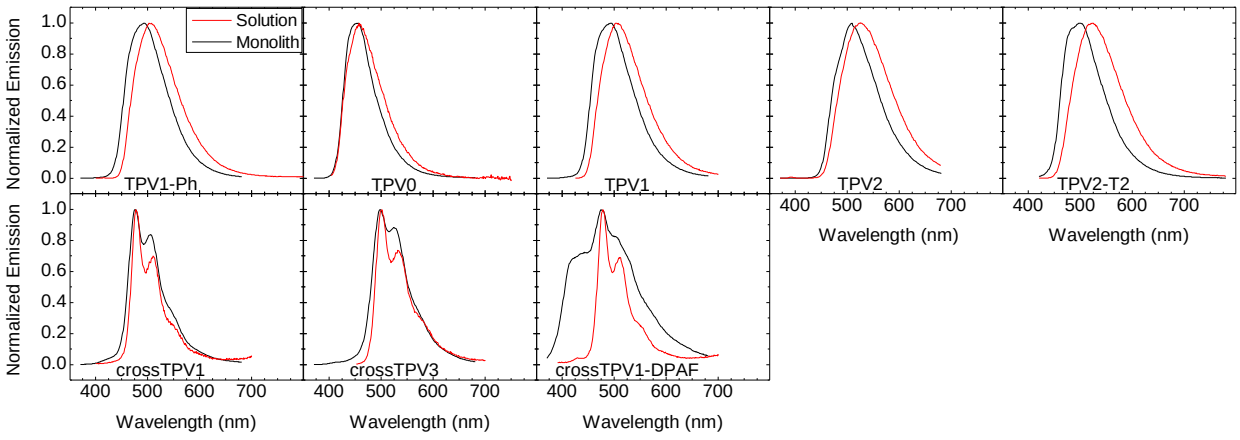

Figure 3-6. Photoluminescence spectra of the linear and cross-conjugated complexes in THF solution (red) and in PMMA monolith (black).

Nanosecond transient absorption was employed to probe the triplet state of the complexes in PMMA monolith and is shown in Figure 3-7. All monoliths displayed strong, broad triplet-triplet absorption similar to the measurements in THF. Transient absorption lifetimes could not be measured in the monoliths because they were longer than could be measured with the current instrumentation (>1 ms). The linear and cross-conjugated complexes in PMMA monolith exhibit a very slight red-shift, except for crossTPV1-DPAF which has a large blue-shift in the monolith transient absorption. This indicates a similar triplet-state in both THF solution and monolith for all complexes but crossTPV1-DPAF.

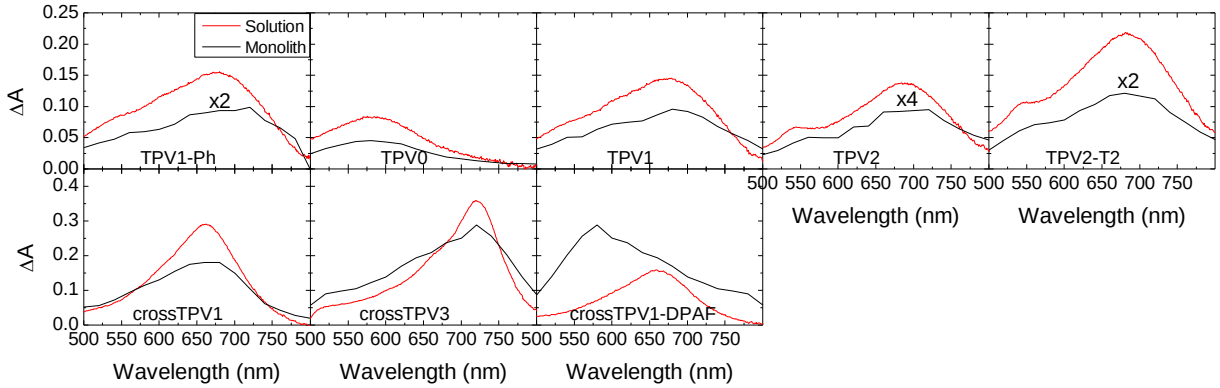

Figure 3-7. Nanosecond triplet-triplet absorption of the linear and cross-conjugated complexes in PMMA monolith (black) compared to the triplet-triplet absorption in THF solution reproduced from Figure 3-3 (red). Pulse energies were approximately 5 mJ/pulse for solution measurements and 800 μJ/pulse for monolith measurements with λ_{exc} = 355 nm.

A blue-shift in the transient absorption spectrum was also observed for two other well-known nonlinear absorbing platinum acetylides, Pt-BTF (benzothiazolfluorene) and Pt-DPAF, after incorporation into PMMA glass monoliths. This effect is probably due to the donor-π-donor or acceptor-π-acceptor structure of the chromophore in the polar PMMA matrix.

Monolith nonlinear absorption properties were measured using the non-linear transmission method for 2PA and open-aperture z-scan method for nonlinear absorption. A summary of their nonlinear photophysical properties, monolith thickness, and calculated concentration can be found in Table 3-2. Monolith thickness was measured with high precision calipers, and the concentration was calculated as described in the experimental section.

Table 3-2. Monolith concentrations and thicknesses and their nonlinear photophysical properties.

Monolith	Thickness (mm)	Calculated Chromophore Concentration (mM)	%Transmission at z=0 from Z-scan	2PA Cross Section at 680 nm (GM)
TPV1-Ph	1.01	2.0	75.9	---[c]
TPV0	2.61	2.8	47.3	---[c]
TPV1	0.99	2.0	59.8	1197[a], 1186[b]
TPV2	1.04	2.8	54.0	---[c]
TPV2-T2	2.40	1.2	56.0	---[c]
crossTPV1	1.02	1.8	61.4	342[a], 285[b]
crossTPV3	1.02	1.9	60.7	1334[a], 1107[b]
crossTPV1-DPAF	2.09	1.7	71.9	---[c]

[a]2PA cross section measured in THF by the NLT method.
[b]2PA cross section measured in PMMA monolith by the NLT method.
[C]2PA was not measured for these monoliths.

Femtosecond 2PA of PMMA monoliths was measured by Dr. Rebane's group at Montana State University using the NLT method with high accuracy. The 2PA cross-sections and values for TPV1, crossTPV1, and crossTPV3 monoliths were measured and compared to the 2PA properties in THF solution (Figure 3-8). The absolute 2PA cross-section values were calculated using the monolith concentrations listed in Table 3-2. The solid-state measurements are very consistent with the 2PA previously

measured in THF solution. In the blue-wavelength region, the 2PA is higher for crossTPV1 and crossTPV3 monoliths compared to the 2PA in THF. This indicates that in the PMMA monoliths more excited state absorption is present, probably due to slower vibrational relaxation in the solid state.

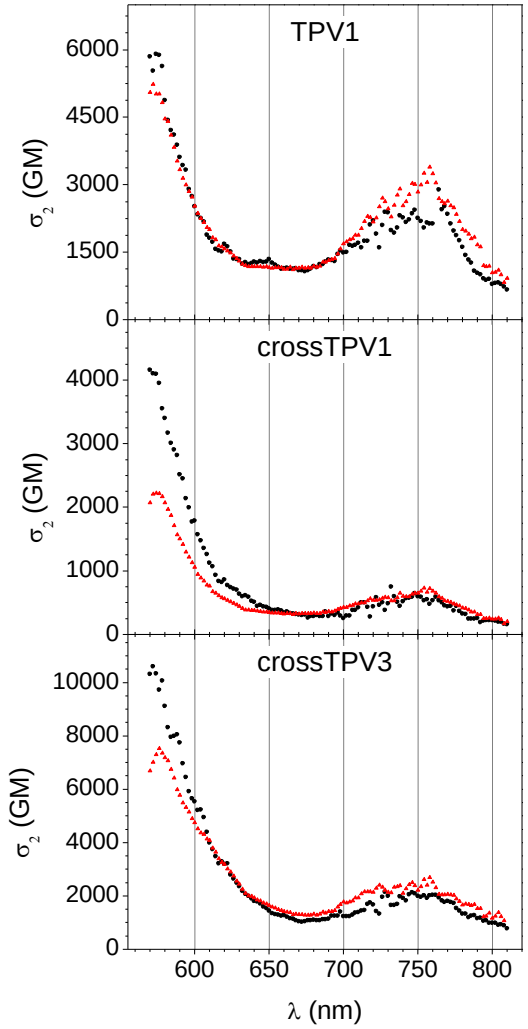

Figure 3-8. Femtosecond 2PA of TPV1, crossTPV1, and crossTPV3 in THF solution (red) and in PMMA monolith (black) acquired by Dr. Rebane's research group at Montana State University by the NLT method.

The dual-mode property of nonlinear absorption is retained in the solid state. The nanosecond open-aperture Z-scan method was used to measure the nonlinear

absorption response to 680 nm laser pulses (Figure 3-9). All PMMA monoliths show strong nonlinear absorption. The monolith thicknesses and concentrations were not matched, so only qualitative information can be obtained from the Z-scan results. In general, similar to the solution z-scan results, the nonlinear absorption increased with increasing length of the conjugated chain, and the linear complexes seemed to have a stronger nonlinear response than the cross-conjugated complexes in PMMA monoliths.

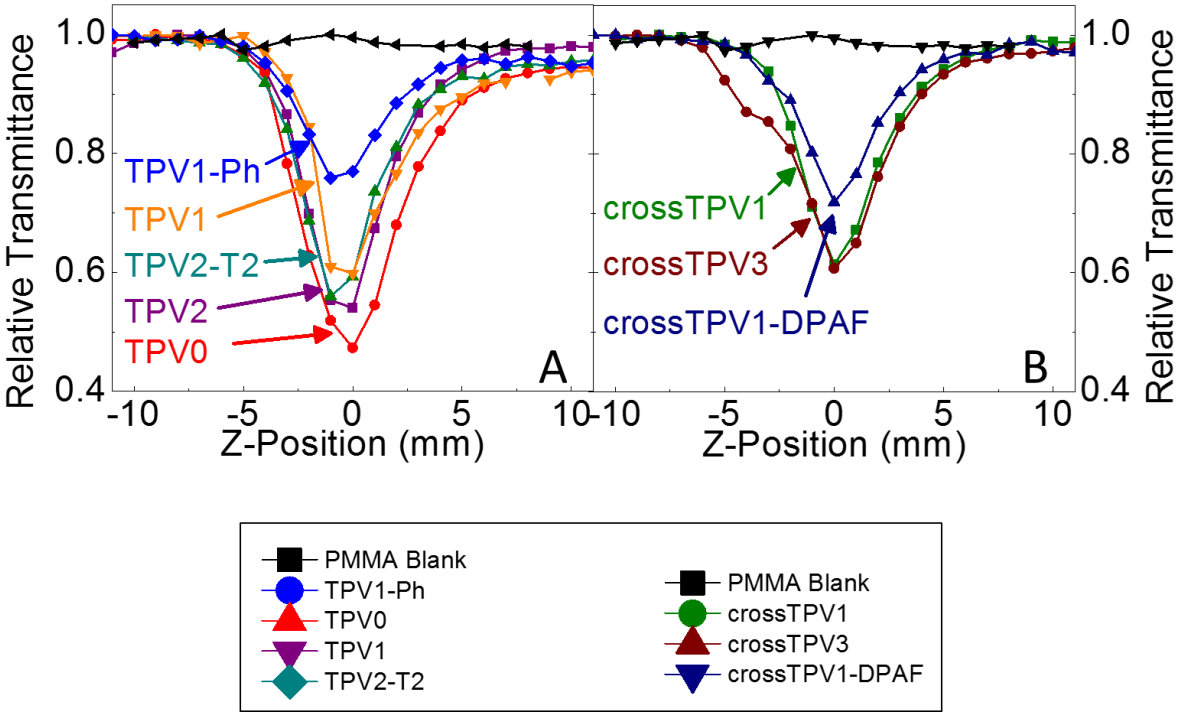

Figure 3-9. Open-aperture Z-scan response to 680 nm nanosecond pulses for the linear (A) and cross-conjugated (B) complexes in PMMA monoliths. A blank PMMA monolith was included as a reference (black). Pulse energies were approximately 700 μJ/pulse.

When the z-scan results for TPV1-Ph, TPV1 and TPV2 are compared, the NLA increases with increasing conjugation of the OPV unit, which supports the trend seen in the solution measurements. The TPV0 monolith has more than double the thickness of the other monoliths, so it displays a surprisingly strong z-scan response. However the

effect of monolith thickness vs. concentration on the nonlinear absorption property measured by the open-aperture z-scan method cannot be elucidated from these results.

Quantitative Analysis of Nonlinear Absorption in Solution and Monolith

In Chapter 1, the calculation of an effective nonlinear absorption coefficient, β_{eff}, was introduced. A β_{eff} can be calculated for each solution and monolith sample by using equation 1-22 and using the transmittance of the sample at z=0 in the open-aperture z-scan data shown in Figures 3-5 and 3-9. The value β_{eff} is a macroscopic quantity that depends on the concentration of chromophore in the material. Because the chromophores in solution and in PMMA monolith do not have the same concentration their β_{eff} values cannot be directly compared. Instead, an effective molecular nonlinear absorption cross-section, σ_2', can also be defined to compare the nonlinear absorption between materials with different chromophore concentrations.[40]

$$\sigma_2' = \frac{\beta_{eff}}{N_A d_0 x 10^{-3}} \qquad (3\text{-}1)$$

The constant, N_A, is Avogadro's number and d_0 is the molar concentration of absorbing molecules in M. The units of σ_2' are cm^4/GW.

The effective nonlinear absorption coefficients and cross-sections for the linear and cross-conjugated platinum(II) acetylide chromophores are listed in Table 3-3. For the calculation, the following values were used. The solution z-scan measurements were performed with 1 mM solutions in 1 mm pathlength cuvette. For the monoliths, the concentrations and pathlengths (monolith thickness) used in the calculations are those listed in Table 3-2. Intensities were calculated based on the laser pulse energies of each experiment: 800 μJ/pulse for solution measurements and 700 μJ/pulse for monoliths.

Overall, there is good agreement between the effective cross section values, σ_2', for each chromophore calculated from the solution and monolith open-aperture z-scan measurements. Discrepancies, which are largest in the case of TPV2-T2, crossTPV1, and crossTPV1-DPAF, may be due to inaccuracy in the measurement of the concentration of the monoliths. The monolith concentrations were estimated based on weight loss when they are polymerized and cured in an oven for 6 days. The assumption is that the weight loss is only due to evaporation of the monomer, methyl methacrylate. There could be some leaking or splashing of the solution out of the Teflon mold which would result in a lower actual concentration than was estimated. Additionally, if the monolith is not truly homogeneous and it is cut and polished, the final calculated concentration will not be very accurate leading to error in the effective nonlinear absorption cross section values.

Table 3-3. Effective nonlinear absorption coefficients, β_{eff}, and effective nonlinear absorption cross-sections, σ_2', for the linear and cross-conjugated platinum acetylides in THF solution and in PMMA monolith.

Compound	β_{eff} (cm/GW) Solution	β_{eff} (cm/GW) PMMA Monolith	σ_2' (10^{-19} cm^4/GW) Solution	σ_2' (10^{-19} cm^4/GW) PMMA Monolith
TPV1-Ph	0.21	0.64	3.5	5.3
TPV0	0.20	0.92	3.4	5.9
TPV1	0.65	1.5	11	12
TPV2[a]	N/A	1.8	N/A	10
TPV2-T2	0.89	0.7	15	4.9
crossTPV1	0.36	1.3	6.0	12
crossTPV3	0.65	1.4	11	12
crossTPV1-DPAF	0.35	0.40	5.8	3.4

[a]Open-aperture Z-scan for TPV2 was not measured in solution.

Using these effective nonlinear absorption cross-section values, the trend seen in the solution z-scan measurements of increasing nonlinear absorption with longer OPV conjugation length is now observed for the monolith measurements of the linear series; however there is no difference in the σ_2' values of the cross-conjugated containing monoliths between crossTPV1 and crossTPV3. Inconsistencies are likely due to error in determining the concentration of chromophore in the monoliths. Overall, this method of calculating a quantitative measure of the nonlinear absorption of chromophores may be a promising way to compare nonlinear absorption properties in solution and solid-state materials. Through future work on OPL materials, more accurate methods of controlling and determining the chromophore concentration in polymer glasses will be devised. Also, this effective nonlinear absorption coefficient and cross-section will be used for other studies, and its usefulness in comparing the nonlinear absorption of chromophores under various conditions will be realized.

Triplet-Triplet Annihilation Studies of Platinum Acetylide Polymers

When a high concentration of triplet excitons is produced and the diffusion of triplet excitons along a polymer chain is very efficient, triplet-triplet annihilation may occur. Triplet-triplet annihilation (TTA) is the deactivation of two triplet excitons into an excited singlet state and a ground state as shown in Equation 3-2. The observation of delayed fluorescence can often be observed from S_1^*.

$$^3T + {}^3T \rightarrow {}^1S^* \tag{3-2}$$

The triplet state plays an important role in platinum acetylide photophysics due to the high yield of intersystem crossing caused by the presence of the heavy platinum atom. Thus, the study of triplet dynamics in these systems is very important. Triplet-triplet

annihilation effectively places a limit on the concentration of triplets that can be present in a conjugated system.

In the study presented here, the effect of triplet-triplet annihilation in conjugated platinum acetylide polymers versus their model molecular complexes is examined by nanosecond transient absorption spectroscopy. The model complexes, crossTPV1 and crossTPV3, contain two cross-conjugated axes where two platinum acetylides are attached to a center phenyl unit of oligo-phenylene vinylene (OPV) with either one or three OPV units between terminal triphenylamine groups in the OPV axis. The copolymers, co-crossTPV1-P and co-crossTPV3-P contain alternating platinum acetylides of an OPV unit and a phenyl ring with long alkyl side-chains to increase solubility. The structures of crossTPV1, crossTPV3, co-crossTPV1-P, and co-crossTPV3-P are shown in Figure 3-10.

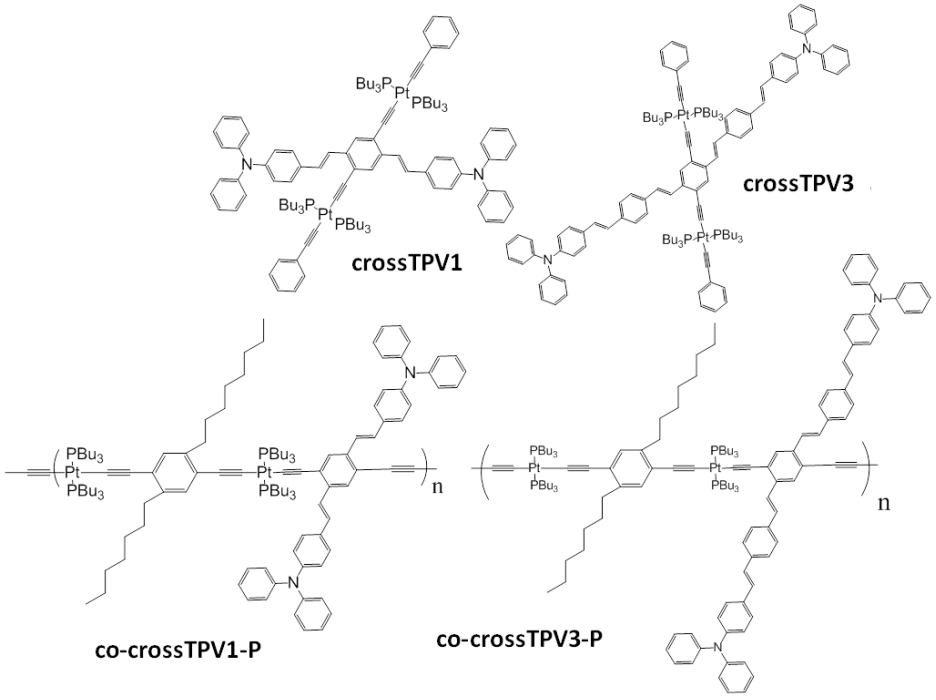

Figure 3-10. Structures and acronyms for the cross-conjugated platinum(II) acetylide *p*-phenylene vinylene model complexes and copolymers synthesized by Galyna Dubinina.

The photophysical properties of the copolymers in comparison to the model complexes were investigated in THF solution. The absorption and emission spectra are shown in Figure 3-11. CrossTPV3 and co-crossTPV3-P, containing the longer OPV unit, are both red-shifted compared to crossTPV1 and co-crossTPV1-P. Both polymers have very pronounced peak around 360 nm due to the conjugation of the polymer along the organometallic platinum acetylide axis. The emission spectra of the polymers are identical to the spectra of the model complexes, indicating that the S1 state is dominated by the OPV chromophore. No phosphorescence from the polymers or model complexes was observed.

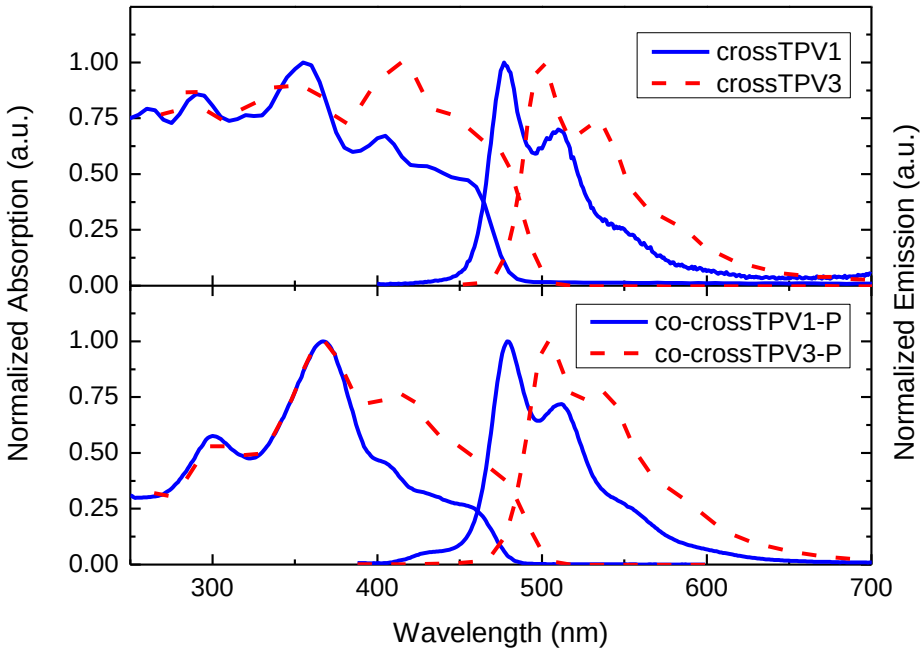

Figure 3-11. Normalized absorption and emission spectra for the model complexes (top) and the copolymers (bottom) in THF solution.

Nanosecond transient absorption was carried out to examine the triplet excited state properties of the complexes and copolymers. Transient absorption spectra are

shown in Figure 3-12. Samples were prepared at matched optical densities at 355 nm in THF. The triplet-triplet absorption spectra of the copolymers is very similar to the spectra of the model complexes, indicating that the triplet state is localized on the OPV chromophore axis with little involvement of the platinum acetylide polymer backbone. Interestingly, the transient absorption intensity of the copolymers is less than half that of the model complexes crossTPV1 and crossTPV3. At matched optical densities and with similar fluorescence quantum yields (1% for crossTPV1 and co-crossTPV1-P, 4% for crossTPV3-P and co-crossTPV3-P), it is expected the triplet yield should be the same between each copolymer and model complex pair. One possibility for marked decrease of triplet state concentration in a conjugated polymer is triplet-triplet annihilation.

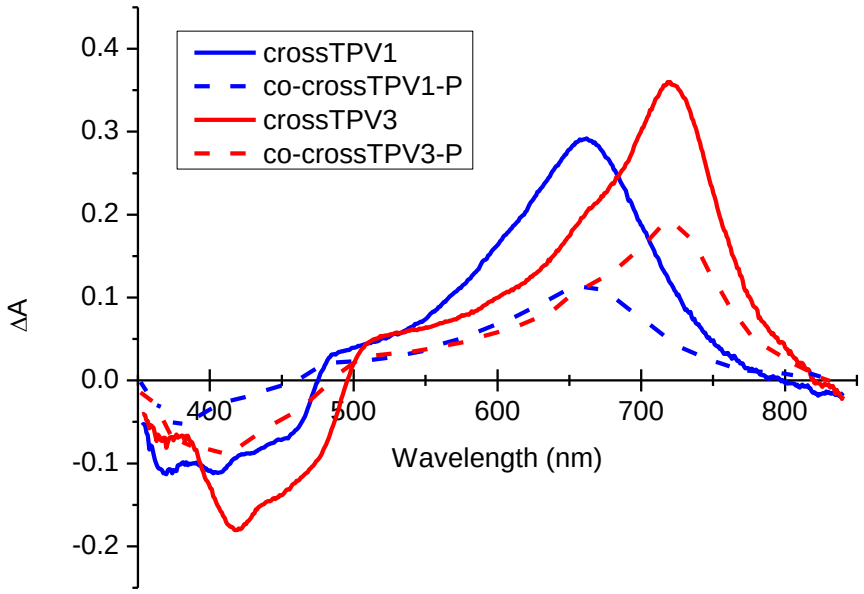

Figure 3-12. Nanosecond transient absorption spectra for the model complexes (red) and the copolymers (blue) in THF solution prepared to OD at 355 nm of 0.57 with λ_{exc} = 355 nm, 5 mJ/pulse (initial camera delay 50 ns, 100 averages).

To confirm the presence of triplet-triplet annihilation in the copolymer solutions, the intensity of the transient absorption at λ_{max} was monitored with increasing laser fluence and is shown in Figure 3-13. The transient absorption of the copolymers saturated with lower laser fluence compared to the monomeric complexes which supports the presence of triplet-triplet annihilation. The model complex and copolymer should share similar triplet molar extinction values since the triplet exciton is localized on the OPV axis as seen by the matching triplet-triplet absorption spectra. So in the absence of other effects like triplet-triplet annihilation, the slope of ΔA versus laser fluence should be the same. Most noticeably for crossTPV3 and co-crossTPV3, it appears that the slopes are indeed similar at very low range (0-1 mJ/cm^2). This effect is not as obvious in crossTPV1 and the corresponding copolymer, due to weaker TA intensity.

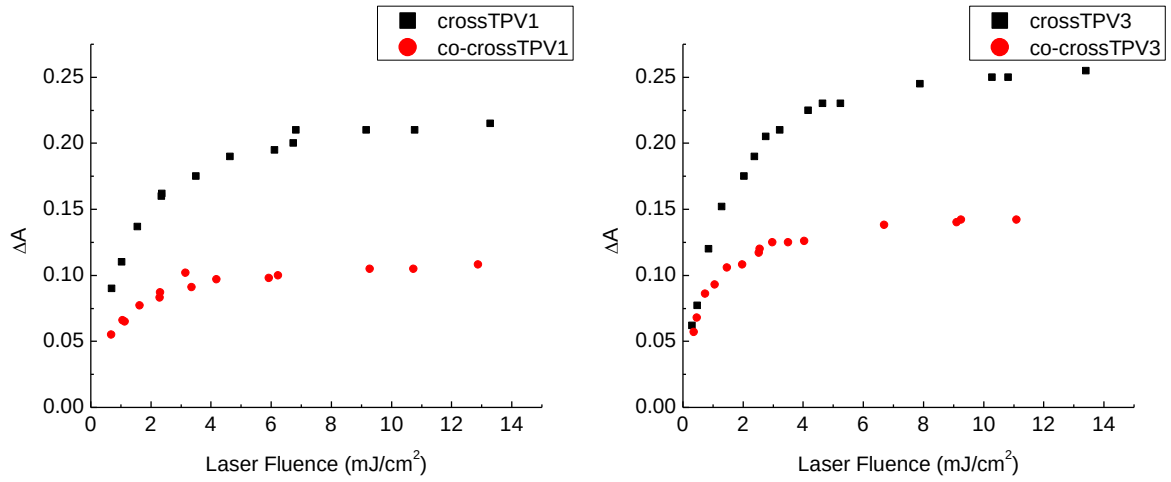

Figure 3-13. Nanosecond transient absorption intensity ΔA at TA_{max} vs. laser fluence for the copolymers and model complexes in THF prepared to an OD at 355 nm of 0.78 (λ_{exc} = 355 nm, 128 averages, detection at λ_{TAmax}).

Additional experiments were performed on crossTPV1 and co-crossTPV1-P to monitor the triplet decay kinetics. Transient decays collected at short timescales (0-200

ns) at λ = TA_{max}, at increasing laser fluence are shown in Figure 3-14. CrossTPV1 shows no fast decay in the timescale monitored, while a very fast initial decay in co-crossTPV1-P appears at higher laser fluences. At low laser fluence (<0.8 mJ/cm^2), no fast decay is observed in the copolymer sample. The amplitude of the fast decay increases with increasing laser fluence which is proportional to the number of triplets present. This supports the presence of triplet-triplet annihilation.

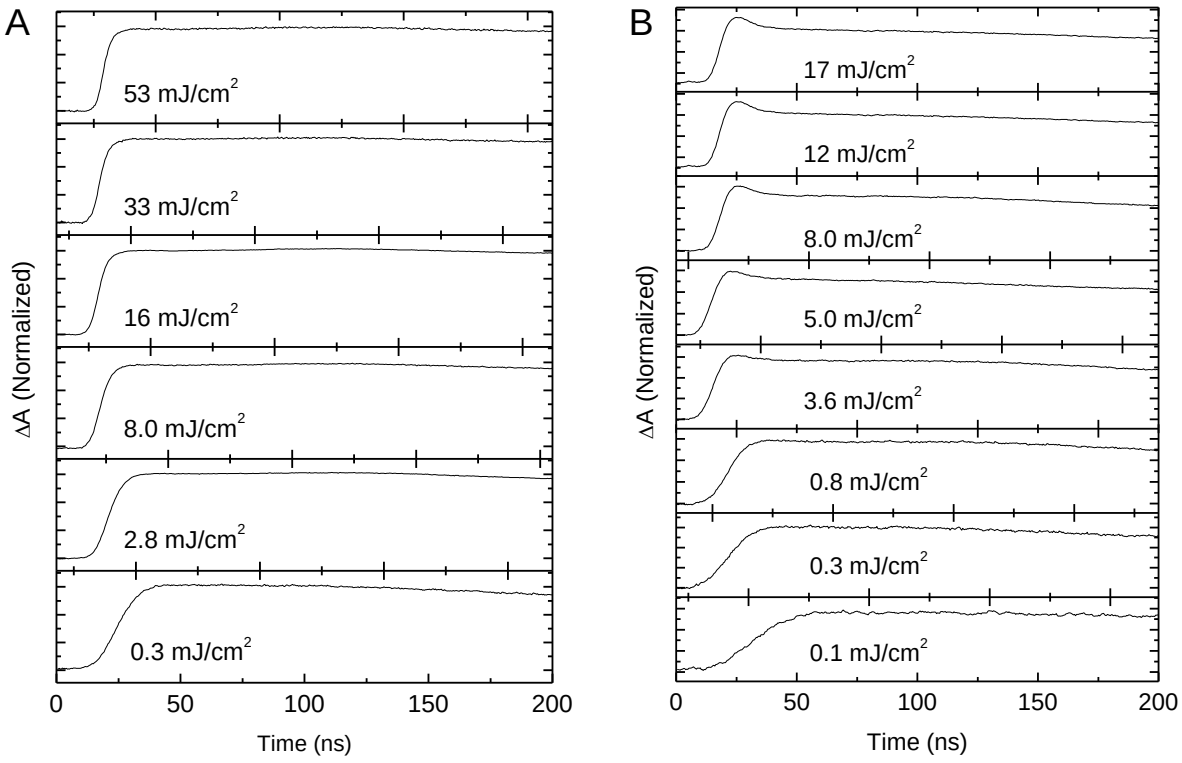

Figure 3-14. Transient decays of crossTPV1 (A) and co-crossTPV1-P (B) in THF at TA_{max} with increasing laser fluence (λ_{exc} = 355 nm, 128 averages, solutions prepared to an OD at 355 nm of 0.78).

While the observation of triplet-triplet annihilation has interesting implications for applications involving the triplet state of platinum acetylide polymers, due to the limited time resolution of our nanosecond instrumentation at such short timescales, the triplet kinetic analysis described here is preliminary. Further in-depth studies will be performed with collaboration with Dr. John Papanikolas and his group at the University

of North Carolina at Chapel Hill. They have femtosecond transient absorption capabilities to more closely study early time-scale dynamics of the triplet state after intersystem crossing. It is hoped that this collaboration with provide a better understanding of the triplet dynamics in polymers with high intersystem crossing yield and efficient exciton diffusion when high concentrations of triplet excited states are produced.

Summary of Results

A series of linear and cross-conjugated phenylene vinylene platinum acetylide complexes with terminal triphenylamine groups were incorporated into PMMA glass monoliths for solid-state study of their one-photon and two-photon photophysical properties with a focus on their application to optical power limiting materials by dual-mechanism nonlinear absorption. All the properties important to nonlinear absorption are retained in the solid state with increased photostability by the polymer host. Absolute two-photon absorption cross-section values measured by NLT method are similar for the complexes in solution and in the monoliths. Open-aperture Z-scan measurement also shows that strong nonlinear absorption is preserved. Alongside the design of increasingly efficient NLA chromophores, future endeavors are focused on improved methods of achieving solid state OPL materials with a focus on greater stability, higher concentrations of incorporated chromophores, and more effective optical power limiting.

The photophysical properties of copolymers consisting of alternating phenylene and cross-conjugated platinum acetylide units were investigated. In the transient decays of copolymers, a significant decrease in TA intensity was observed which indicated that triplet-triplet annihilation may be present. The transient decays of the

copolymer had a fast component in the decay which exhibited increasing amplitude with higher laser fluence, which confirmed the presence of triplet-triplet annihilation. The monomer complexes did not show evidence for triplet-triplet annihilation. Further investigations using femtosecond transient absorption are in progress with a collaboration with Dr. Papanikolas and his group at the University of North Carolina at Chapel Hill.

Experimental Section

Preparation of Monoliths. The synthesis of the linear and cross-conjugated complexes in Scheme 1 have been reported previously.[82,83] PMMA monoliths were prepared by a procedure adapted from Westlund and coworkers.[73] The platinum(II) acetylide chromophores (initial concentration 1 mM) and 6 mg of azoisobutyronitrile (AIBN) were dissolved in 1.1 mL of inhibitor-free methyl methacrylate (MMA). The solution was poured into a 0.5" circular Teflon mold and placed in an oven to polymerize at 50°C for 3 days, then at 80°C for 3 days. Some of the initial PMMA monoliths showed a darkening of the top surface of the monolith indicative of decomposition of the chromophore, so the procedure was modified with a gentle nitrogen flow into the oven to reduce oxygen-sensitized degradation. All monoliths prepared under N_2 appeared homogeneous with no evidence of degradation and were highly transparent (Figure 1). Some gas bubbles were trapped near the edges of the monoliths; however, they did not obstruct the photophysical measurements. Trapped bubbles did not occur in the monoliths prepared without N_2 flow.

The monoliths were cut to about 1 mm thickness using a thin rotary blade (Dremel Tools) and polished by hand using fine grit sandpaper placed on a flat surface for photophysical measurement. Different concentrations of chromophore were

attempted, but monoliths containing higher initial concentrations (>2 mM) of chromophore were not transparent due to phase separation. Monolith solutions were prepared to 1 mM initial concentration before polymerization. Final calculated concentrations of the polymerized monoliths were approximated by using the density of PMMA (1.2 g/mL) and the final weights after polymerization. Weight loss due to the evaporation of MMA in the monoliths was inconsistent due to uncontrolled flow of N_2 into the oven. It is assumed that the monoliths are homogenous and that cutting and polishing the monoliths do not change their concentration. Table 3-2 lists the final thickness and calculated concentration of each monolith.

Photophysical Measurements. One-photon photophysical properties for solutions were measured using a 1-cm pathlength quartz or borosilicate cuvette in spectroscopic grade, dry THF. Solutions were deoxygenated by purging with argon for phosphorescence and transient absorption measurements. Ground state absorption spectra were collected on a Varian Cary 100 dual-beam spectrophotometer with THF as the instrument baseline blank. Corrected steady-state emission measurements were collected by a Photon Technology International (PTI) photon counting fluorescence spectrophotometer with optically dilute solutions, $OD_{max} < 0.10$. Fluorescence quantum yields were measured at room temperature in air-saturated THF using 9,10-diphenylanthracene in cyclohexane as a standard ($\Phi_{fl} = 0.75$).[77] Nanosecond triplet-triplet transient absorption was measured in a continuously circulating 1-cm pathlength borosilicate cuvette in argon-purged THF solutions. The third harmonic of a Continuum Surelite II-10 Nd:YAG laser at 355 nm (10 mJ/pulse) was used as the pump and a Perkin-Elmer LS1130-3 pulsed xenon lamp was used as the probe source. The

transient absorption signal was detected with a gated-intensified CCD mounted on a 0.18 M spectrograph (Princeton PI-Max/Acton Pro 180) after an initial camera delay of 50 ns. Samples were prepared to an optical density of 0.4 at the excitation wavelength. Triplet lifetimes were calculated with a single-exponential global fitting of the transient absorption decay data using SpecFit analysis software. Triplet molar extinction coefficients were determined by relative actinometry using benzophenone (Φ_T = 1.00, ε_T = 7870 L mol^{-1} cm^{-1})[78,79] as the actinometer.

Monolith photophysics were measured freestanding, open to atmosphere without a cuvette. Absorption spectra were not obtained due to saturated OD. Emission spectra were obtained by a front-face alignment on a Spex Fluorolog 3 spectrophotometer. Transient absorption measurements on monoliths cut to a thickness of approximately 1 mm were made using an in-house designed TA instrument dedicated to solid-state measurements. The third harmonic of a Continuum Surelite I-10 Nd:YAG laser at 355 nm (600 μJ/pulse) was used as the pump beam in an antiparallel alignment to the probe beam provided by a 250 W QTH lamp (Newport). Single-wavelength transient absorption decays were acquired as an average of 128 shots every 25 nm using a Hamamatsu R928 PMT and an in-house modified base using 5 of the 9 stages for amplification. The transient absorption spectrum was acquired by using a custom Matlab program to convert the transient absorption decays at each wavelength to a transient absorption spectrum at t=0. The transient absorption of the monoliths did not fully decay to the baseline in the timescale of the instrument (2 ms) so transient absorption lifetime data could not be obtained.

Fluorescence lifetimes for both THF solutions and monoliths were obtained by time-correlated single photon counting technique (TCSPC) with a PicoQuant FluoTime 100 compact fluorescence lifetime spectrophotometer. A UV-pulsed diode laser provided excitation at 375 nm (power < 10 mW). The laser was pulsed by a PDL800-B pulsed diode laser driver. Fluorescence decays were obtained for at least five wavelengths across the emission spectrum using 10 nm bandpass interference filters for solution measurements in air-saturated THF and analyzed by a global fit as average amplitude-weighted from the fluorescence decays using biexponential fitting parameters (FluoFit software). For monolith fluorescence lifetime measurements, the monoliths were placed at 45° in the sample holder with respect to the incoming laser beam. Fluorescence lifetimes were acquired and fit at one wavelength for comparison to solution measurements.

Nonlinear transmission measurements were performed via an open-aperture z-scan apparatus. The excitation wavelength, 680 nm, was generated by a Continuum Surelite OPO Plus pumped with the third harmonic (355 nm) of a Continuum Surelite II-10 Nd:YAG laser. The laser beam was split with a 50:50 beam splitter to two pyroelectric detectors, which measured the transmitted pulse energy through the sample as a function of the input pulse energy using an Ophir Laserstar dual-channel optical laser energy meter. The beam was focused with a 25.4 mm diameter, 50.8 mm focal length concave lens. A ThorLabs motorized translation stage (Z825B and TDC001) allowed millimeter movement along the z-axis. Solution samples were prepared with dry-THF to a concentration of 1 mM and put into a 1-mm pathlength quartz cuvette for analysis. A sample of Pt-DPAF was used as a reference standard for

comparison between different runs. Monolith samples cut to approximately 1-mm thickness were placed between two glass slides with a few drops of refractive index matching fluid on each side of the monolith (Newport F-IMF-105, 1.52 at 589 nm).

The femtosecond 2PA measurements were performed using collimated-beam nonlinear transmission (CB-NLT) technique by Dr. Aleks Rebane and his group at the Montana State University. A detailed description of the laser system is described elsewhere.[84] Briefly, the laser system comprised of a Ti:Sapphire femtosecond oscillator (Lighthouse Inc.), femtosecond regenerative amplifier (Legend H, Coherent Inc.), and an optical parametric amplifier, OPA (TOPAS-C, Light Conversion). The second harmonic of the signal output of the OPA was continuously tunable from 540 to 810 nm with the maximum pulse energy, 10-200 μJ. The maximum average pulse duration was 80-120 fs (fwhm). The OPA output beam was slightly expanded and then collimated with long focal length lenses (f = 500 – 1000 mm) to give an average beam diameter on the sample, d = 0.3- 1.0 mm. Minimum beam diameter was chosen to eliminate spurious nonlinear effects such as self-focusing, which may occur in the sample and in the optical elements at high photon flux density values. The pulse energy incident at the sample was changed by means of a continuously-variable reflective circular attenuator (Thorlabs, maximum OD = 2.0). Nonlinear transmittance of the sample as a function of the incident pulse energy was determined by measuring the relative pulse energy before and after the sample with two silicon photodiodes (Thorlabs, PDA10A). The measured nonlinear transmittance at each wavelength was fitted with a linear function. The 2PA cross sections at each wavelength were determined by comparing the CB-NLT slope values in the sample with those obtained in 1 cm path length solution of 2PA

reference standards under same experimental conditions. Rhodamine B solution in methanol., fluorescein solution in water and bis-diphenylanimostilbene solution in dichloromethane were used as reference standards.[84]

Triplet Molar Extinction Determination by Relative Actinometry

Triplet absorption properties are generally difficult to characterize due to the transient nature of the triplet excited state. The triplet absorption spectrum is relatively easy to measure in regions where little to no ground state absorption exists; however if strong ground state absorption is present, the triplet absorption can usually not be detected. Particularly difficult to measure is the quantity of the molar triplet extinction coefficient. The molar triplet extinction coefficient, ε_T (M^{-1} cm^{-1}), is a quantitative measure of the amount of light absorbed by the triplet excited state, T_1, of a molecule and depends on the concentration of T_1 (c) and the absorbance of T_1 (A) along a given optical pathlength (l) as shown in Equation (3-3).

$$\varepsilon_T = \frac{A}{c\,l} \tag{3-3}$$

The absorbance is calculated experimentally from the transmittance of light through a sample as in Equation (3-4), where T_0 and T are the transmitted light through the sample in the absence and presence, respectively, of the transient species.

$$A = \log_{10}\frac{T_0}{T} \tag{3-4}$$

Some considerations of any experiment to calculate the triplet extinction coefficient should be taken into account.[85] First, the beam used for analyzing the absorbance of the sample should not suffer from reflection or scattering, such that the beam is only transmitted or absorbed. Also, the measured transmittance should only be due to the transmitted beam and not to other light sources such as emission from the

sample. This is relatively easy to control with good optical design of the beam path and sample conditions. Second, the instrumental parameters of the experiment should be well characterized, with a linear response curve of detected transmittance and a temporal response that is substantially shorter than the decay time of the triplet excited state. Most importantly, care must be taken to ensure the analyzed volume of the sample has a homogenous distribution of the triplet excited state and perfectly overlaps the volume of the excitation used to produce the excited state. Ideal homogeneity of the sample and overlap of the excitation and analysis beams is difficult to manage due to many reasons; however most methods for calculating the triplet extinction coefficient allow correction factors for these experimental imperfections.

One method commonly used is the ground-state depletion method, where a two-species system is assumed, first used by Porter and Windsor in the 1950s during their study of triplet states of aromatic complexes by flash photolysis.[86-88] This method assumes that the ground state is converted into the triplet state T_1 by intersystem crossing after excitation to S_1 with a 100% yield. So there are no other ground state depletion pathways. The ground state is repopulated by decay of the triplet state. So the concentration of the triplet state can be calculated by Equation 3-5.

$$[T] = \Delta[G] = [G]_0 - [G] \tag{3-5}$$

At a wavelength, λ_1, where the ground state depletion can be monitored (the transient has no absorption) and within the transient's absorption band at another wavelength, λ_2, where there is no ground state absorption, the change in absorbance can be described by Equations 3-6 and 3-7, where l is the pathlength of the sample.

$$\Delta A(\lambda_1) = -\varepsilon_G(\lambda_1)[T]l \tag{3-6}$$

$$\Delta A(\lambda_2) = \varepsilon_T(\lambda_2)[T]l \quad (3\text{-}7)$$

Combining these two equations, the triplet molar extinction coefficient can be calculated by the following relation:

$$\varepsilon_T(\lambda_2) = \varepsilon_G(\lambda_1)\frac{\Delta A(\lambda_2)}{\Delta A(\lambda_1)} \quad (3\text{-}8)$$

The uncertainty in this method is determining a wavelength λ_1 where one can be certain there is no triplet-triplet absorption. Depending on the sample this can be difficult because there is often at least some overlap between the ground state absorption spectrum and the triplet-triplet absorption spectrum. Using this method, other reasons for ground state depletion, such as photodecomposition, can contribute significant error to the calculation of ε_T.

To calculate the molar triplet extinction coefficients of the series of linear and cross-conjugated *p*-phenylene vinylene platinum(II) acetylides (Figure 3-1), a different method was used called the relative actinometry method. Use of an actinometer, whose ε_T and Φ_{isc} are known, is an accurate way of determining the triplet molar extinction coefficients for unknown samples. The sample and actinometer solutions are prepared in benzene to matched optical density (OD_{355nm} = 0.78) at the excitation wavelength. At λ_{max} of their transient absorption, the ΔA intensity is measured at increasing laser fluence in a region where the response is linear and no nonlinear effects are observed. The laser fluence is increased while keeping the same beam quality by use of a variable beamsplitter. The slopes of ΔA vs. laser fluence for the sample and the actinometer are used to calculate the triplet molar extinction coefficient by Equation (3-9).

$$\varepsilon_{sample} = \frac{slope_{sample}\Phi_{ISCref}\varepsilon_{ref}}{slope_{ref}\Phi_{ISCsample}} \quad (3\text{-}9)$$

The actinometer used was benzophenone, which has a known triplet molar extinction coefficient $\varepsilon_{T,525\ nm}$ = 7870 ± 1200 M^{-1} cm^{-1} and triplet quantum yield Φ_{ISC} = 1.0.[78,79] Under the conditions used in this experiment benzophenone in benzene is linear for laser energies up to about 1 mJ/pulse (Figure 3-15).

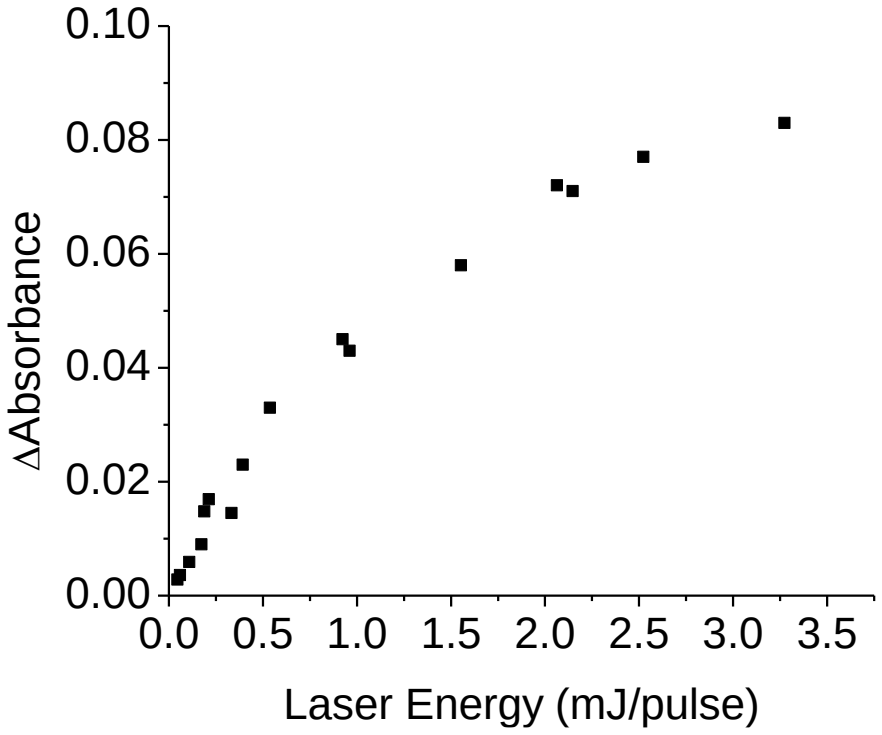

Figure 3-15. ΔAbsorbance vs. Laser Energy for the nanosecond transient absorption monitored at 525 nm for benzophenone in benzene (OD_{355nm} = 0.78).

To obtain $\Phi_{ISCsample,}$ the approximation that $\Phi_{ISCsample}$ is equal to one minus the fluorescence quantum yield, Φ_F, can be used. The singlet oxygen quantum yield, Φ_Δ, was used, but the singlet oxygen measurement typically has a higher degree of uncertainty due to the reactivity of the singlet oxygen produced and the sensitivity of some of the platinum acetylide complexes to singlet oxygen sensitized photodegradation. At higher laser energies, the ΔA response of the platinum acetylides

becomes nonlinear either due to saturation or self-quenching effects, and so lower laser energies were used for the platinum complexes (Figure 3-16).

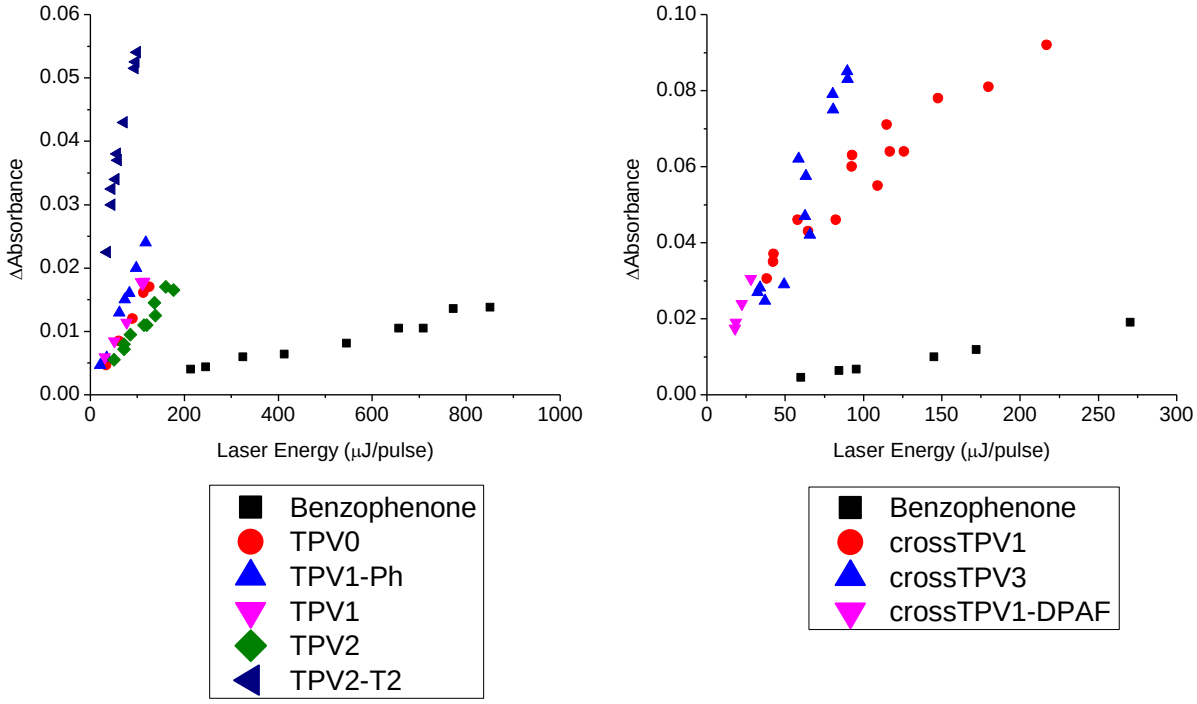

Figure 3-16. Relative actinometry plots of ΔAbsorbance vs. Laser Energy (μJ/pulse) for the linear (TPVn) and cross-conjugated (crossTPVn) series against benzophenone measured at $\lambda = \lambda_{TAmax}$. Solutions were prepared to an OD at 355 nm of 0.78 in benzene. The linear and cross-conjugated series relative actinometry experiments were performed on different days.

The triplet molar extinction coefficients calculated for both series in Table 3-4 demonstrate the strong triplet-triplet absorption present in these complexes. Pulse radiolysis studies on oligomeric *p*-phenylene vinylenes (OPVs) to measure the triplet state properties reported triplet molar extinction coefficients of 140,000 M^{-1} cm^{-1} to 190,000 M^{-1} cm^{-1} increasing with the length of the OPV chain (2 to 8 oligomeric units).[89] Benchmark platinum acetylide complexes which do not contain OPV units, Pt-BTF and

Pt-DPAF, have triplet molar extinction coefficients of 64,300 and 30,300 M^{-1} cm^{-1}, respectively.[67] The OPV ligands on the platinum significantly enhances the triplet molar extinction coefficient.

Table 3-4. Calculated values of the triplet molar extinction coefficients, εT, for the platinum(II) acetylides from the slope of the relative actinometry experiment and $\Phi_{ISC} = [1 - \Phi_F]$ according to Equation 2-7 above. The linear and cross-conjugated series were analyzed on different days in THF solutions prepared to OD_{355nm} of 0.77 and 0.79, respectively.

Compound	Slope (10^{-5})	Φ_F	ε_T (M^{-1} cm^{-1})	Compound	Slope (10^{-5})	Φ_F	ε_T (M^{-1} cm^{-1})
Benzophenone	1.6	---	7870[78,79]	Benzophenone	7.0	---	7870[78,79]
TPV0	13.7	0.10	74,000	crossTPV1	52.3	0.01	77,000
TPV1-Ph	20.2	0.46	180,000	crossTPV3	87.8	0.04	81,000
TPV1	15.9	0.30	110,000	crossTPV1-DPAF	105	0.005	118,000
TPV2	9.9	0.52	100,000				
TPV2-T2	58.3	0.28	390,000				

increasing with the length of the OPV chain (2 to 8 oligomeric units).[89] Benchmark platinum acetylide complexes which do not contain OPV units, Pt-BTF and Pt-DPAF, have triplet molar extinction coefficients of 64,300 and 30,300 M^{-1} cm^{-1}, respectively.[67] The OPV ligands on the platinum significantly enhances the triplet molar extinction coefficient.

CHAPTER 4
TRIPLET SENSITIZATION OF CONJUGATED POLYMERS BY Hg3

Introduction

Conjugated polymers such as MEH-PPV (poly(2-methoxy,5-(2'-ethylhexyloxy)-1,4-phenylene vinylene)) are studied for a variety of organic electrooptical devices such as photovoltaic cells, light-emitting diodes, lasers, and thin-film transistors due to their exceptional charge-carrier transport, electroluminescent, and photoluminescent properties.[90-94] In addition to desirable photoluminescent properties, conjugated polymers can act as semiconductors due to the highly π-conjugated backbone along the polymer chain with delocalized π and π* orbitals which can act as valence and conduction bands which support charge carrier transport along the polymer chain. Compared to inorganic semiconductors, organic polymers can offer mechanical flexibility, optical transparency and easy processibility. Indeed, the field of organic/plastic electronics has such vastly impacted current technology that the study of π-conjugated polymers and their semiconductor properties earned Alan J. Heeger, Alan G. MacDiarmid, and Hideki Shirakawa the 2000 Nobel Prize in Chemistry. Furthering the technological applications of these polymer materials, there has been much attention on understanding the phenomena that control the photophysics and carrier transport such as conformation of the polymer chains,[95-99] interchain aggregation,[100-102] and intramolecular dynamics.[101,103,104]

Recently, some focus has shifted to the study of triplet states of small molecules and conjugated polymers for photoactive applications.[105] Triplet states, due to the spin-forbidden nature of intersystem crossing, have substantially longer lifetimes than singlet

states. Thus, triplet excitons may have a greater probability of travelling throughout the medium to the desired interface in a device where charge separation (for photovoltaic cells) or photoluminescence (for LEDs) can occur. The trade off to this longer lived excited state is that singlet excitons can travel long distance by Förster energy transfer, whereas triplet exciton diffusion is governed by Dexter exchange and is dependent on orbital overlap between neighboring chromophores.[17,106] The triplet excitons move along a polymer chain or efficiently π-stacked adjacent chains in a "hopping" motion according to a random walk pattern.[107-109]

Organometallic small molecules and polymers are actively being studied as materials for triplet solar cells.[110,111] Shao and Yang in 2005 reported a heterojunction solar cell device using PtOEP (platinum(II) octaethylporphyrin) as the donor with PCBM (phenyl-C61-butyric acid methyl ester) as the acceptor and found relatively high performance of the device with a triplet exciton diffusion length of 30 nm.[112] The Reynolds and Schanze groups in 2006 studied a phosphorescent platinum acetylide polymer and acceptor PCBM in a bulk-heterojunction solar cell and demonstrating for the first time that the involvement of the triplet-excited state in photoinduced charge separation leads to efficient charge generation.[113] Numerous organometallic polymers have been studied since then for triplet photovoltaic devices incorporating heavy metals such as Pt(II),[114,115] Ir(III),[116] Ru(II),[117,118] and others

In 2009, a group from University of Missouri reported a ladder-type poly(*para*-phenylene) polymer (LPPP) containing trace amounts of Pd impurity (less than 100 ppm), PhLPPP, that was used to study the effect of triplet excitons on power conversion efficiency in photovoltaic cells.[119] They compared LPPP:PCBM photovoltaic cells,

which contain the Pd impurity, to a MeLPPP, which does not contain any heavy-metal impurity. Remarkably, the cells made with PhLPPP:PCBM containing the heavy metal impurity had an external quantum efficiency (EQE) higher by a factor of 8 than that for the metal-free MeLPPP:PCBM in the blue region of the spectrum. Their work introduced the possibility of enhancing efficiency using the triplet state without complicated synthetic routes to introduce heavy metals into the backbone of the polymer itself.

These studies demonstrate that the triplet states of conjugated polymers have interesting implications for the performance of photovoltaic devices. The next step is to devise the best methods of introducing triplet excited states in conjugated materials. The results presented here involve the mixing of conjugated polymers with a planar mercury-containing complex in solution and films in order to investigate the effects on the photophysics by the presence of a heavy metal, mercury. It is postulated that a planar heavy metal complex may be able to coordinate with a highly conjugated, aromatic polymer backbone by π-π interaction to efficiently enhance intersystem crossing to the triplet state by spin-orbit coupling while simultaneously stabilizing the planarity of the polymer backbone to improve the charge transport ability.

Triplet Sensitization by Hg3

Trimeric perfluoro-*ortho*-phenylene mercury, “Hg3”, shown in Figure 4-1, is a colorless solid with no photoluminescence in room temperature solutions of CH_2Cl_2 and with intense orange photoluminescence in its crystalline form when irradiated by UV light. At low temperatures, 77 K, a very broad emission band with λ_{max} = 440 nm (exc = 355 nm) appears with a broad shoulder centered at 530 nm and extending past the

visible region of the spectrum, possibly due to the formation of tight dimers in its crystalline state.[120] Hg3, and similar organomercurial fluoroarenes, have been shown to complex with planar aromatic compounds such as benzene,[121,122] biphenyl,[120] naphthalene,[120] triphenylene,[120] and acetone,[123] among others,[124-126] forming compact alternating stacks in “sandwich”-type configurations due to the Hg-π interaction in the solid state. These interactions are likely electrostatic, as DFT calculations suggest the center of the trinuclear macrocycle of Hg3 has a positive electrostatic potential while the perimeter is negative.[127] Also the HOMO-LUMO gap for Hg3 is particularly high, 3.357 eV,[128] so orbital mixing between Hg3 and the organic aromatics is highly unlikely. Most importantly, in these studies, the Hg3/arene complexes exhibit phosphorescence from the T_1 state of the arene due to heavy atom effect from the proximity of the mercury atoms.[120,124,126]

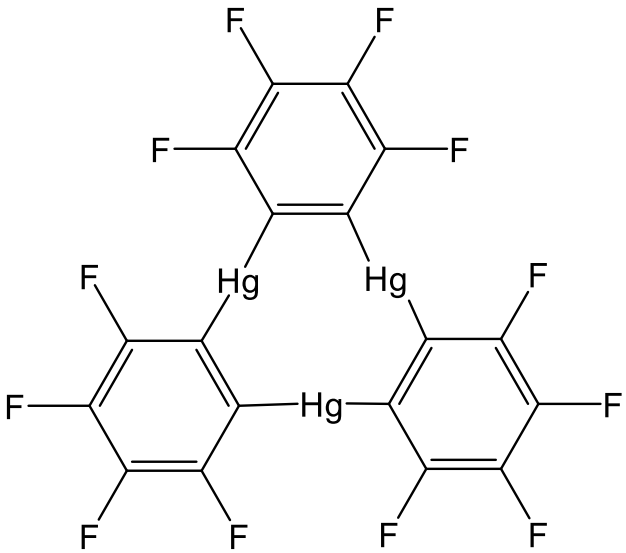

Figure 4-1. Structure of trimeric perfluoro-*ortho*-phenylmercury, “Hg3”.

Gabbai and his group at Texas A&M University have done extensive research on the supramolecular interactions between conjugated molecules and Hg3, along with

similar fluorinated organomercurials.[120,121,123-126] In 2008, they reported the supramolecular structure between Hg3 and tolane (diphenylacetylene) which is comprised of an alternating stacked configuration where mercury atoms interact with both the acetylenic and aromatic carbons on the tolane (Figure 4-2).[124] The tolane adopts a non-planar geometry with a dihedral angle between phenyl groups of 5.9°. It was mentioned that the interaction of Hg3 and tolane was heavily dependent on the presence of the solvent, CH_2Cl_2, as upon complete evaporation of the solvent to form crystals, decomposition of the supramolecular complex occurred. Thus no phosphorescence of the crystalline supramolecular structure could be observed.

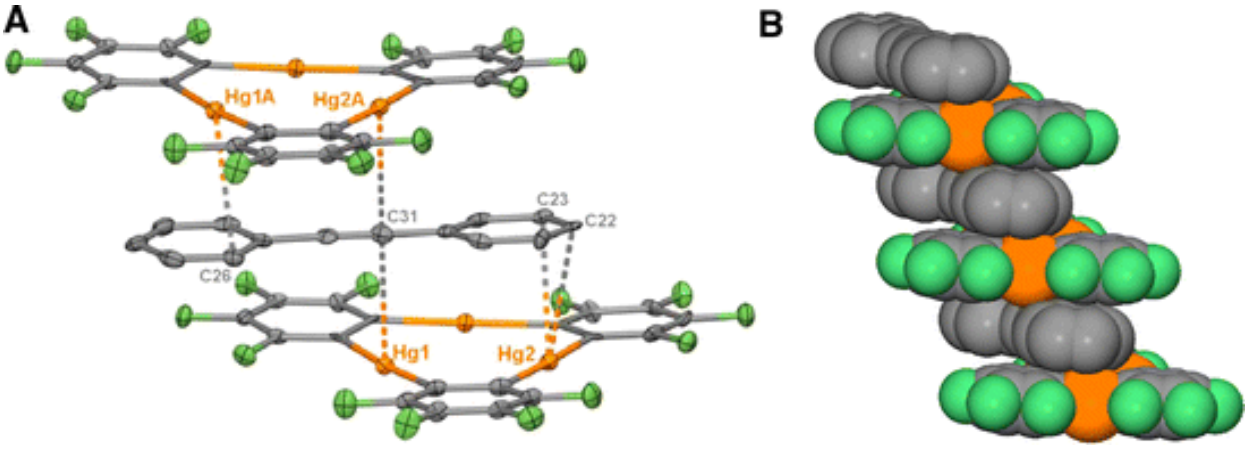

Figure 4-2. Crystal structure of Hg3 and tolane reported by Gabbai.[124] (a) ORTEP view (50% ellipsoids) of compound [3·tolane·CH2Cl2]. (b) Space filling model of the binary stack present in [3·tolane·CH2Cl2]. H atoms and solvate CH_2Cl_2 molecules omitted.

Conjugated Polymers and Hg3

MEH-PPV

MEH-PPV, poly[2-methoxy-5-(2-ethylhexyloxy)-1,4-phenylene vinylene], is one of the most well studied electroluminescent polymers. It and other poly(phenylene vinylene), PPV, analogs are commonly used in LED applications due to their excellent

luminescent properties.[93,94,129,130] These polymers have also been studied for use in photovoltaic devices with an acceptor like fullerene, for example, due to its charge transport properties and high absorption coefficient in the visible region of the spectrum.[131-133] MEH-PPV is an amorphous polymer, with a glass transition temperature of T_g = 65 °C.[134,135] The structure of MEH-PPV is shown in Figure 4-3 below.

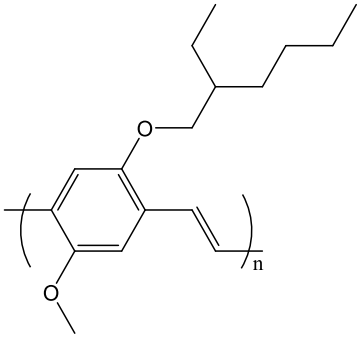

Figure 4-3. Structure of MEH-PPV.

Solution Photophysical Studies

The interaction between MEH-PPV and the trimeric mercury complex, Hg3, was found to be strongly solvent dependent as is shown in Figure 4-4. In a nonpolar aromatic solvent, such as benzene, the addition of Hg3 to MEH-PPV causes a visible color change of the solution after stirring for several minutes; however, in a polar chlorinated solvent such as o-dichlorobenzene or chloroform, the addition of Hg3 complex to the polymer MEH-PPV has no effect on the absorption spectrum, indicating no interaction between the Hg3 and the polymer. The solvent dependency of this interaction indicates that the interaction may be forced due to the insolubility of the Hg3 complex in benzene at room temperature. The Hg3 results in “solvation” into the polymer chains, ordering the polymer chains as seen in the absorption and emission

spectra. Furthermore, others have reported properties of a solid-state complex of benzene and Hg3 produced by dissolving Hg3 in boiling benzene and slow evaporation of the solvent,[122] so the interaction between the Hg3 and the polymer may also be mediated by pi-stacking of the solvent between polymer chains.

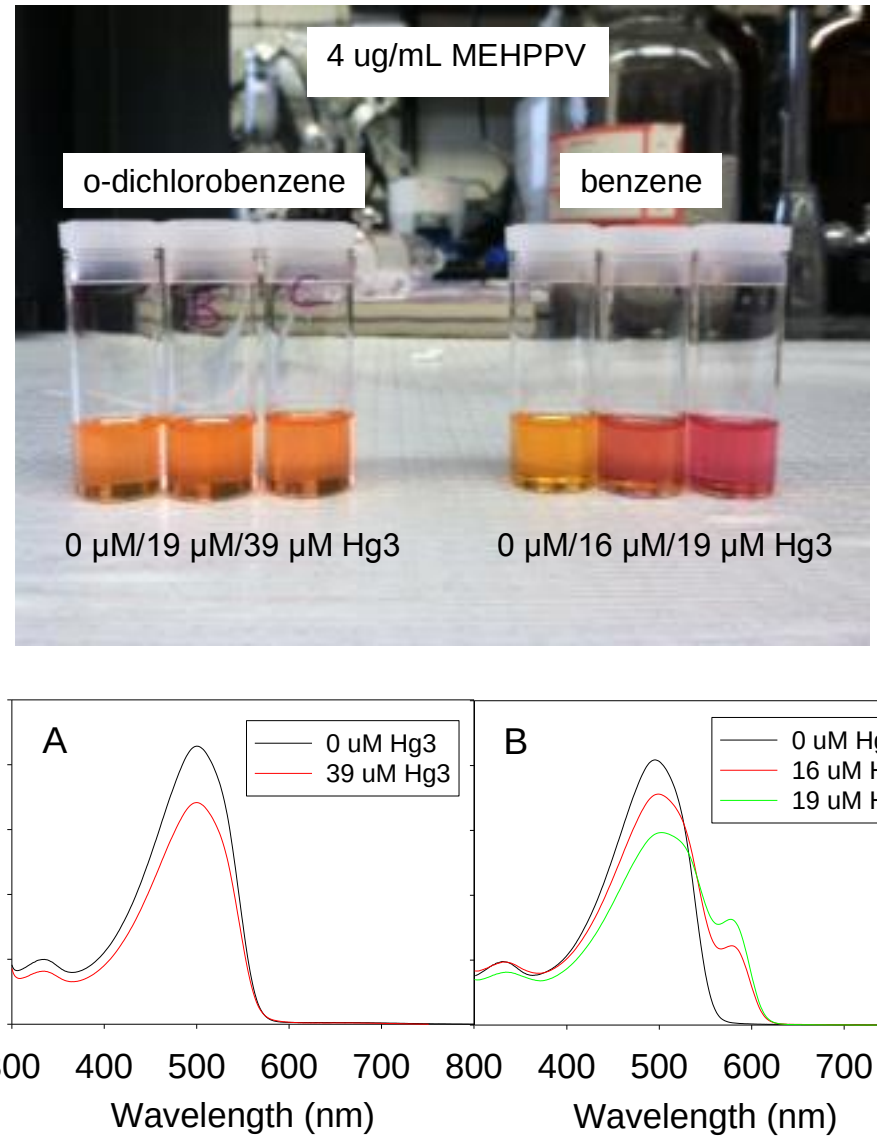

Figure 4-4. Visible color change of the solution and the absorption spectra of MEH-PPV upon addition of Hg3 in o-dichlorobenzene (A) and benzene (B).

The changes in the absorption and emission spectra were monitored carefully with addition of Hg3. MEH-PPV in good solvents like benzene or toluene exists as

isolated, unaggregated polymer chains with an absorbance maximum at ~497 nm due to relatively short conjugation lengths from twisting along the polymer backbone.[98] Upon addition of increasing amounts of the Hg3 complex to the polymer solution, aggregation of the MEH-PPV polymer occurs, shown by a red-shifted absorption spectrum and the growth of a shoulder at 578 nm as shown in Figure 4-5. Visibly, the color changes from a bright orange to a deep red. Large aggregated particles can be seen floating in solution at higher concentrations of Hg3 where the absorption spectrum nears the saturation point of Hg3 addition, at concentrations greater than about 200 μM. These particulates settle to the bottom if the solution is left to sit overnight, although the solution still remains a deep red color indicating that not all Hg3-aggregated polymer precipitates from solution.

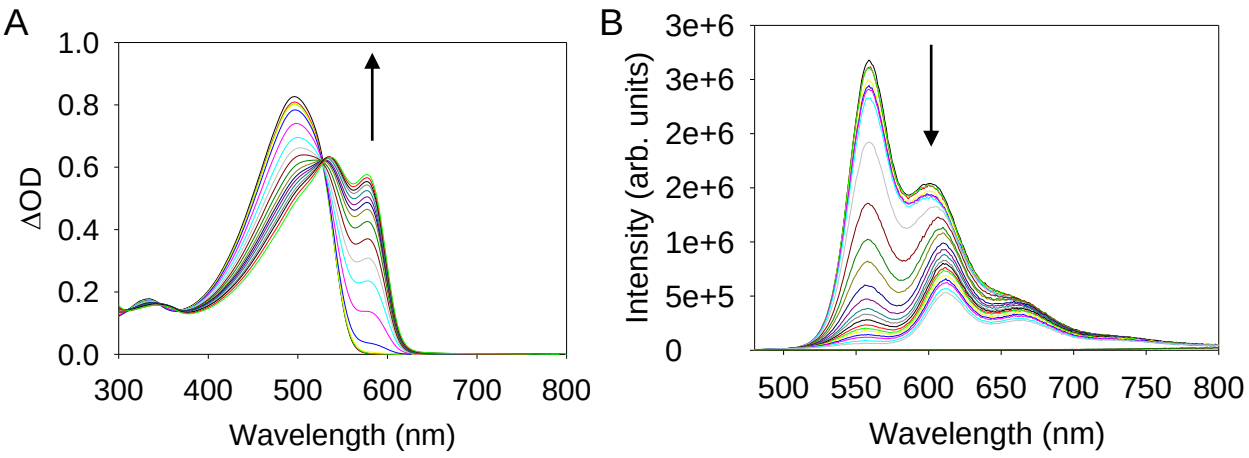

Figure 4-5. Absorption (A) and emission (B) spectra of MEH-PPV in benzene with a concentration of 10 μg/mL (15 μM repeat unit) with increasing additions of Hg3 from 0 μM to 240 μM. Excitation for the emission measurements was at 490 nm.

The fluorescence spectrum also shows interesting changes upon addition of Hg3 (Figure 4-5). The fluorescence of MEH-PPV in benzene is seen as a structured

emission with maxima at 558 nm and 602 nm with a shoulder around 660 nm. When Hg3 is added, the fluorescence intensity was effectively quenched and the structured emission was red-shifted. This quenching may indicate that intersystem crossing occurs in the presence of the heavy metal atom Hg; however the decreased emission intensity is more likely due to the aggregated polymer. Additionally, self-absorption of the emission may also be present due to the red-shifted absorption when Hg3 is added. Hg3 in benzene exhibited no absorption or photoluminescence in the detection range.

The changes in the absorption and emission spectra upon addition of Hg3 in benzene are strikingly similar with reported aggregation of pure MEH-PPV under various conditions reported in the literature.[136,137] In fact, reported results by Collison et. al. in 2001 mentioned an instantaneous visible color change when the poor solvent hexane was added to a toluene solution of MEH-PPV accompanied with a red-shifted structured absorption and emission along with a lower fluorescence quantum yield.[98] In this report, the authors concluded that the formation of "locally-ordered" MEH-PPV chains in poor solvent that were torsionally-constrained effectively increased the conjugation length of the polymer. Using a two-species model, they were able to describe the changes seen in the absorption and emission spectra.

Time resolved emission measured with excitation at 375 nm showed decreased fluorescence lifetimes upon addition of Hg3. The measured fluorescence lifetime of pure MEH-PPV in benzene was τ_{ave} = 270 ps (monitored at λ = 520 nm) which agrees with fluorescence lifetimes previously reported for MEH-PPV.[138,139] Upon addition of Hg3, the fluorescence lifetime decreased as shown in Table 4-1; however because the lifetime of pure MEH-PPV is close to the instrument response function (IRF), accurate

lifetime quenching data could not be obtained. Low temperature emission (80 Kelvin) measurements were attempted to observe phosphorescence from MEH-PPV upon addition of the Hg3, but the experiments were unsuccessful due to instrumental constraints.

Table 4-1. Average fluorescence lifetimes, τ_{ave}, for MEH-PPV in benzene upon addition of increasing amounts of Hg3 using narrow band filters (10 nm).

Concentration Hg3 (μM)	Fluorescence Lifetime, τ_{ave} (520 nm)	Fluorescence Lifetime, τ_{ave} (600 nm)	Fluorescence Lifetime, τ_{ave} (670 nm)
0 μM added	270 ps	280 ps	266 ps
15 μM added	246 ps	172 ps	171 ps
30 μM added	<IRF	<IRF	<IRF

Nanosecond transient absorption spectroscopy was used to observe the excited state dynamics of the polymer in the presence of Hg3. Solutions of MEH-PPV in benzene were prepared to an optical density at λ_{exc} = 532 nm of 0.61 from a stock solution (3 mg/mL in benzene). Hg3 crystals were added directly to the solutions. Solutions were stirred for 2-3 hours until the color change was complete and all Hg3 was dissolved. Three concentration regimes were examined for TA analysis as shown in the absorption spectra in Figure 4-6: (1) pure MEH-PPV with no Hg3 added, (2) low Hg3 concentration, 40 μM, such that the aggregation peak in the absorption spectrum is rising, and (3) high Hg3 concentration, 100 μM, where the complex is near the saturation point of the polymer. Solution (1) was bright orange in color, solution (2) was a bright pink grapefruit color, and solution (3) was a deep red.

Transient absorption spectra and decays were obtained with excitation using nanosecond pulses (λ_{exc} = 532 nm) at approximately 2.5 mJ/pulse laser energies for all measurements under both deoxygenated and oxygen-saturated conditions. It is

important to note that the solutions were matched in polymer concentration and not optical density at the laser excitation wavelength. Solution (3) with the highest Hg3 concentration was free from visible particulates during TA measurement, although after

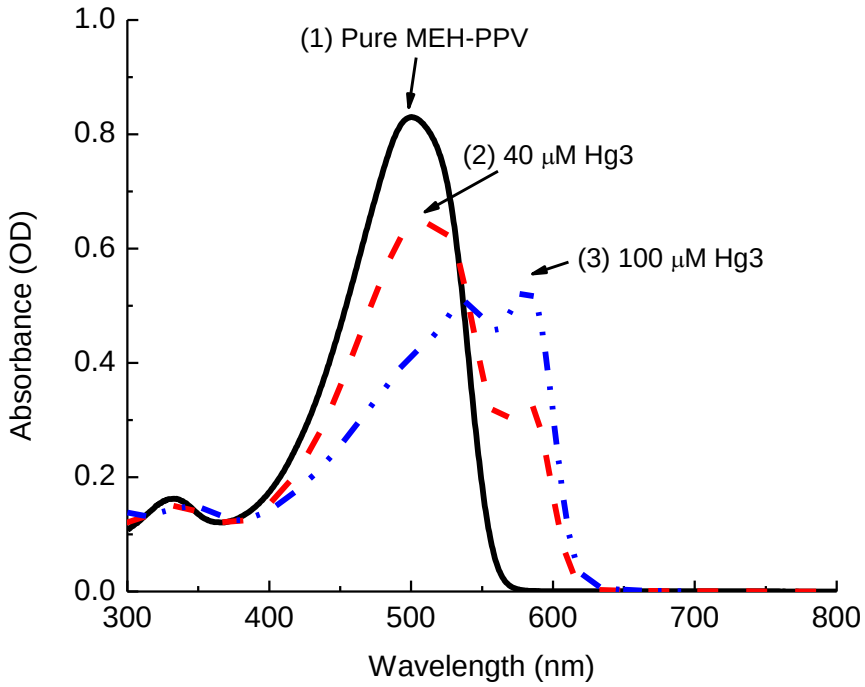

Figure 4-6. Ground state absorption spectra of the MEH-PPV solutions in benzene used for the transient absorption spectroscopy experiments.

the solution sat overnight some particulates had settled on the bottom of the solution vial. Hg3 in benzene shows no transient absorption. The transient absorption spectra are shown in Figure 4-7.

Initially, the transient absorption measurements were taken in argon-purged solutions (Figure 4-7A). In all solutions there is a transient absorption peak centered around 830 nm which matches reported triplet-triplet absorption for MEH-PPV.[140] The intensity of the triplet-triplet absorption peak decreases with increasing Hg3, but that may be due to lower optical density at the excitation wavelength as the aggregation

peak in the ground state absorption spectrum around 600 nm rises. It can be concluded, however, that the addition of Hg3 to the polymer does not greatly increase the concentration of triplet excitons produced upon excitation as would be expected by the increased presence of heavy metal atoms in the polymer.

As the concentration of added Hg3 increases another peak arises around 950 nm, which indicate the formation of MEH-PPV radical cations that are reported to absorb at 955 nm.[141] Triplet states are readily quenched by molecular oxygen, which is a ground state triplet, to form singlet oxygen while the radical cation should be unaffected by the presence of oxygen in solution. After purging the solutions with oxygen (Figures 4-7 B and C), the peak around 830 nm is efficiently quenched after 88 ns, while the peak at 950 nm remains. Therefore, the peak at 830 nm must be the triplet state. The rise of 950 nm upon addition of Hg3 indicates that Hg3 may be acting as an electron acceptor in benzene solution. Little, if any, photodegradation of the polymer occurred from the production of singlet oxygen during this experiment, as repurging the oxygen-saturated benzene solutions with argon recovers the original long-lived transient absorption at 830 nm.

The transient absorption of solution (1), pure MEH-PPV, is shown in Figure 4-8. In deoxygenated solution, a relatively strong transient absorption peak is present centered at 810 nm and tails off with no transient absorption after 925 nm. When the solution is saturated with oxygen, the transient absorption is very quickly quenched, disappearing within 88 ns. Looking at the transient decays at 830 nm, there is a very fast component in both the deoxygenated and O_2-saturated measurements. The

longer-lived component of the transient decay at 830 nm is nearly completely quenched in the presence of molecular oxygen, confirming the assignment of this peak to the

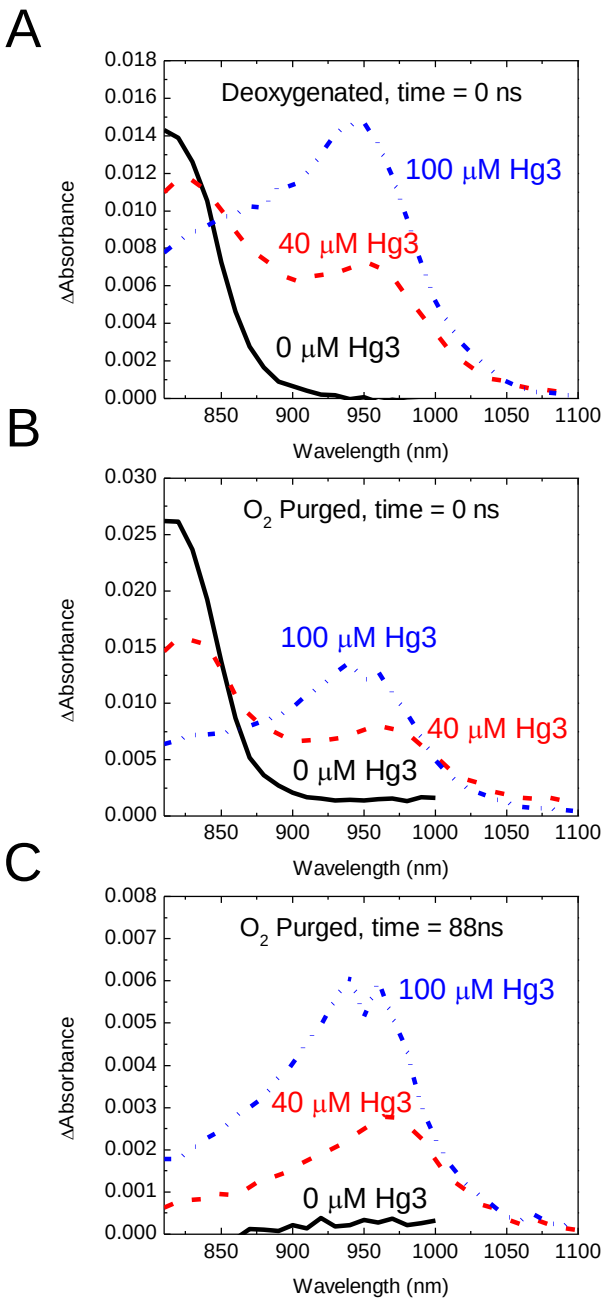

Figure 4-7. Nanosecond transient absorption spectra for MEH-PPV with three concentrations of Hg3 added: 0 μM, 40 μM, and 100 μM with λ_{exc}= 532 nm, 2.6 mJ/pulse. A: Transient absorption spectra at time = 0 ns (immediately after laser pulse) under deoxygenated benzene solutions. B: Transient absorption spectra at time = 0 ns in oxygen-saturated benzene. C: Transient absorption spectra at time = 88 ns in oxygen-saturated benzene.

triplet-triplet absorption of MEH-PPV. An exponential fit including the initial fast component could not be found with good results, so only the longer lived decay was fit to an single exponential function with a lifetime of τ_{TA} = 299 ns (R^2 = 0.989). This lifetime is surprisingly short compared to lifetimes reported in benzene for MEH-PPV triplets created by triplet energy transfer from a donor, like biphenyl, which are typically on the order of 100 μs.[140] The best exponential fit to the weak, noisy decay in the oxygen-saturated solution at 830 nm shows a decreased lifetime of 30 ns (R^2 = 0.455).

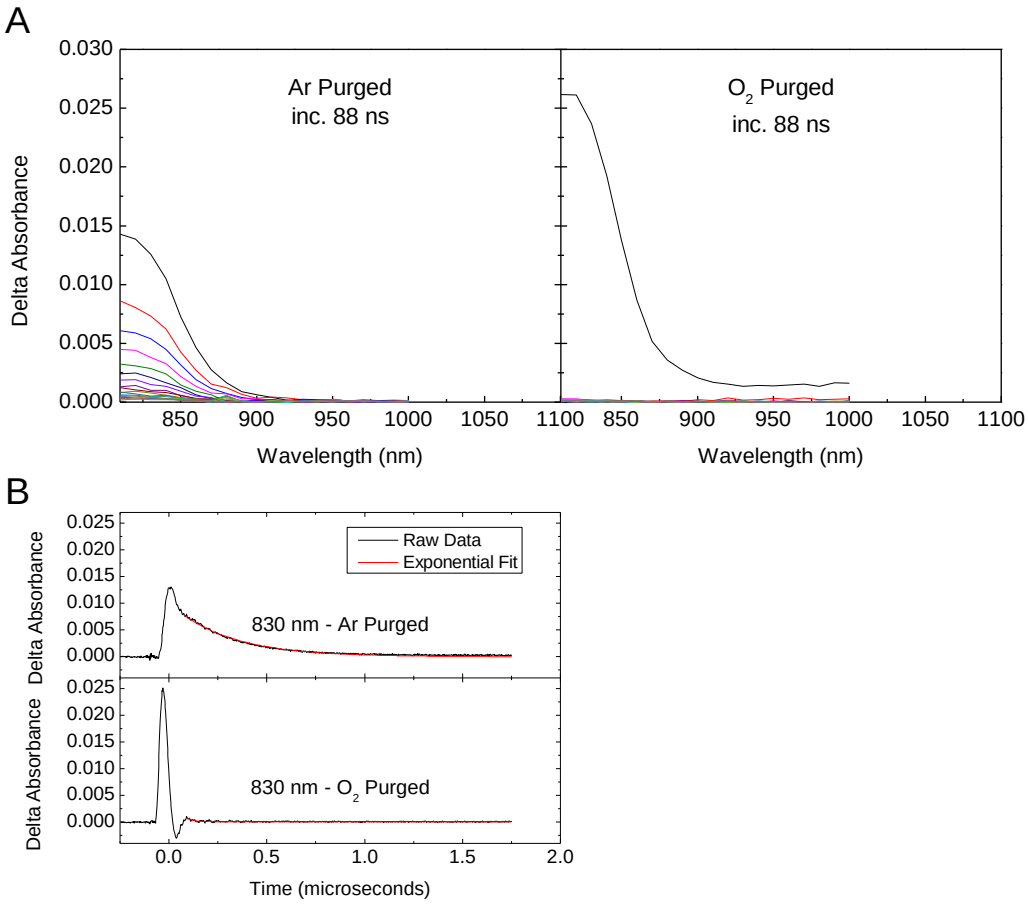

Figure 4-8. Transient absorption spectra (A) and transient decays (B) of pure MEH-PPV (solution 1) in benzene, under deoxygenated and oxygen-saturated conditions (λ_{exc}= 532 nm, 2.6 mJ/pulse).

The transient absorption spectra of solution (2), MEH-PPV with 40 μM Hg3, are shown in Figure 4-9. In deoxygenated solution, the triplet-triplet absorption peak at 830 nm is observed, and another peak, tentatively assigned to MEH-PPV$^{+\bullet}$, appears at 950 nm. There is a slight red-shift of the triplet-triplet absorption peak from 810 nm in the pure MEH-PPV solution to 830 nm. When the solution is saturated with oxygen, the transient absorption at 830 nm is very quickly quenched, disappearing within 88 ns, while the absorption at 950 nm remains. Looking at the transient decays, the very fast component appears to maintain the same temporal profile although it changes in magnitude between wavelength and purging conditions.

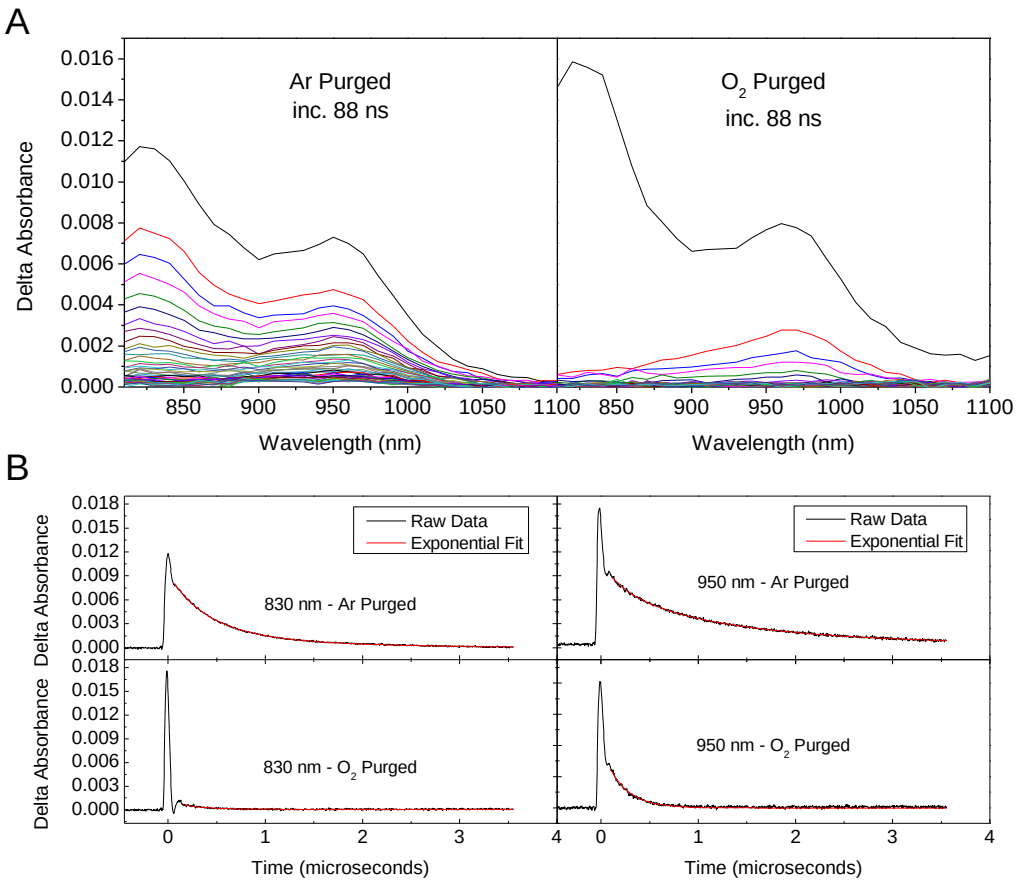

Figure 4-9. Transient absorption spectra (A) and transient decays (B) of MEH-PPV with 40 μM Hg3 in benzene (solution 2) under deoxygenated and oxygen-saturated conditions (λ_{exc}= 532 nm, 2.6 mJ/pulse).

Figure 4-10 shows the transient absorption spectra of solution (3), MEH-PPV with 100 μM Hg3 in deoxygenated and oxygenated solution. In deoxygenated solution, the triplet-triplet absorption peak at 830 nm is almost completely overwhelmed by the absorption band at 950 nm, tentatively assigned to MEH-PPV$^{+\bullet}$. After purging the solution with oxygen, little change in the absorption spectrum is apparent. The small peak visible at 830 nm is quickly quenched after the first 88 ns, and the 950 nm peak decays more slowly, less affected by the presence of oxygen.

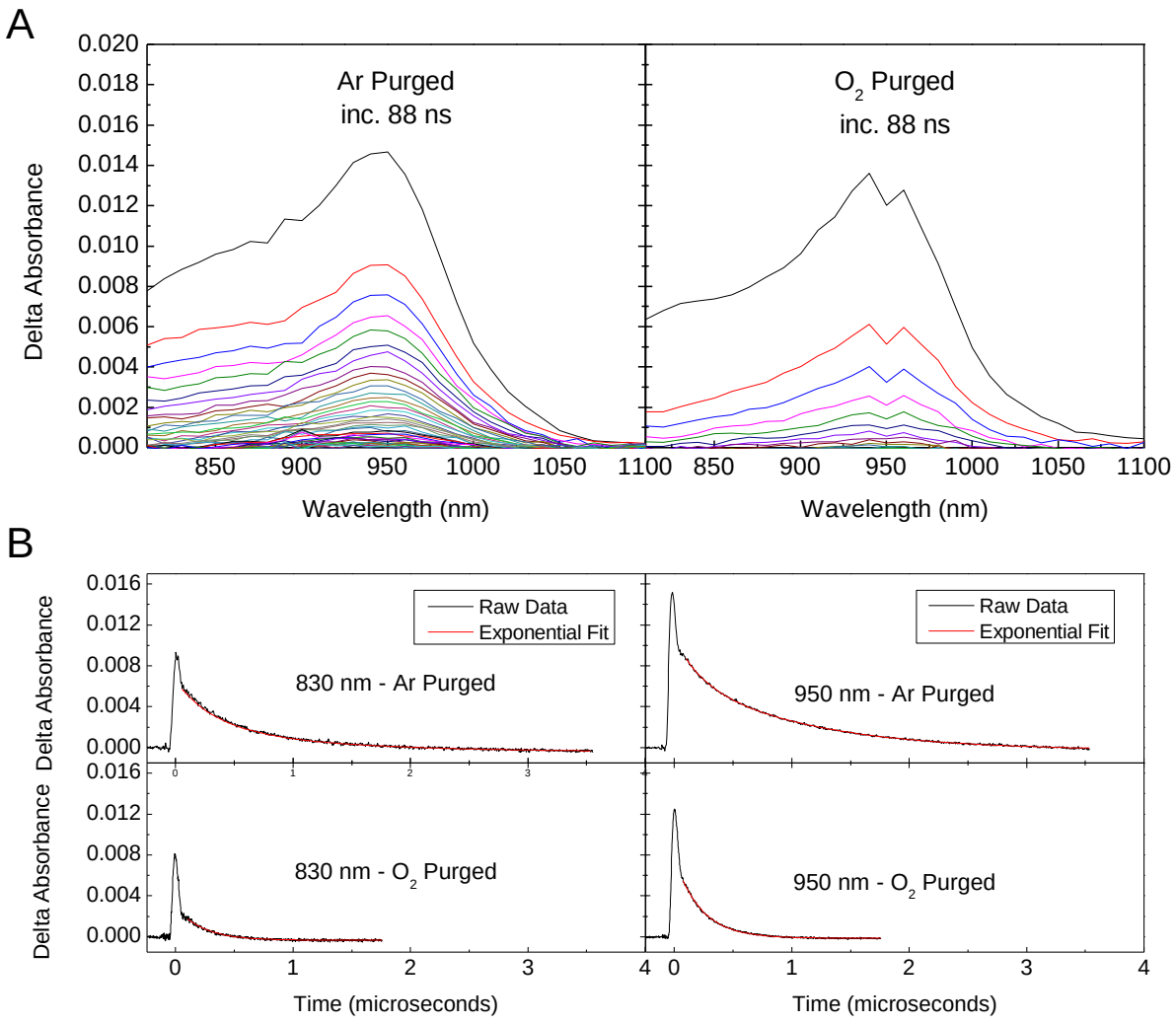

Figure 4-10. Transient absorption spectra (A) and transient decays (B) of MEH-PPV with 100 μM Hg3 in benzene (solution 3) under deoxygenated and oxygen-saturated conditions (λ_{exc}= 532 nm, 2.6 mJ/pulse).

The transient decays reveal interesting information as shown in Table 4-2. These decays are fitted without including the initial very fast feature in the transients, which will be discussed later. First, upon addition of Hg3 to the MEH-PPV, the single-exponential decay becomes obviously bi-exponential with a short (200-400 ns) and a longer (1-2 μs) lifetime, indicating a transition from a single-component, $[MEH\text{-}PPV]^3$, to a two-component, $[MEH\text{-}PPV]^3$ and $[MEH\text{-}PPV]^{+\bullet}$, system. Second, the lifetimes after oxygen-purge are very consistent between both 40 μM and 100 μM Hg3 solutions with lifetimes around 200 ns, while the average lifetime decreases upon increased Hg3 addition.

Table 4-2. Exponential fits to the transient decays at 830 nm and 950 nm for MEH-PPV and Hg3 solutions in argon-purged and oxygen-saturated benzene. All fits were to single or bi-exponential decays with R^2 values of >0.997 except for pure MEH-PPV, O_2 purged which had an R^2 value of 0.455.

	Pure MEH-PPV	MEH-PPV + 40μ M Hg3		MEH-PPV + 100μ M Hg3	
λ =	830 nm	830 nm	950 nm	830 nm	950 nm
Ar purged	262 ns	418 ns (82%) 2.63 μs (18%)	400 ns (40%) 1.62 μs (60%)	329 ns (82%) 1.18 μs (18%)	199 ns (75%) 1.03 μs (25%)
O_2 Purged	30 ns	218 ns	190 ns	224 ns	222 ns

The origin of the initial very fast feature in the transient decays shown in Figure 4-8, Figure 4-9, and Figure 4-10 is unknown. Preliminary experiments find that the proportion of this fast component to the longer triplet decay is independent of the laser excitation energy (from 200 μJ/pulse to 2 mJ/pulse), so concentration-based effects such as triplet-triplet annihilation can be ruled out. Interestingly, regardless of whether the transient-absorption spectrum is extrapolated from the peak of the fast component or from the start of the longer-lived component at each wavelength, the resulting spectra

are equivalent. This holds true even for solution (2) and solution (3), where Hg3 has been added and the spectrum includes a rising peak at 950 nm. Experiments performed on a benzene blank solution and other compounds in solution under similar conditions do not show this fast-lived component, so it does not seem to be an instrumental effect.

Cyclic voltammetry (CV) measurements were performed on the Hg3 complex to support the observation of the polymer cation by transient absorption as shown in Figure 4-11. Reduction of the Hg3 complex dichloromethane (3 mM concentration) in argon-purged was observed with a non-reversible reduction peak around -1.4 V (vs. Ag/AgCl). The CV shown in Figure 4-11 is the first scan of a freshly-prepared solution. The reduced Hg3 complex was not stable, and a shift of the peak to higher potential and eventual disappearance of the peak with precipitation occurred after subsequent CV measurements.

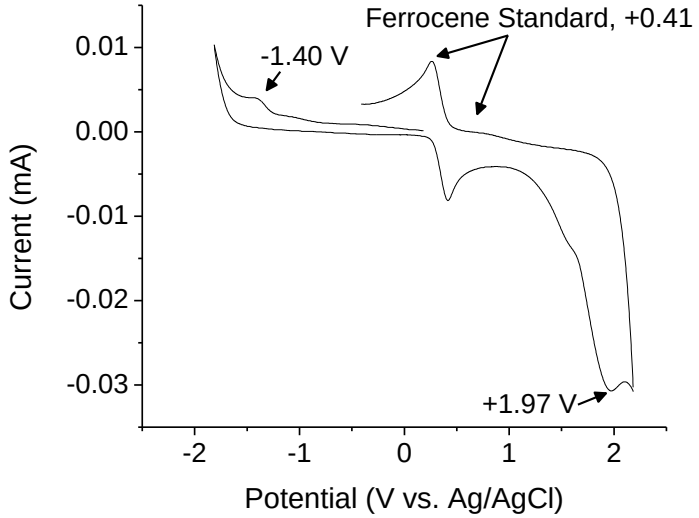

Figure 4-11. Cyclic voltammetric response from a 3 mM solution of Hg3 at a scan rate of 100 mV/s in dichloromethane at platinum working electrode (supporting electrolyte: 0.1 M TBAH). Ferrocene was used as a standard.

Film Photophysical Studies

Films were prepared with varying amounts of Hg3 added to examine the photophysics in the solid state. Solutions were prepared in o-dichlorobenzene or benzene and drop-coated onto clean glass slides with similar optical properties between films made with different solvents. As shown in Figure 4-12, pure MEH-PPV films prepared in o-dichlorobenzene solutions are a bright orange color, but the color changes from bright orange to deep red with increasing amounts of Hg3 as the solvent is evaporated to match the visible color change in benzene solution. This illustrates that the aggregation between Hg3 and MEH-PPV, forced by the evaporation of solvent does not require the presence of benzene to form aggregates. Even in a solvent where Hg3 is fairly soluble, like o-dichlorobenzene, as the solvent evaporates and the polymer and mercury complex are forced closer together by the shrinking volume, aggregation of the MEH-PPV occurs similarly as in a poor solvent.

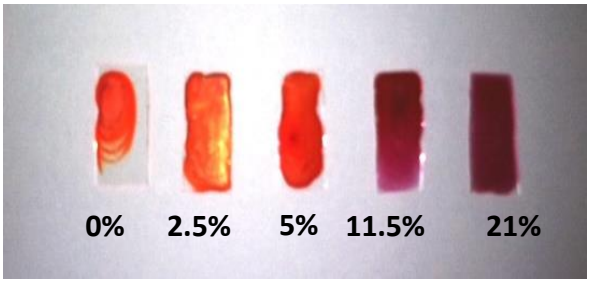

Figure 4-12. Visible color change of films made with o-dichlorobenzene with increasing weight % of Hg3 added (where 50% wt. means equal weights of polymer and Hg3).

The absorption and emission spectra for drop-coated films prepared from MEH-PPV solutions in benzene with increasing amounts of Hg3 added are shown in Figure 4-13. The films varied in thickness due to aggregation, so the intensity of the absorption

or emission cannot be directly compared. Interestingly, the structure of the absorption and emission spectra of the films evolve similarly upon increased concentration of Hg3 compared to the spectra measured in benzene solution shown in Figure 4-5 of MEH-PPV (~25 μM repeat unit) with 0-240 μM Hg3 added. In general, upon addition of Hg3, there is a red-shift in the absorption and emission with more structured bands indicative of the aggregation of MEH-PPV.

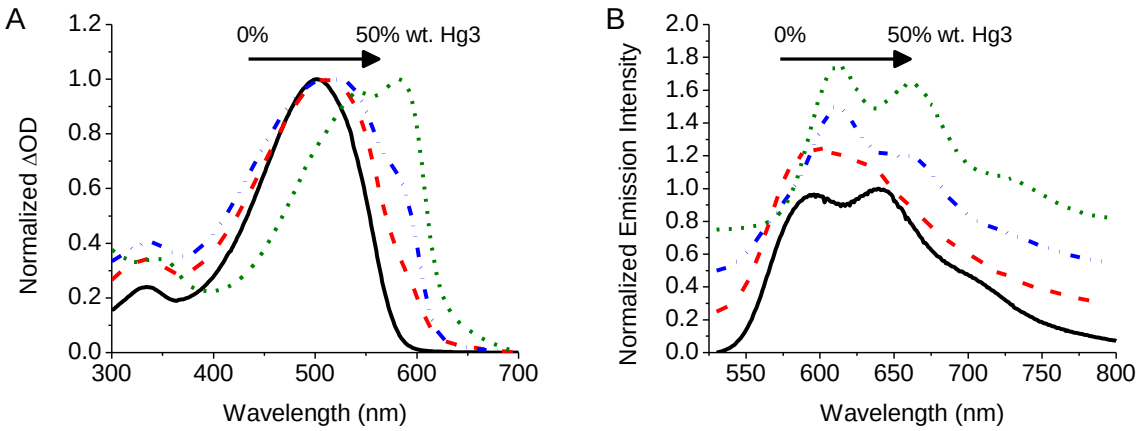

Figure 4-13. Absorption (A) and emission (B) spectra of drop-coated films of MEH-PPV with increasing wt.% of Hg3 prepared in benzene: 0% wt., 10% wt., 20% wt., and 50% wt. Hg3.

Nanosecond transient absorption measurements shown in Figure 4-14 on dropcoated films of MEH-PPV and Hg3 are a remarkable parallel to the solution experiments. Initially, upon addition of Hg3, a rising peak centered around 825 nm appears, and when the concentration is increased to 20% wt. Hg3 and finally 35% wt. a prominent peak around 925 nm takes over. The biexponential fits to the transient decays at λ_{max} of the 10%, 20%, and 35% wt. films give lifetimes similar to those measured in benzene solution with a longer component that ranges from 877 ns to 1.09 μs and a shorter component that ranges from 162 ns to 235 ns as the amount of Hg3 increases. The longer component around 1 μs has a larger contribution to the overall

decay (from 48% to 68%) as the amount of Hg3 increases. This trend resembles the trend seen in solution TA measurements. The increasing lifetime is probably due to the restrictive organization of the polymer when it is aggregated by the Hg3.

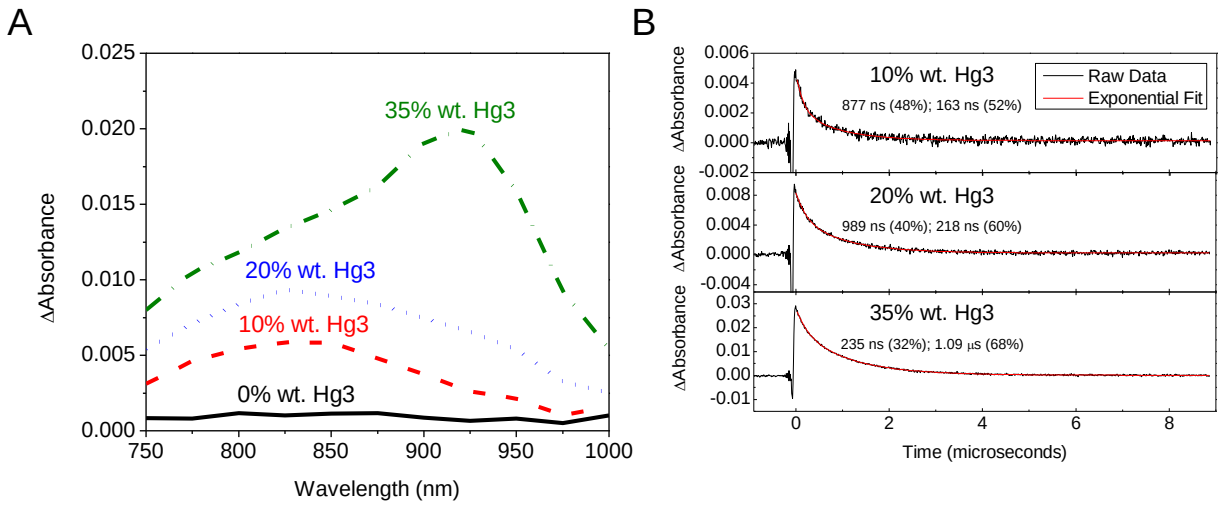

Figure 4-14. Nanosecond transient absorption spectra (A) and decays at $\lambda = TA_{max}$ (B) for dropcoated films of MEH-PPV prepared in benzene containing increasing wt. % Hg3 (λ_{exc}= 532 nm, 800 μJ/pulse, 128 averages, 1 kΩ termination, smooth 10). Transient decays were fit to biexponential decays shown in red.

Structure/Morphology Studies

An interesting effect was noticed while attempting to perform low temperature emission experiments on MEH-PPV. When MEH-PPV was frozen in the glass-forming solvent, methyl-THF, the color of the solution changed from orange to pink, as shown in Figure 4-15. This is analogous to the color change upon addition of Hg3 to MEH-PPV in benzene solution at room temperature. The increased conjugation length, intermolecular interactions, and exciton migration of MEH-PPV and other PPVs at decreasing temperature in organic glasses leads to red-shifted and narrower emission bands as has been well-documented with many detailed studies by other groups.[103,142-145] For the purposes of this work, the observed color change offered further evidence that Hg3 simply acts as an instigator for MEH-PPV to self-aggregate and motivated

further experiments to examine how the structure and morphology of MEH-PPV changes when Hg3 is added.

Figure 4-15. Color change of MEH-PPV in methyl THF upon freezing to liquid nitrogen temperatures. Vial, right: MEH-PPV in methyl THF at room temperature. Tube, left: MEH-PPV in frozen methyl THF.

The Hg3 complex does not contain any protons, so ^{1}H NMR experiments were performed in deuterated benzene to examine at the structural changes of MEH-PPV when increasing amounts of the Hg3 complex were added (Figure 4-16). The ^{1}H NMR spectrum of pure MEH-PPV in benzene-d6 matches the spectra of MEH-PPV previously reported.[97,146] When Hg3 is added, there is a dramatic change in the NMR spectrum. Due to the insolubility of Hg3 in benzene, as Hg3 is added and associates with MEH-PPV, the polymer also becomes less soluble. The NMR signal becomes noticeably weaker. The protons around the aromatic ring in the polymer labeled as peaks A and B in the spectra almost completely disappear indicating significant interaction between Hg3 and the aromatic protons. The shift of A and the side-chain proton signals C and D downfield indicates significant shielding of the aromatic region by large planar molecule Hg3.

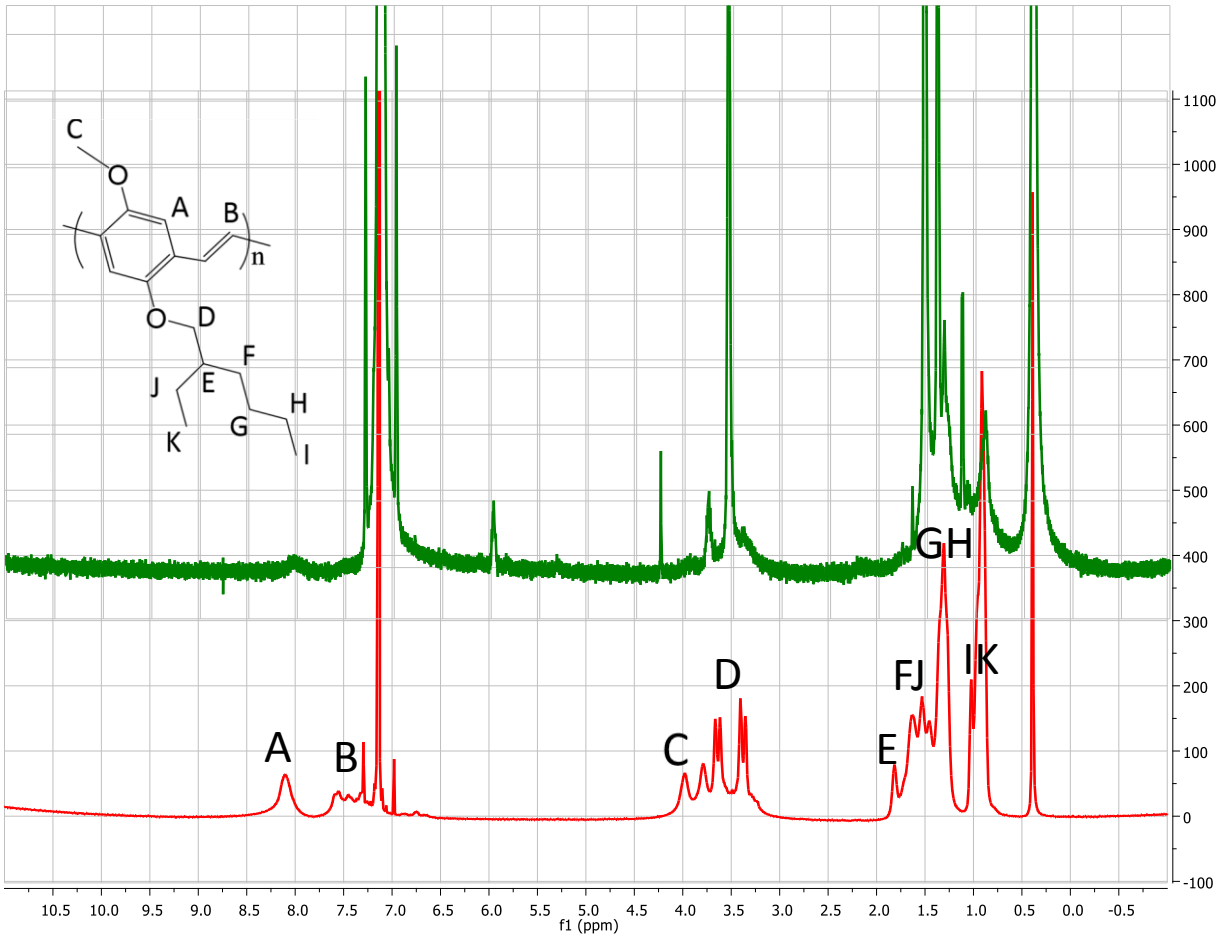

Figure 4-16. ^{1}H NMR of pure MEH-PPV in benzene-d6 (red, bottom) and ^{1}H NMR of MEH-PPV with Hg3 in benzene-d6 (green, top). NMR experiment performed by Russ Winkel.

X-ray diffraction (XRD) experiments at room temperature shown in Figure 4-17 were carried out on drop-coated films containing MEH-PPV and 0%, 5%, 15%, 30%, and 50% wt. Hg3. The pure MEH-PPV (0% wt. Hg3) film had a featureless diffraction pattern between 2θ = 0 - 25° indicating that MEH-PPV has amorphous structure. Relatively weak diffraction peaks in the scattering angle range of 2θ = 4.5° to 7.5° for the MEH-PPV + 5% wt. Hg3 film and increasingly strong diffraction peaks for the higher % wt. Hg3 films up to the scattering angle range of 2θ = 3.5° to 8.5° for the MEH-

PPV + 50% wt. Hg3 film were observed. This indicates efficient packing of the side-chains of MEH-PPV polymer in the presence of the Hg3. Studies of MEH-PPV after thermal annealing treatment by other groups report a peak around 5° in XRD owing to the regular packing of the polymer side-chains.[147,148] This XRD data supports the photophysical results that Hg3 templates ordering of the MEH-PPV. Powder XRD on the Hg3 crystals show a strong diffraction peak at 2θ = 9.6°. Because the Hg3 peak at 9.6° is not seen in the MEH-PPV + Hg3 films, it's likely that all the Hg3 is associated with the polymer creating the strong diffraction pattern at ~5°.

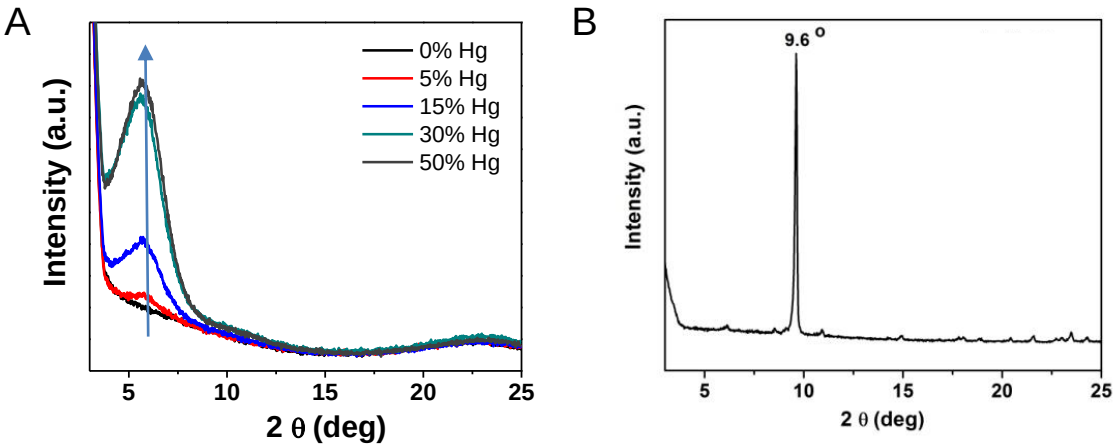

Figure 4-17. X-ray diffraction profiles at room temperature obtained by Gyu Leem of (A) films of MEH-PPV with increasing wt. % of Hg3 added and (B) Hg3 powder.

To examine the morphology of MEH-PPV films containing Hg3 at various concentration conventional bright-field transmission electron microscopy (TEM) was used. The images shown in Figure 4-18 demonstrates the remarkable effect on the morphology of MEH-PPV in films by the presence of Hg3. The pure MEH-PPV film at room temperature gives a featureless TEM image due to the amorphous nature of the polymer. From the 5% wt. Hg3 film, some aggregation of the polymer is visible as worm-rod shapes on the TEM image. As the concentration of Hg3 increases to 50%

wt., the worm-rod shapes become interconnected and the TEM image becomes strikingly similar to the image of MEH-PPV after heat treatment reported by Chen in 2004.[149] Taken together with the XRD results, these TEM studies show that the increasing the amount of Hg3 from 0% to 50% wt. led to increased aggregation and higher ordered structures of MEH-PPV containing Hg3.

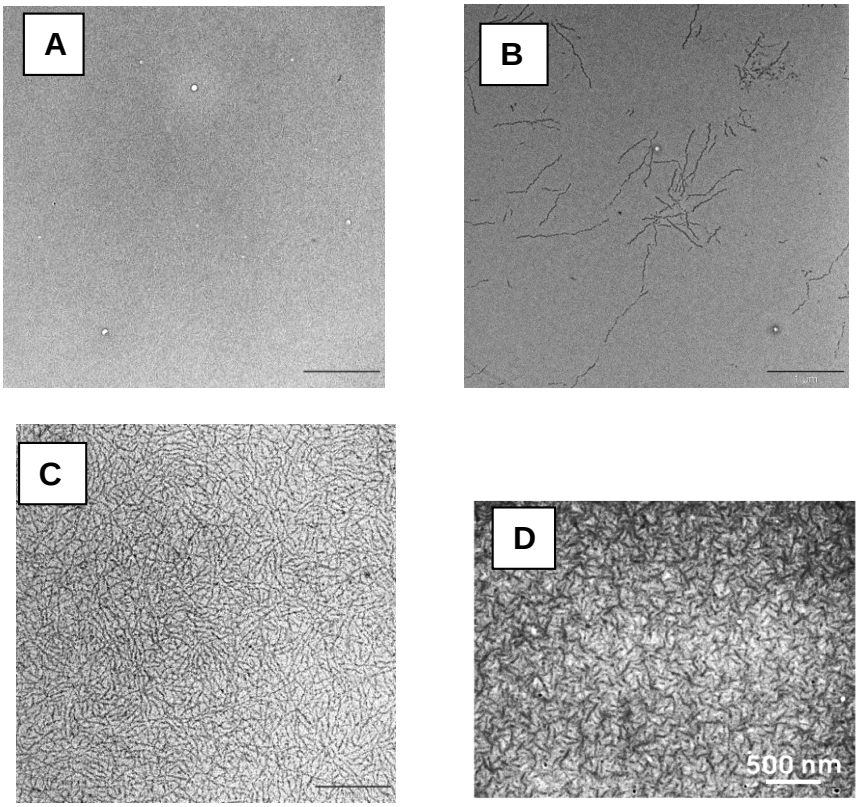

Figure 4-18. TEM images of MEH-PPV films acquired by Gyu Leem (scale bar is 1 μm). Various concentrations of Hg3 were added (A) 0% wt., (B) 5% wt., and (C) 50% wt. (D) For comparison, a TEM image of MEH-PPV after annealing treatment reported by Chen in Langmuir 2004.[149]

P3HT

The interaction between P3HT and Hg3 was also investigated. P3HT (Poly(3-hexylthiophene-2,5-diyl)) shown in Figure 4-19. Organic solar cells comprising of P3HT and their derivatives are the most promising of all organic polymers with reported

efficiencies of up to 5%.[150,151] P3HT can be prepared in two flavors: regioregular and regiorandom depending on the alignment of the polymer chains. Regioregular P3HT is aligned in a head-to-tail stereoregular order and forms high-mobility films due to the formation of nanocrystalline lamellae.[152,153] Regiorandom P3HT does not display supramolecular structure in films and generally has very small hole mobility in contrast to the high mobility found in regioregular P3HT[154-156].

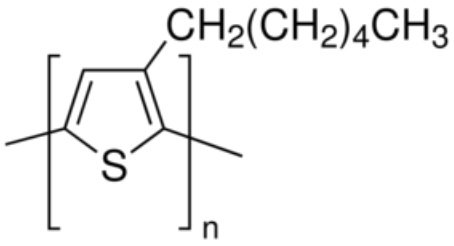

Figure 4-19. Structure of P3HT (Poly(3-hexylthiophene-2,5-diyl)).

The interaction between P3HT (regioregular) and Hg3 was investigated. There was found to be some solvent dependence as shown in Figure 4-20. Unlike MEH-PPV, P3HT tends to aggregate in benzene, so the addition of Hg3 only darkens the purplish-red color slightly. In chloroform, initially the P3HT is unaggregated and the solution is orange, but with addition of Hg3, the solution quickly darkens.

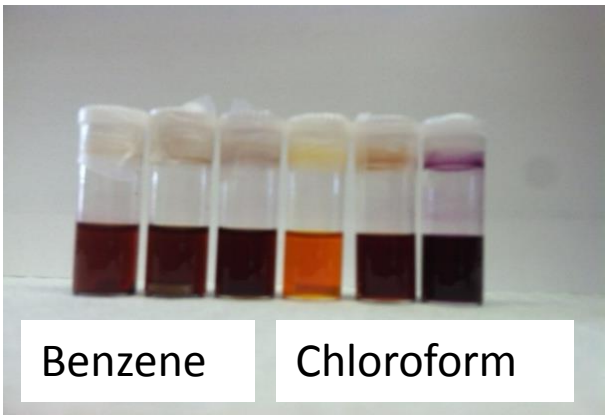

Figure 4-20. P3HT solutions with increasing amount of Hg3 in benzene and chloroform.

P3HT in chloroform has an absorption peak at 450 nm. When Hg3 is added, the shoulder around 595 nm rises and a peak appears at 551 nm. Ordered P3HT aggregates in solution, such as is induced by poor solvent, is reported to absorb at 551 nm where the intensity is dependent on the degree of interchain ordered aggregation of the polymer possibly due to π-π stacking.[157-159] The fluorescence of P3HT occurs with maxima at 580 and 620 nm with a shoulder at 690 nm. This fluorescence was effectively quenched upon addition of Hg3 with little red-shift, but the peak-ratios at high concentrations of Hg3 compared to pure P3HT in chloroform are changed. Unlike MEH-PPV, large aggregates were not visible in solution at the highest concentrations of Hg3. This may be due to the fact that Hg3 is soluble in chloroform whereas in benzene it is mostly insoluble.

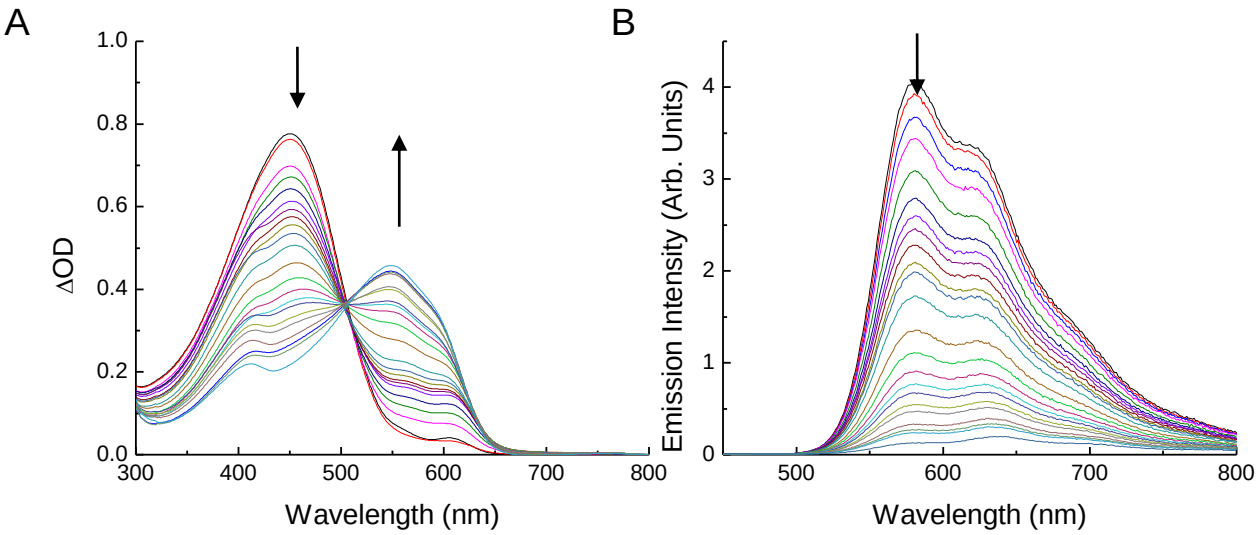

Figure 4-21. Absorption (A) and emission (B) spectra of P3HT (14 μg/mL, 9 μM repeat unit) upon addition of increasing concentration of Hg3 from 0 μM – 105 μM.

Preparing films from P3HT in chloroform with varying concentrations of Hg3, it is interesting to note that although the solution color varies from orange to purple depending on the amount of Hg3 present, upon evaporation of the solvent, all films

become a similar dark purple in color (Figure 4-22). This is seen most clearly in the 0% film. The pure P3HT film starts out a bright orange color, but as the solvent evaporates, the P3HT undergoes self-organization and the purple color that appears is that of the aggregated polymer.

Figure 4-22. P3HT films dropcoated from chloroform solution as the solvent evaporates. Left: 0% Hg3, Right: 50% Hg3

The absorption and emission spectra of the P3HT films prepared in benzene and chloroform containing increasing weight % of Hg3 are shown in Figure 4-23. The P3HT films have similar absorption and emission properties regardless of the solvent used for casting. The structured absorption of the pure P3HT films is lost when Hg3 is added, and the absorption maxima slightly red-shifts. However, a dramatic change in the absorption spectrum seen in the presence of Hg3 such as with MEH-PPV does not occur with P3HT. It appears as though the P3HT polymer naturally self-organizes in a film, and the Hg3 only has a small effect. The emission of P3HT seems to be quenched by the addition of Hg3, and the peak ratios in the emission change similarly to the effect seen in chloroform solution shown in Figure 4-20.

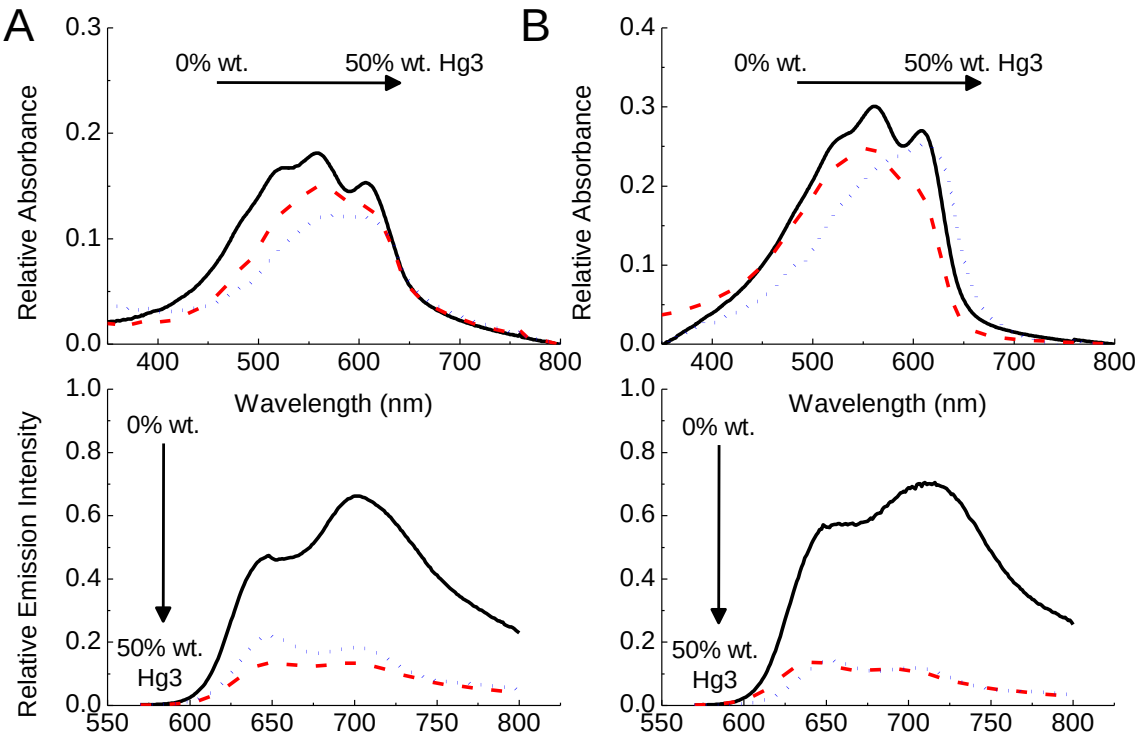

Figure 4-23. Absorption and emission spectra of P3HT films prepared in benzene (A) and chloroform (B) with increasing concentrations of Hg3: 0% wt. (black), 20% wt. (red), and 50% wt. (blue). Spectra are scaled on a relative scale for comparison.

The triplet-triplet transient absorption for regiorandom-P3HT films occurs around 800 nm, while regioregular-P3HT is not reported to show triplet-triplet absorption.[160-162] Nanosecond transient absorption measurements were attempted on P3HT in chloroform and P3HT films (0-50% wt. Hg3) with addition of Hg3 with no transient absorption detected.

Summary of Results

In solution, the interaction between MEH-PPV and Hg3 is strongly solvent dependent. In solvents such as o-dichlorobenzene, no interaction between the Hg3 and the polymer is observed; however, in benzene, which does not dissolve Hg3, the Hg3 complex “solvates” into the polymer chains leading to aggregation of the polymer. In

films prepared by either solvent, aggregation of the polymer occurs as the solvent is evaporated.

The photophysical data suggests increased conjugation length of the polymer due to self-organization of the polymer chains promoted by the interaction with Hg3. The fluorescence emission intensity is quenched indicating that the presence of the heavy mercury atoms may be promoting intersystem crossing in the polymer to the triplet state; however, the transient absorption results in solution do not show evidence of increased triplet concentration as Hg3 concentration increases. Instead, the polymer cation is detected in increasing magnitude due to electron transfer to Hg3 which was shown to have irreversible reduction by cyclic voltammetry.

The aggregation of the polymer by interaction with Hg3 was confirmed by XRD and TEM analysis. With increasing Hg3 concentration, XRD analysis shows efficient packing of the polymer side-chains, and the TEM analysis demonstrates the templated ordering of the polymer backbone by the appearance of worm-rod shapes. Taken together with the NMR results, which show shielding of the aromatic protons with Hg3, this ordering of the polymer is likely due to an intercalation of Hg3 between the aryl regions of adjacent polymer chains.

Another conjugated polymer, P3HT, was examined for its interaction with Hg3. Aggregation of P3HT occurred in chloroform with increasing amounts of Hg3 added observed by changes in the absorption and emission spectra. Fluorescence quenching suggested enhanced intersystem crossing; however no transient absorption in solution or in film was observed. P3HT naturally forms well-ordered films, so it's not surprising that Hg3 had little observed effect on the photophysical properties.

From these results, it can be concluded that Hg3 may enhance ordering of amorphous conjugated polymer chains without the need for complicated heat treatments. While the P3HT polymer showed little benefit from addition of Hg3, the MEH-PPV/Hg3 system showed interesting properties. While there is no evidence to support that Hg3 sensitizes the triplet excited state of the polymer, it is proven that the addition of Hg3 leads to efficient packing of the long, branched alkyl side-chains, increased conjugation length along the polymer chain, and overall increased crystallinity of the polymer in untreated films. These properties are important to the design of efficient optoelectronic devices. Future studies will be focused on experiments to measure the charge and exciton transport of the polymer in the presence of Hg3.

Experimental Section

Preparation of Polymer Solutions and Films. The mercury complex Hg3 was synthesized by a former postdoc, Kye-Young Kim, and the purity was checked by ^{19}F NMR. The molecular weight of Hg3 is 1046 g/mol. MEH-PPV was obtained from a commercial supplier, American Dye Source Inc., and stored in an oxygen and moisture-free environment although portions were taken out and kept in tightly closed vials covered with foil for up to several weeks before use. The molecular weight and purity of the polymer were checked by GPC. Polymer solutions for photophysical measurement and the preparation of films were prepared by first dissolving the polymer into high-purity spectroscopy-grade solvent, stirring for at least 2-3 hours to obtain a homogenous solution. A polymer solution was prepared by dilution of a concentrated MEH-PPV stock solution (3 mg/mL) which was left to stir overnight to a 3 mL quartz cuvette to a final concentration of 15 μM repeat unit for spectrophotometric analysis. The Hg3 complex is not completely soluble in benzene, so a dispersion was prepared at 0.6 mM

concentration and was continuously stirred during the experiment to ensure as consistent additions as possible to the polymer solution. After each addition, the solution in the cuvette was stirred for at least 1 minute before data acquisition.

For very concentrated polymer solutions, such as for films, the solutions were stirred for at least 24 hours before addition of the Hg3 complex. Due to the insolubility of Hg3 in most solvents, Hg3 powder was weighed and directly added into the polymer solution for all TA measurements. The Hg3 particles are initially colorless, but when they were added to bright orange MEH-PPV polymer solution, the particles became reddish from aggregation with the polymer and fell to the bottom of the orange MEH-PPV solution. After stirring for 3-4 hours or overnight, the Hg3 particles dissolved and the MEH-PPV+Hg3 solution changed in color from orange to red depending on the amount of Hg3 added. At “saturated” concentrations of Hg3, some visible chunks of aggregated polymer became stick to the side of the vial. Sometimes the aggregated polymer could be redissolved by sonication, but the highest Hg3 concentrations always had aggregated polymer along the sides of the sample vial. Solutions were wrapped with foil to protect from light when not in use. Films were prepared by dropcoating from concentrated solutions and allowing the solvent to evaporate at room temperature in the dark overnight before measurement. A 50% weight film means equal mass of polymer and Hg3.

P3HT solutions and films were prepared and analyzed similarly. Hg3 is soluble in chloroform, so a stock solution of Hg3 in chloroform was easily prepared. P3HT, regioregular was obtained from Sigma-Aldrich, and PFO was obtained from American Dye Source, Inc.

Photophysical Measurements. Photophysical properties for solutions were measured using a 1-cm pathlength quartz or borosilicate cuvette in spectroscopic solvents. Solutions were deoxygenated by purging with argon or oxygen-saturated by purging with oxygen for transient absorption measurements. Ground state absorption spectra were collected on a Varian Cary 100 dual-beam spectrophotometer with the appropriate solvent as the instrument baseline blank. Corrected steady-state emission measurements were collected by a Photon Technology International (PTI) photon counting fluorescence spectrophotometer.

Nanosecond triplet-triplet transient absorption was measured in a continuously circulating 1-cm pathlength borosilicate cuvette. The second harmonic of a Continuum Surelite II-10 Nd:YAG laser at 532 nm (2.4 mJ/pulse) was used as the pump and a Newport xenon arclamp was used as the probe source. The transient absorption signal was detected in the nIR between 810-1100 nm, every 10 nm with a Thorlabs Si Photodiode PDA8A. The transient absorption spectra were obtained by using a custom Matlab program to convert the transient absorption decays at each wavelength to spectra at specified time intervals. MEH-PPV samples were prepared to an optical density of 0.61 at 532 nm before Hg3 addition. Transient absorption lifetimes were calculated using exponential fitting in Origin 8.5 software.

Polymer film photophysics were measured freestanding, open to the atmosphere. Absorption spectra were measured on a Varian Cary 100 dual-beam spectrophotometer with a clean glass slide as the instrument blank. Emission spectra were obtained by a front-face alignment on a Fluorolog 3 spectrophotometer. Transient absorption measurements were made using an in-house designed TA instrument dedicated to

solid-state measurements. The second harmonic of a Continuum Surelite I-10 Nd:YAG laser at 532 nm (600 μJ/pulse) was used as the pump beam in an antiparallel alignment to the probe beam provided by a 250 W QTH lamp (Newport). Single-wavelength transient absorption decays were acquired as an average of 128 shots every 25 nm using a Thorlabs Avalanche Photodetector APD 110A. The transient absorption spectrum was acquired by using a custom Matlab program to convert the transient absorption decays at each wavelength to a transient absorption spectrum at t=0.

Other Measurements. To characterize the morphology of the MEH-PPV with Hg, analysis by transmission electron microscope (TEM), JEM-2000 FX electron microscope, JEOL, was performed at a bias voltage of 100 kV. Polymer solutions were prepared at 1 mg/mL MEH-PPV in benzene. Hg3 powder was weighed and directly added to the solution, stirring moderately overnight. For the lower wt.% solutions, a stock solution in benzene (0.6 mg Hg3 dispersed per mL) was prepared and while stirring the stock solution, an aliquot of Hg3 was transferred into the TEM solution. For TEM, sample preparation involved the deposition of the polymer solution onto a 300-mesh Holey carbon-coated copper grid and allowing the sample to dry before analysis. Vapor phase staining with OsO_4 is used for imaging the polymer samples by TEM.

X-ray powder diffraction measurements (XPert Powder) with monochromatic Cu Kα radiation (λ = 1.540562 Å) were performed to determine the structure of the powder. Diffraction data were collected at room temperature by step scanning in the range $3° \leq 2\theta \leq 25°$ with a step size of 0.0167° and a counting time of 30 s at each step. Films were prepared from sample solutions in benzene with 5 mg/mL MEH-PPV concentration stirred overnight. Hg3 powder was weighed and added directly to the solution, stirring

vigorously for 2 days. Films were made by doctor-blading the solutions onto clean-glass slides for XRD analysis. The doctor-blading procedure is as follows: Three layers of Scotch Magic Tape were used to section off a portion of the glass slide (about 3 cm x 2.5 cm) and 150 µL of solution was pipetted to one edge of the slide. A flat edge was used to sweep along the tape, evenly covering the glass slide between and wiping off excess solution. The films were allowed to dry for several hours before analysis.

The cyclic voltammetry measurement was performed in dichloromethane with a conventional three electrode cell configuration on a BAS CV-50W voltammetric analyzer equipped with a platinum disk working electrode (2 mm^2), and platinum and silver wires were used as the counter and reference electrodes, respectively. All electrodes were polished and rinsed with water before use. Tetrabutylammonium hexafluorophosphate (TBAH), 0.1 M, was used as the supporting electrolyte. The concentration of Hg3 was approximately 3 mM. The cyclic voltammogram was calibrated using ferrocene as a standard taking its potential as 0.41 vs. Ag/AgCl.[163] The scan rate was 100 mV/s and the sensitivity was 10 µA/V.

CHAPTER 5
PHOTOPHYSICAL STUDY OF CATIONIC OLIGOMERS IN A CLAY HOST

Introduction

Poly(phenylene ethynylene) (PPE) and oligo(phenylene ethynylene) (OPE) derivatives have been studied extensively in recent years due to their photophysical and photochemical properties. One application of PPEs with cationic endgroups are aseffective light-activated biocides in water solution due to their ability to coordinate with the anionic bacterial membrane which can itself cause cell death.[164-167] It has also been shown that singlet oxygen plays a vital role in the light-inactivation of bacteria.[168-171] Upon irradiation with light, singlet oxygen is readily produced by energy transfer from the triplet state.[172] There is a positive correlation between the triplet quantum yield and lifetime of oligo(phenylene)ethynylenes and their biocidal activity.[165]

Immobilizing light-induced biocidal complexes onto a material surface has been a topic of study in recent years as more efficient and effective antimicrobial agents are needed to combat increasing antibiotic-resistent bacterial strains.[173-175] In an article by Tiller and coworkers in 2001, methods were explored for attaching *N*-alkylated poly(4-vinylpyridine) to a glass surface and evaluated the cell killing on the dry glass surface.[176] The biocidal activity of polymer films containing singlet-oxygen sensitizers such as fullerene have also been reported.[177] Incorporating photoactive chromophores into clay scaffolds can produce interesting effects relevant to photocatalysis, photoluminescence, photochromism, and nonlinear optics.[178,179] Layered materials, such as clay, offer an expandable interlayer space where guest compounds can be intercalated. This intercalation constrains and organizes the geometry of the guest compound resulting in nanostructured materials with unique properties.[180,181] Further,

nanofilms of clays containing cationic dyes or polymers can be produced with two levels of organization: an association: an organization of molecules onto the clay surface and a secondary organization on the individual clay sheets.[182,183]

In 1999, Winkler reported the solution intercalation of poly(p-phenylene)vinylene into a smectite clay host and the resulting photoluminescent and electroluminescent properties including those of a single layer LED device containing the polymer-clay hybrid.[184] An interesting report by Neumann, Cione, and Gessner in 2001 shows that the emission properties of aromatic hydrocarbons in a Laponite clay can be modified by the exchange of the Na^+ or Li^+ cations in the clay with heavier metals Rb^+, Cs^+, and Tl^+.[185] In this study, decreased singlet lifetimes and increased phosphorescence were observed as an effect from enhanced spin-orbit coupling provided by the presence of the heavier metal atoms. Additionally, the hydrocarbons on the clay surface exhibited aggregation dependence on the concentration of heavier cations due to a decrease in surface area of the heavy-cation exchanged clay. Their results illustrate the ability to tune the photophysical properties of chromophores by incorporation into a clay framework.

Conjugated oligomers and polymers in clay hosts have received considerable attention for their novel electronic and optical properties in the confined interlayer space.[186,187] One of the major difficulties in working with conjugated oligomers and polymers is controlling aggregation because of the presence of strong interchain interactions.[136,188] An investigation of the effect of supramolecular organization on oligo(phenylene)ethynylenes by Whitten and coworkers in 2009 when the OPEs were assembled to anionic nanoparticulate scaffolds such as Laponite.[189] The cationic OPEs

participated in strong host-guest interactions with these anionic scaffolds and the formation of J-dimers upon intercalation into the clay suggested an increase in effective conjugation length. More recently, a polyfluorene derivative was incorporated into a clay nanocomposite by Tozoni resulting in a blue-shifted photoluminescence with a significant increase in intensity.[190] In this case, it was observed that the strong tendency for polyfluorenes to aggregate by π-stacking was overcome simply by stirring a solution of the polymer with clay particles.

This current study involves the solution intercalation of oligo-phenylene ethynylenes (OPEs) into a clay matrix as represented in Figure 5-1, and the properties of the oligomer/clay hybrid are investigated.

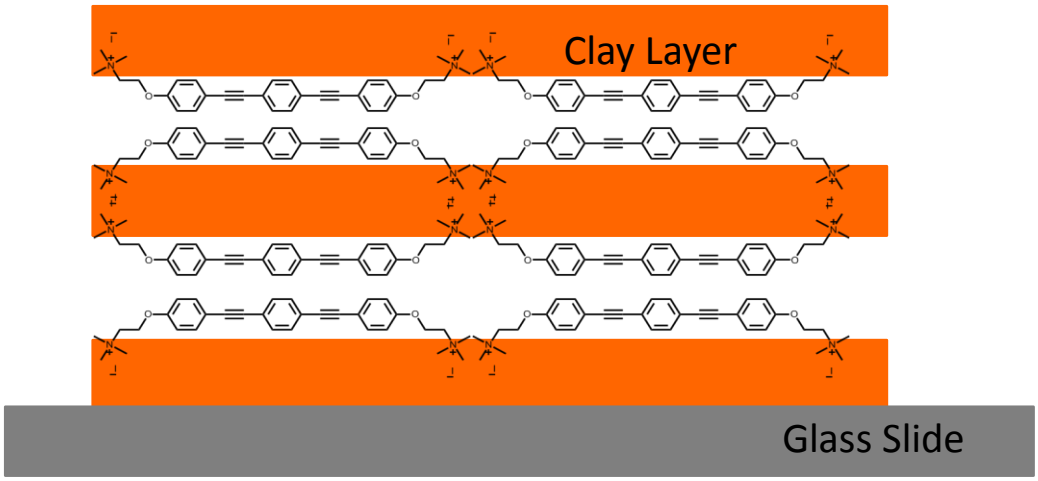

Figure 5-1. Representative drawing of the intercalation of a cationic oligomer into the clay interlayer spaces in a film.

Sumectin SA (SSA) is an artificially synthesized cation-exchangeable clay (synthetic saponite) obtained from Kuminine Ind. Co. with a stoichiometric formula of $[(Si_{7.20}Al_{0.80})\ (Mg_{5.97}Al_{0.03})\ O_{20}\ (OH)_4]^{-0.77}\cdot(Na_{0.49}\text{-}Mg_{0.14})^{+0.77}$ as shown in Figure 5-2.[191] It is a layered silicate which consists of a layer of Al or Mg octahedra between two layers of Si tetrahedra. SSA a highly pure clay that is easily dispersed in water and

transparent in the UV-visible region. The cationic exchange capacity (CEC) of SSA is 99.7 meq./100 g and the layer thickness is 0.96 nm. This CEC means that a solution of SSA prepared to 20 mg/L will be approximately 20 µeq./L (2.0×10^{-5} anionic sites per L). Between anionic sites, the average distance is approximately 1.2 nm.[191,192]

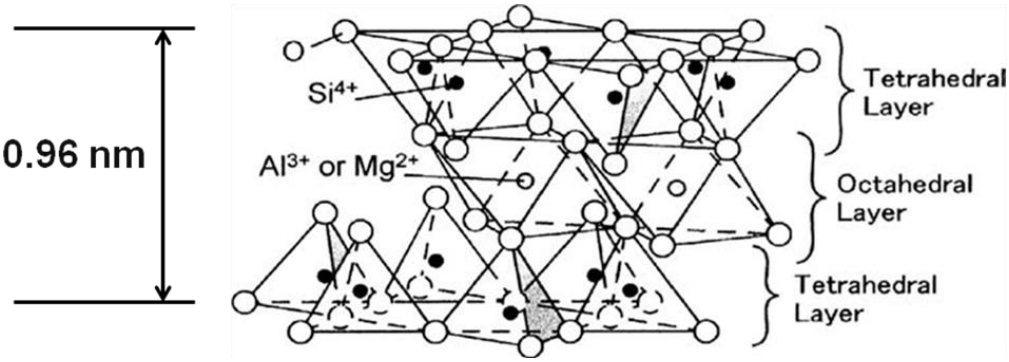

Figure 5-2. Structure of Sumectin SA (SSA) clay that was used in this analysis.[191]

Two cationic oligomers shown in Figure 5-3, EO-OPE-C2 and EO-OPE-Th, which were synthesized by Anand Parthasarathy and Subhadip Goswami were used in this study. These oligomers have been previously studied for their light-activated killing of bacteria and their photophysical properties in methanol and in water have been fully characterized.[165] Both oligomers have two quaternary nitrogen endgroups capable of cation exchange with the ions present in the clay. The goal of this research is to intercalate the oligomers into the clay interlayer spacings and examine the effect on the photophysical properties of the oligomers.

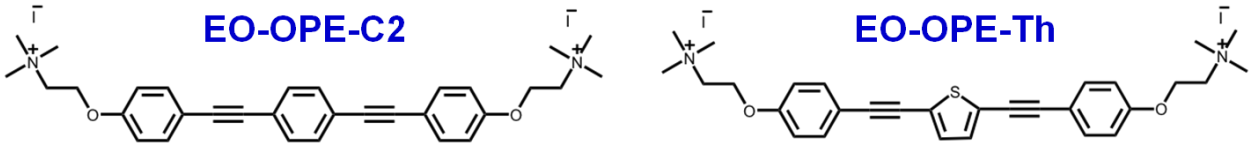

Figure 5-3. Structures of the cationic oligomers EO-OPE-C2 and EO-OPE-Th.

Absorption and emission measurements show aggregation of the oligomers onto the clay surface, and XRD analysis is used to verify insertion of the oligomers into the

interlayer spaces of the SSA. TGA allows a quantitative measurement of the amount of oligomer incorporated onto the clay substrate, which is supported by the absorption/fluorescence titration data. Transient absorption of the oligomer/clay thin films shows strong triplet-triplet absorption of both oligomers which indicates that these materials may have a promising future for triplet state applications such as singlet-oxygen sensitized light-activated biocides.

Solution Studies

The cationic oligomers EO-OPE-C2 and EO-OPE-Th in water have absorption in the near-UV region with maxima of 327 and 354 nm, respectively.[165] The absorption of the thienylene-containing oligomer, EO-OPE-Th, is slightly red-shifted. Upon addition of SSA to water solutions of the oligomers, there is an increasing red-shift in the absorption maxima accompanied with a growth of a structured red-shifted absorption peak which indicates the presence of aggregation of the oligomers onto the clay substrate as shown in Fig. 5-4.

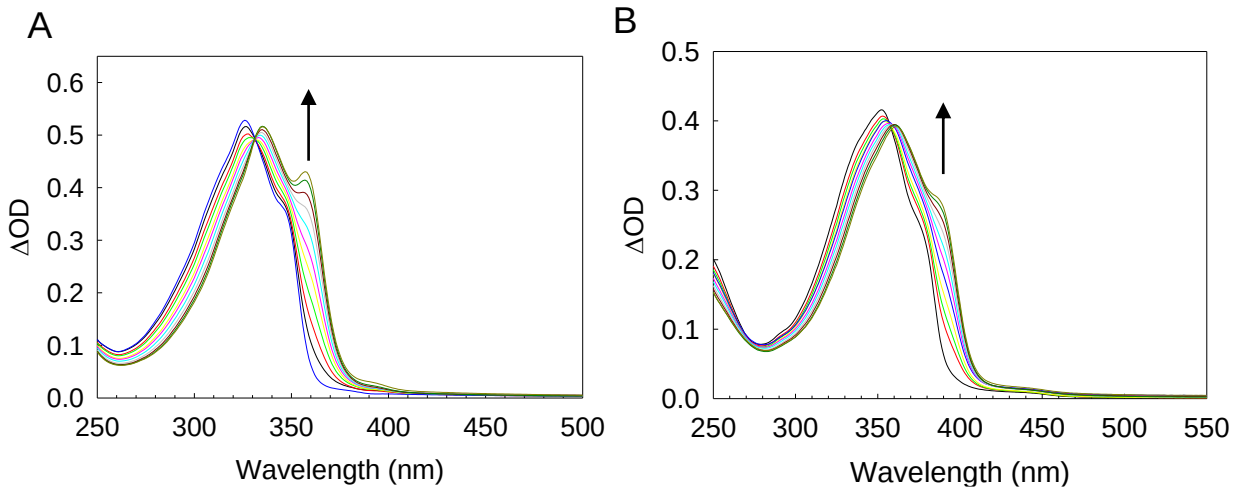

Figure 5-4. The absorption spectra acquired by Eduardo Acosta of 4 μM of oligomers EO-OPE-C2 (A) and EO-OPE-Th (B) with increasing concentration of SSA in water from 0 to 16 μeq./L.

The fluorescence of the oligomers is shown in Fig. 5-5. The emission is quenched with increasing additions of SSA and a new peak appears around 470 nm which can be assigned to the oligomer/SSA hybrid. In both cases, the fluorescence emission after addition of SSA becomes broadened, and in the fluorescence spectrum of EO-OPE-Th, the fluorescence loses its vibronic structure in the clay substrate. An isosbestic point is present in both oligomer/SSA titrations indicating a two-component system whose components are the free oligomer and the oligomer/clay hybrid. After a certain amount of SSA has been added, the original oligomer fluorescence is nearly entirely quenched and settling of the clay-oligomer hybrid occurs as indicated by a loss of the isosbestic point in the fluorescence spectrum. This settling occurred at a concentration of 16 μeq./L SSA for EO-OPE-C2 and 18 μeq./L for EO-OPE-Th. This corresponds to 25% (vs. CEC) for EO-OPE-C2 and 22% (vs. CEC) for EO-OPE-Th. This provides a minimum approximation of the saturation point of the clay surface.

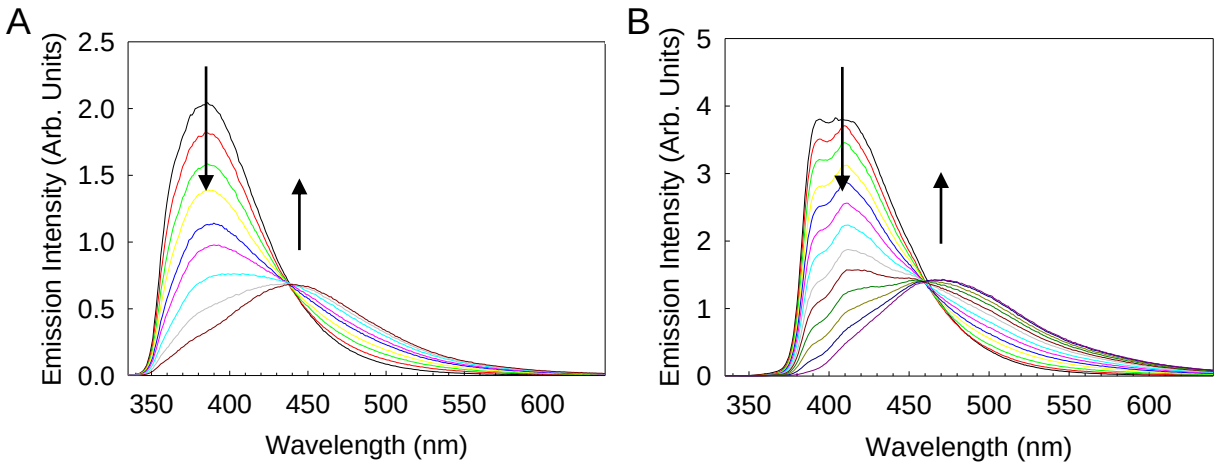

Figure 5-5. The emission spectra acquired by Eduardo Acosta of 4 μM of the oligomers (A) EO-OPE-C2 and (B) EO-OPE-Th upon addition of SSA in water from 0 to to 16 μeq./L.

The fluorescence lifetimes of the oligomers at 410 nm in water were measured to be τ_{ave} = 0.54 ns for EO-OPE-C2 and τ_{ave} = 0.29 ns for EO-OPE-Th, which is similar to

previously reported fluorescence lifetimes in methanol.[165] At 470 nm in the 25% CEC oligomer/SSA solutions, the fluorescence lifetimes become more complex reflecting an increasingly heterogeneous environment. Fitting the lifetimes to a triexponential, the average lifetime at 470 nm increases to τ_{ave} =1.4 ns for EO-OPE-C2 but decreases for EO-OPE-Th to τ_{ave} = 0.034 ns. The increased lifetime in the EO-OPE-C2 oligomer indicates a reduction of the nonradiative decay processes such as vibrational relaxation due to restricted movement in the rigid clay substrate. The EO-OPE-Th oligomer has a shorter fluorescence lifetime than EO-OPE-C2 because of spin-orbit coupling induced by the heavy sulfur atom. When the EO-OPE-Th oligomer is incorporated into the clay interspace, molecular movement is restricted. A decreased fluorescence lifetime is observed because this enhances the conjugation along the backbone leading to increased intersystem crossing by spin-orbit coupling.

Solid-State Measurements

Films of the oligomer-clay hybrids were prepared by the filter paper transfer method. Oligomer/SSA solutions were prepared in water with an excess of oligomer to ensure saturation of the clay. The solutions were filtered and rinsed with copious amounts of water to remove any free oligomer. The wet filter paper was then pressed firmly onto clean glass slides and peeled gently to leave behind the oligomer/clay hybrid film. Films were dried in an oven overnight.

Oligomer/SSA film emission spectra are reported in Fig. 5-6. The emission spectra of the oligomer/SSA films are very similar to the solution measurements with the highest concentration of clay. There is only a slight red-shift of the emission maxima compared to the solution measurements revealing that the excited state of the oligomer after incorporation into the SSA is very similar to that present in water solution.

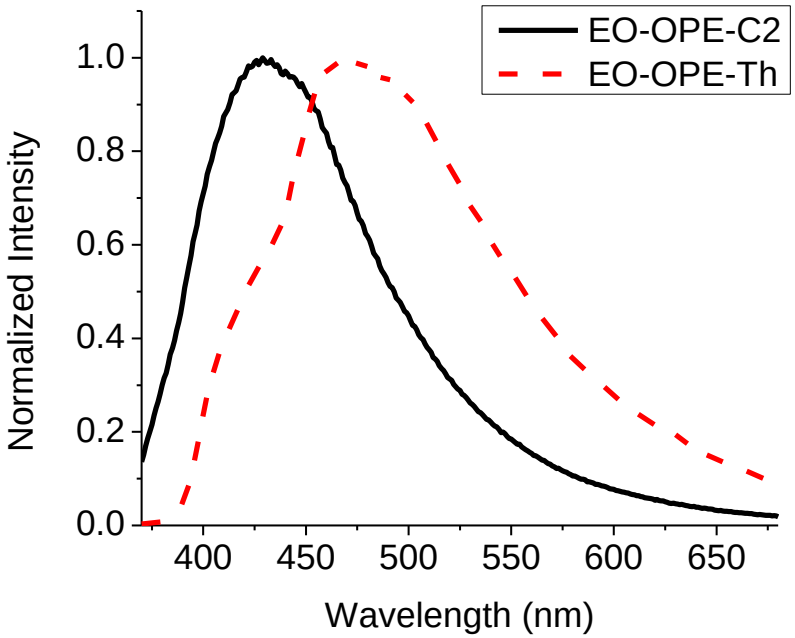

Figure 5-6. Emission spectra of oligomer/SSA hybrid films. Emission scans were performed using a front-face configuration with excitation at 350 nm.

There is a short-wavelength shoulder on the EO-OPE-Th fluorescence spectrum may indicate the presence of unbound oligomer on the film. Since the films were rinsed copiously with water, this is unlikely. Most likely, due to the non-linear structure of EO-OPE-Th, there is less uniform packing of the oligomer into the interlayer. Possibly, some oligomers are absorbed to the clay at only one of the two cationic side-groups causing a “free-oligomer”-like band in the emission spectrum of EO-OPE-Th.

The transient absorption spectra of the oligomer/SSA films are shown in Figure 5-7. Both films display triplet-triplet transient absorption between 500-800 nm with excitation at 355 nm nanosecond pulses. The transient absorption intensity of the EO-OPE-C2/SSA hybrid compared to the EO-OPE-Th/SSA hybrid is very weak. A higher triplet yield in the EO-OPE-Th oligomer is expected due to the enhanced intersystem crossing by the presence of the thiophene unit.

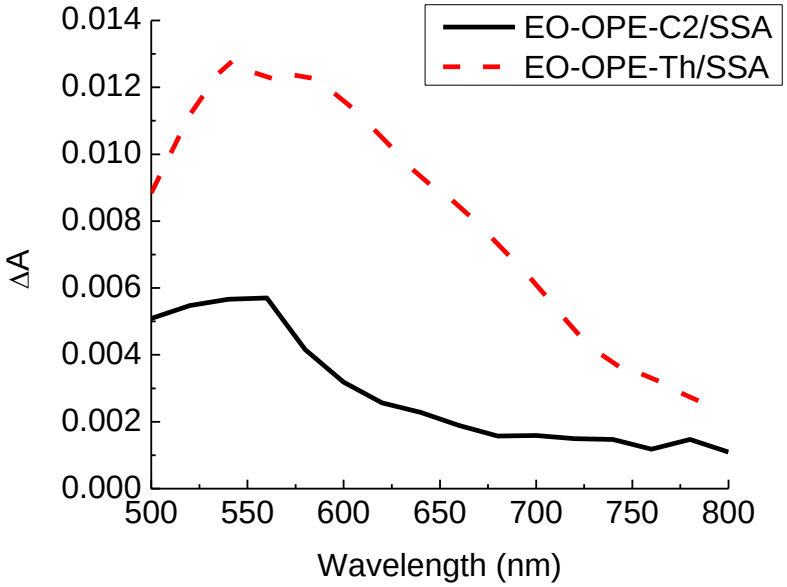

Figure 5-7. Transient absorption spectra of oligomer/clay hybrid films. Excitation was with nanosecond pulses at 355 nm, 800 μJ/pulse (128 averages, 1 kΩ termination, smooth 10).

The transient decays at λ_{max} appeared biexponential with a very long lived component and a shorter component. The long component of the EO-OPE-C2 was out of the instrumental range, >10 ms, but the shorter component was measured to be 18.5 μs. Previous measurements of the free EO-OPE-C2 oligomer in water give a lifetime of 18.7 μs.[165] This again illustrates the similarity between the excited state properties in solution and in the clay substrate. The average lifetime of the EO-OPE-Th oligomer was measured to be τ_{ave} = 144 μs ($\tau_{1\ (67.3\%)}$ = 24.4 μs and $\tau_{2\ (32.7\%)}$ = 391 μs). The solution transient absorption lifetime for EO-OPE-Th in water was previously reported to be 7.2 μs.[165]

Oligomer/SSA hybrid solid was subjected to XRD analysis compared to unmodified SSA powder to verify intercalation of the oligomer into the interlayer of the clay and measure the interlayer spacing. The XRD spectra are shown in Figure 5-8.

Pure SSA shows a peak around 6.7° that shifts to smaller angles upon addition of EO-OPE-C2 and EO-OPE-Th, 5.7° and 5.5°, respectively. From these results, it is evident that the layer spacing of the SSA is increased upon addition of both oligomers and that intercalation of the oligomers into the interlayer spaces of the SSA has occurred. The width of a single layer of SSA is 0.960 nm with an interlayer distance of 0.360 nm. The layer spacing of EO-OPE-C2/SSA hybrid is 1.530 nm giving an interlayer distance of 0.570 nm. The layer spacing of the more nonplanar oligomer EO-OPE-Th/SSA hybrid is 1.571 nm giving an interlayer distance of 0.611 nm.

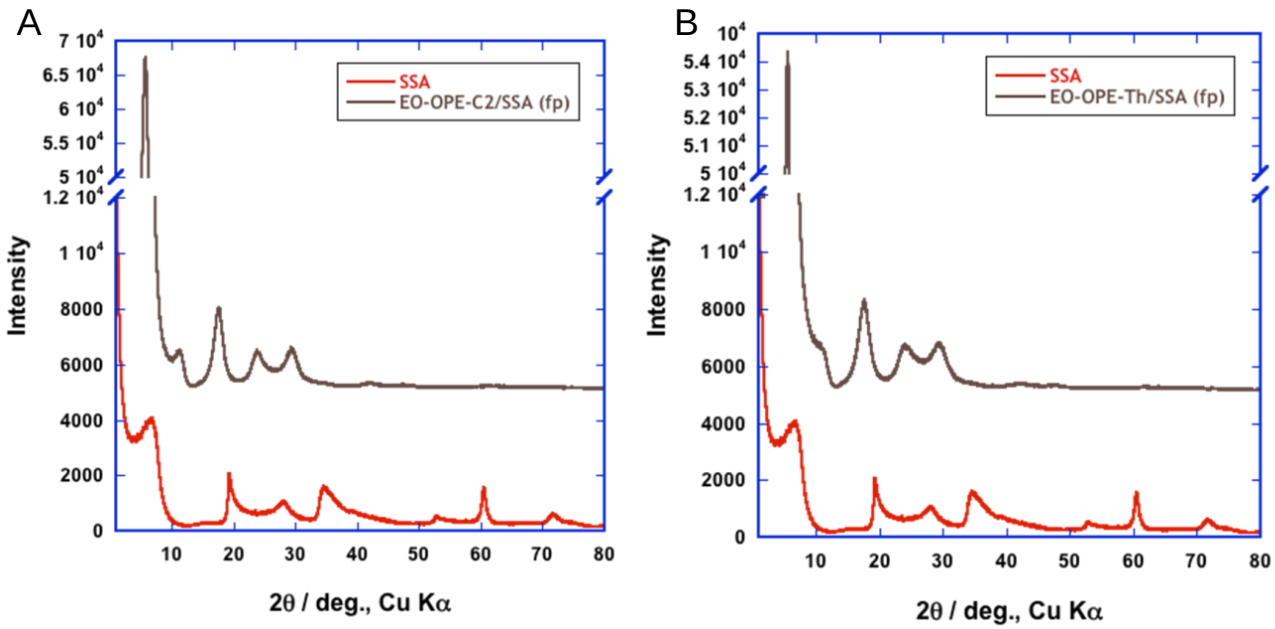

Figure 5-8. X-ray diffraction patterns of the oligomer/SSA hybrids acquired by Akino Uchikoshi at Tokyo Metropolitan Univesity (A) EO-OPE-C2 and (B) EO-OPE-Th. The unmodified SSA powder XRD is shown in red while the oligomer/SSA hybrid XRD is shown in brown.

With the assistance of Dr. Galyna Dubinina, Chimera 1.8 software (after MM2 geometry optimization) was used to estimate the length and width of the oligomers in order to get a better understanding of the orientation of the oligomers in the clay

interlayer space. The distances are measured from atom center to atom center. Distances between the van der Waals radii will be slightly larger. The 3D structures and

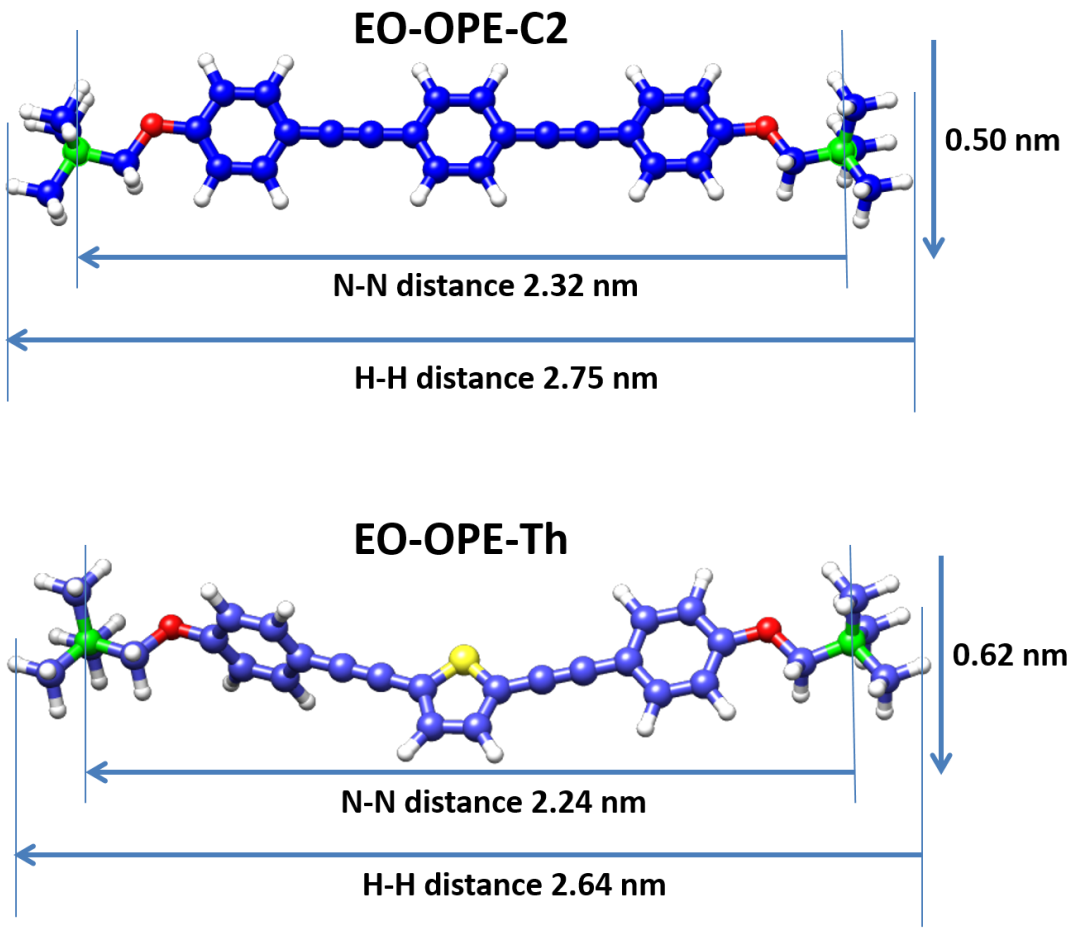

Figure 5-9. 3D structures of the cationic oligomers made by Chimera 1.8 software after MM2 geometry optimization. Distances are measured from the atom centers.

approximate distances are shown in Figure 5-9. The widths of the oligomers, 0.50 nm for EO-OPE-C2 and 0.62 nm for EO-OPE-Th calculated by Chimera, are similar to the interlayer spacing of the SSA layers after insertion of the oligomer measured by XRD in Figure 5-8 (0.570 nm for EO-OPE-C2/SSA the film and 0.611 nm for the EO-OPE-Th/SSA film). This suggests that the oligomers are intercalated into the clay in a single layer. The lengths between the nitrogen atoms of the cationic endgroups are 2.32 nm

for the EO-OPE-C2 oligomer and 2.24 nm for the EO-OPE-Th oligomer. Since the distance between anionic sites in the clay is about half the length of the oligomers, it's likely that at least one "unused" anionic site will lie between the two anionic sites in the clay layer which are accessed by the cationic endgroups of the oligomer. Thus this A es the limit to adsorption at less than 2/3 of the sites, or ~66% (vs. CEC).

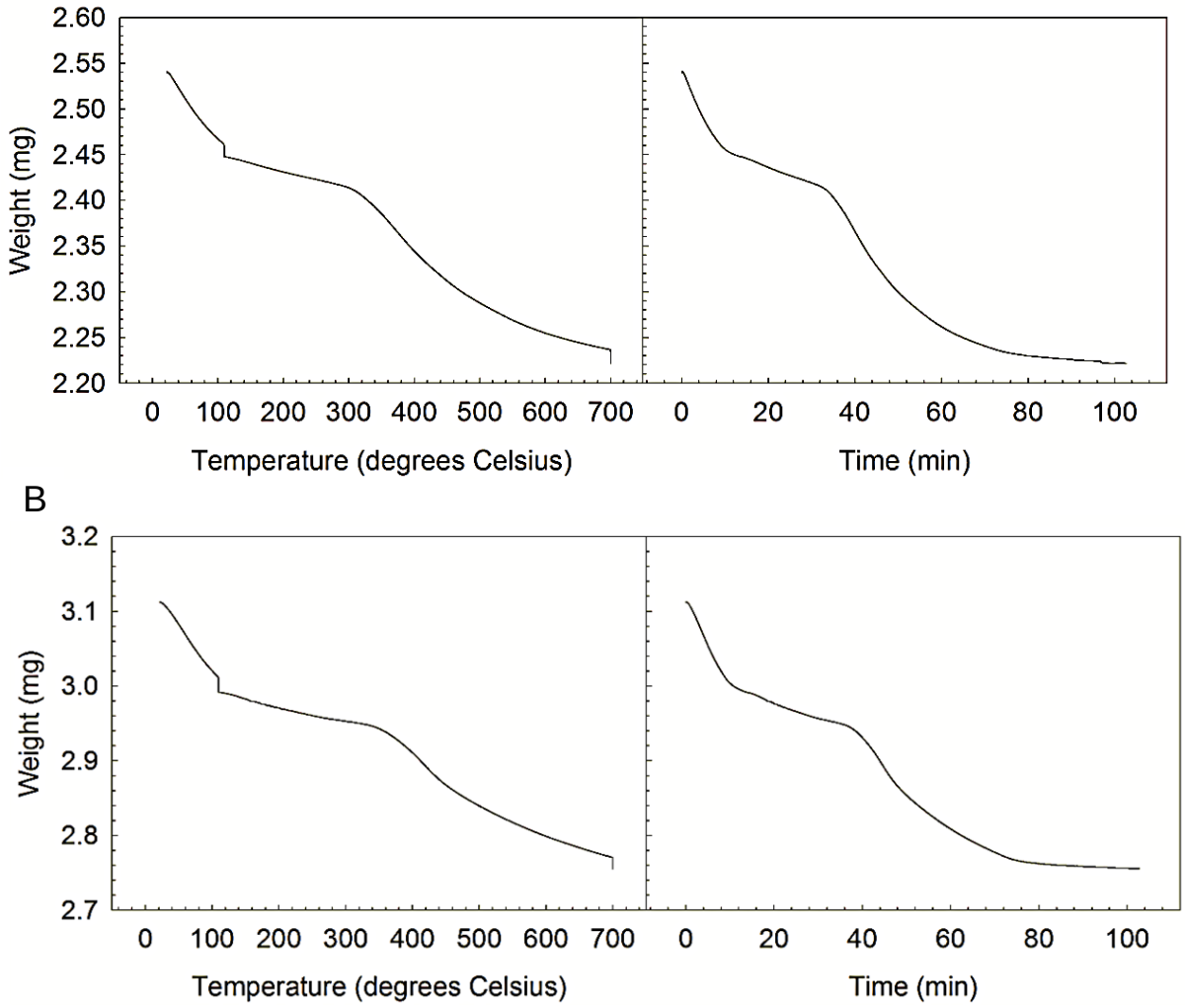

Figure 5-10. TGA analysis of the (A) EO-OPE-C2/SSA and (B) EO-OPE-Th/SSA solid. Correcting for water loss, the weight change due to loss of EO-OPE-C2 is 8.32% and the weight change due to loss of EO-OPE-Th is 7.55%.

To determine the amount of oligomer adsorbed into the clay substrate, solids of each oligomer/SSA hybrid were subjected to TGA analysis as shown in Figure 5-10 with

a temperature ranging from room temperature up to 700°C. The inorganic clay SSA is stable at 700°C, so the mass loss of the hybrid can be attributed to water and oligomer. The oligomer mass was calculated as the difference in the ending mass at 700°C/100 minutes and the mass after water evaporation during a hold at 110°C. The adsorption calculated from the TGA data is 37.7% (vs. CEC) for EO-OPE-C2 and 33.5% (vs. CEC) for EO-OPE-Th.

Summary of Results

The intercalation of cationic oligomers, EO-OPE-C2 and EO-OPE-Th, into Sumectin SA clay and the effect on the photophysics of the oligomers was studied. In solution, the interaction with the clay led to a slight red-shift in both the absorption and emission spectra. In the absorption spectra, with increasing concentrations of clay added there was a more structured emission indicating ordered aggregation of the oligomers onto the clay. The fluorescence of the oligomers with increasing amounts of clay is quenched and a very broad, structureless band appears. Precipitation occurred at concentrations of clay corresponding to 25% (vs. CEC) for EO-OPE-C2 and 22% (vs. CEC) for EO-OPE-Th placing a lower limit on the amount of oligomer adsorbed onto the clay. The fluorescence lifetimes in solution of the oligomers in concentrated clay solutions became more complex. The fluorescence lifetime of the EO-OPE-C2/SSA solution increased compared to free EO-OPE-C2 in water from τ_{ave} = 0.54 ns to 1.4 ns. Conversely, for the EO-OPE-Th/SSA solution, the fluorescence lifetime increased from τ_{ave} = 0.29 ns measured of the pure EO-OPE-Th solution to τ_{ave} = 0.034 ns. Both changes in lifetime can be explained by the more restrictive environment of the rigid clay substrate. The molecular geometry of the oligomers in the clay interlayer is more confined and reduces the rate of internal conversion by vibrational relaxation, thus

increasing the lifetime of the radiative process. In EO-OPE-Th, a heavy sulfur atom is present. A more restrictive geometry can improve orbital overlap and enhance intersystem crossing by increased spin-orbital coupling leading to a decreased fluorescence lifetime.

In oligomer/SSA film measurements, the emission spectra is only slightly red-shifted compared to the solution measurements after addition of SSA indicating similar excited state energetics. The EO-OPE-C2/SSA film exhibited a broad-featureless emission whereas the EO-OPE-Th/SSA film emission displayed a red-shifted band which may correspond uneven intercalation of the oligomer. The nanosecond transient absorption spectra of the films show relatively strong, broad, and long-lived transient absorption for both EO-OPE-C2/SSA and EO-OPE-Th/SSA. In agreement with the fluorescence lifetime results for EO-OPE-Th in solution, the transient absorption for EO-OPE-Th/SSA was significantly more intense compared to EO-OPE-C2 due to the triplet yield of the EO-OPE-Th oligomer.

The interlayer spacing of the clay increased upon addition of the oligomer as was measured by XRD confirming that intercalation has occurred. For EO-OPE-C2/SSA, the interlayer space increased from 0.360 nm in pure SSA to 0.570 nm upon intercalation of the oligomer. The EO-OPE-Th/SSA film had an interlayer space of 0.611 nm. The interlayer spacing is larger for EO-OPE-Th/SSA than that for EO-OPE-C2/SSA due to the rigid, non-linear backbone introduced by the thiophene unit present in the middle of the oligomer. 3D models of the oligomers support the interlayer spacings calculated from the XRD data suggesting that the oligomers are unagreggated and in a single layer in the interlayer space. The amount of oligomer absorbed onto the

clay was measured by TGA. It was found that the amount of the oligomer adsorbed was at 37.7% (vs. CEC) for EO-OPE-C2/SSA and 33.5% (vs. CEC) for EO-OPE-Th/SSA. These findings are consistent with the observed precipitation during the fluorescence titration in water.

Experimental Section

Materials. Sumectin SA was a gift from Dr. Haruo Inoue from Tokyo Metropolitan University and was purchased from Kunimine Industries Co., Ltd. The oligomers, EO-OPE-C2 and EO-OPE-Th were synthesized in the Schanze group by Anand Parthasarathy and Subhadip Goswami. Water was purified using a Millipore system to a resistivity of 18.0 megaohms.

Preparation of Films. Films were prepared by the filter paper transfer method. A solution of clay saturated with oligomer was prepared in ultrapure water and filtered through filter paper, washing at least 3 times with copious amounts of water to eliminate any excess oligomer. The wet filter paper was pressed firmly onto a clean glass slide and slowly peeled away leaving behind a clay-oligomer hybrid film.

Photophysical Measurements. Photophysical properties for solutions were measured in ultrapure water using a 1-cm pathlength quartz or borosilicate cuvette. Ground state absorption and emission experiments were performed by undergraduate research student, Eduardo Acosta. Ground state absorption spectra were collected on a Varian Cary 100 dual-beam spectrophotometer with water as the instrument baseline blank. Corrected steady-state emission measurements were collected by a Photon Technology International (PTI) photon counting fluorescence spectrophotometer.

Fluorescence lifetimes were obtained by time-correlated single photon counting technique (TCSPC) with a PicoQuant FluoTime 100 compact fluorescence lifetime

spectrophotometer. A UV-pulsed diode laser provided excitation at 375 nm (power < 10 mW). The laser was pulsed by a PDL800-B pulsed diode laser driver. Fluorescence decays were obtained using 10 nm bandpass interference and analyzed from the fluorescence decays using exponential fitting parameters (FluoFit software). The emission lifetimes of the pure oligomers in water were fit to biexponential decays: 0.84 ns (20.5%) and 0.46 ns (79.5%) for EO-OPE-C2 and 1.1 ns (3.2%) and 0.19 ns (96.8%) for EO-OPE-Th at 410 nm. Upon addition of SSA to an approximate CEC of 25%, at 410 nm the EO-OPE-C2/SSA solution lifetime was fit to a triexponential decay: 7.9 ns (2.1%), 2.4 ns (12.8%), and 0.48 ns (85.1%) and for EO-OPE-Th/SSA solution triexponential fit is 3.3 ns (0.8%), 0.96 ns (8.9%), and 0.20 ns (90.3%). The lifetime was also measured for both oligomers at 470 nm, where the new emission peak arises after addition of the SSA. In the 25% CEC EO-OPE-C2/SSA solution, the lifetime components were the same, but the long lifetime components have a larger contribution to the overall lifetime than in the emission at 410 nm: 7.6 ns (7.0%), 2.3 ns (30.7%), 0.34 ns (62.3%). However in the 25% CEC EO-OPE-Th/SSA solution measured at 470 nm, all the lifetime components at 470 nm are significantly shorter than the lifetime components at 410 nm: 1.4 ns (<1%), 0.19 ns (7.5%), 0.007 ns (92.4%).

Film photophysics were measured freestanding, open to atmosphere without a cuvette. Absorption spectra were not obtained due to saturated OD. Emission spectra were obtained by a front-face alignment on a Fluorolog 3 spectrophotometer. Transient absorption measurements on films were performed using an in-house designed TA instrument dedicated to film measurements. The third harmonic of a Continuum Surelite I-10 Nd:YAG laser at 355 nm (600 μJ/pulse) was used as the pump beam in an

antiparallel alignment to the probe beam provided by a 250 W QTH lamp (Newport). Single-wavelength transient absorption decays were acquired as an average of 128 shots every 25 nm using a Hamamatsu R928 PMT and an in-house modified base using 5 of the 9 stages for amplification. The transient absorption spectrum was acquired by using a custom Matlab program to convert the transient absorption decays at each wavelength to a transient absorption spectrum at t=0. The transient decay at λmax for the EO-OPE-C2/SSA film shows a biexponential decay with a shorter lifetime of 18.5 μs (54.8%) and a very long-lived component of 431 ms (45.2%). The lifetime fitting of the EO-OPE-Th/SSA to a biexponential decay yields lifetimes of 24.4 μs (67.3%) and 391 μs (32.7%).

TGA was measured on a TA instruments model Q5000. About 2.5 - 3 mg of solid was placed into the sample pan, and the temperature program used was as follows, a ramp of 10°C/min from room temperature to 110°C, a 5 minute hold, a 10°C/min ramp to 700°C, and a final 30 min hold.

XRD analysis was carried out at Tokyo Metropolitan University by Akino Uchikoshi on a Rigaku RINT-TTR II instrument with monochromatic Cu Kα radiation (λ = 1.540562 Å, 50 kV, 30 mA). Scan rate was 1°/min in 2θ/θ mode. The oligomer/clay films studied by XRD were prepared by the filter paper transfer method and compared against the XRD profile of pure SSA powder.

CHAPTER 6
CONCLUSION

The work reported here investigated the excited state dynamics of conjugated molecules, oligomers, and polymers in solution and in the solid-state with a focus on the triplet state properties for applications such as optical power limiting, photovoltaic devices, and biocidal action. Demonstrated were three methods of designing solid-state materials with desired triplet state properties. The first was by covalent bonding of a two-highly conjugated ligand with a heavy metal, such as platinum, and incorporating the complex into an inert polymer matrix, which was discussed in Chapter 3. Another approach was to prepare blended films containing a conjugated polymer and a heavy-metal containing compound, such as Hg3, as described in Chapter 4. Lastly, intercalation of a cationic oligomer into a solid matrix like clay that contains heavy metals was investigated in Chapter 5.

Transient Absorption Instrumentation for Thin Films

In all the work herein, the triplet state properties were investigated by use of a newly constructed nanosecond transient absorption spectroscopy system specifically designed for solid-state analysis. A Surelite I-10 Q-switched Nd:YAG laser was used as the pump source, and a Newport 250 W quartz tungsten halogen lamp is used as the probe. Detection is with either a Hamamatsu R928 photomultiplier tube (using 5 of the 9 stages for amplification) or a Thorlabs A110 avalanche photodiode for detection in the UV-Vis and nIR regions, respectively. The transient absorption system for thin films was used and validated using thin films made by spin-coating solutions of a model platinum acetylide polymer, pPtPh, in toluene under various conditions. The optimal settings for routine analysis were deduced by systematically varying the experimental parameters

and observing the quality of the transient decay collected of pPtPh films. Transient absorption of lower than $\Delta A = 10^{-3}$ was achieved which makes this system a valuable tool for analyzing the triplet state properties of thin films.

Solid State Materials for Optical Power Limiting

A series of *p*-phenylene vinylene platinum acetylide complexes were incorporated into PMMA monoliths with high transparency, stability, and optical quality for optical power limiting application. The mechanism for optical power limiting in these complexes is nonlinear absorption by combined simultaneous two-photon absorption and triplet-triplet excited state absorption. The photophysical properties of the PMMA monoliths were studied and compared to the properties of the *p*-phenylene vinylene platinum acetylides in solution. The important photophysical properties to nonlinear absorption, such as strong two-photon absorption, intense triplet-triplet excited state absorption, and good spectral overlap between the two, were retained in the PMMA monolith.

The PMMA monoliths containing the platinum acetylide complexes exhibited nonlinear absorption to nanosecond pulses. An effective nonlinear absorption coefficient, β_{eff}, was used to compare the nonlinear absorption of the chromophores in solution and in the PMMA monoliths. Similar values for β_{eff} were found between the solution z-scan results and those of the monolith measurement, especially for the linear *p*-phenyene vinylene platinum acetylide series indicating that these platinum acetylide chromophores are as effective optical power limiters in PMMA monolith as in solution.

Triplet-triplet annihilation was present in conjugated co-polymers containing phenylene and *p*-phenylene vinylene platinum acetylide units which was observed as very fast initial decay with increasing amplitude at increasing laser fluence in the

transient absorption. Representative “monomer” complexes did not show evidence of triplet-triplet annihilation. Tripet-triplet annihilation reduces the concentration of triplets after a certain threshold population is present which can affect nonlinear absorption by reducing the amount of photons absorbed by the triplet excited state. These results demonstrate that discrete molecules capable of two-photon absorption and strong triplet-triplet excited state absorption which are incorporated into polymer monoliths are a promising route to producing solid-state optical power limiting materials.

Triplet Sensitization of Conjugated Polymers by Hg3

The addition of trimeric perfluoro-*p*-phenylene mercury, Hg3, to conjugated polymers was investigated to determine whether Hg3 could sensitize the triplet state of the polymers by spin-orbit coupling which could be useful in photovoltaic applications where long-lived excitons may increase efficiency. The addition of Hg3 to MEH-PPV had interesting effects on the photophysical properties. Aggregation peaks in the absorption and emission of MEH-PPV characteristic of self-organization of the polymer were observed with increasing concentration of Hg3 added. Quenching of the fluorescence suggested enhanced intersystem crossing to the triplet state; however nanosecond transient absorption in solution did not show evidence of increased triplet state population upon addition of the Hg3. The transient absorption did show an absorption corresponding to the MEH-PPV radical cation which suggested that Hg3 can act as an electron acceptor which was confirmed by cyclic voltammetry experiments.

In MEH-PPV films containing increasing amounts of Hg3, there was a small increase in the transient absorption intensity of the triplet exciton peak of MEH-PPV., and the MEH-PPV radical cation absorption at 950 nm was also observed at high concentrations of Hg3. Additionally, the structure and morphology of MEH-PPV in films

upon addition of Hg3 was observed using ^{1}H NMR, powder XRD, and TEM. It was found that the side-chains of MEH-PPV become efficiently packed when Hg3 is added, and worm-rod shapes observed in the TEM point to templated aggregation of the polymer backbone by Hg3 similar to the ordering that is seen when MEH-PPV films are annealed after casting. This may be due to intercalation of the Hg3 between the aryl groups of adjacent polymer chains since the ^{1}H NMR shows significant shielding of the aromatic protons of the polymer once Hg3 is added.

The interaction of another conjugated polymer, P3HT, with Hg3 was also investigated. The absorption and emission spectra in solution displayed an increasing aggregation peak with increasing concentration of Hg3; however since P3HT inherently produces crystalline films, there was little effect on the photophysical properties of P3HT films when Hg3 was added. From these results, it is concluded that Hg3 may benefit photovoltaic applications of amorphous conjugated polymers such as MEH-PPV by improving the morphology of films without the need for additional treatment such as annealing.

Photophysical Study of Cationic Oligomers in a Clay Host

The intercalation of cationic oligomers into a synthetic saponite clay, SSA, was reported. Absorption and emission measurements revealed ordered aggregation of the oligomers upon addition of the SSA. A red-shift in both the absorption and emission spectra occurred and a quenching of the fluorescence was observed when SSA was added to solutions of the oligomers in water. Fluorescence quenching may be due to the presence of heavy atoms in the clay promoting intersystem crossing to the triplet state. The nanosecond transient absorption spectra of the films show relatively strong, broad, and long-lived transient absorption for both EO-OPE-C2/SSA and EO-OPE-

Th/SSA. Greater transient absorption was present in the EO-OPE-Th/SSA film than in the EO-OPE-C2/SSA film which is as expected due to the presence of the sulfur atom in the thiophene unit of EO-OPE-Th.

Analysis by XRD confirmed that the interlayer spacing of the clay increased upon addition of the oligomer. The interlayer space measured for the EO-OPE-C2/SSA film was 0.570 nm, and for the EO-OPE-Th/SSA film it was 0.611 nm. The interlayer space of pure SSA was 0.360 nm. A larger interlayer space for EO-OPE-Th/SSA is expected due to the more rigid, non-linear backbone. The XRD results and 3D models of the oligomers suggest that the oligomers are unagreggated and in a single layer in the interlayer space. The amount of oligomer absorbed onto the clay measured by TGA was 37.7% (vs. CEC) for EO-OPE-C2/SSA and 33.5% (vs. CEC) for EO-OPE-Th/SSA.

APPENDIX A
USER MANUAL FOR THE TRANSIENT ABSORPTION INSTRUMENT FOR THIN FILMS

TA System for Films

Randi Price
Installed June 2010
Latest revision: July 2013

This is the instruction manual for a transient absorption system for films installed 2010. These instructions are intended for users already aware of the safety precautions and operating limitations of all the components. Please check with Dr. Schanze or the TA Lab Manager if you are unsure how to operate any part of this system.

For more detailed explanations of each component, please refer to the manufacturer's original booklet. For a detailed explanation of experimental settings and calculations, refer to the additional information included at the end of this manual. Common troubleshooting problems are also included at the end of the acquisition instructions.

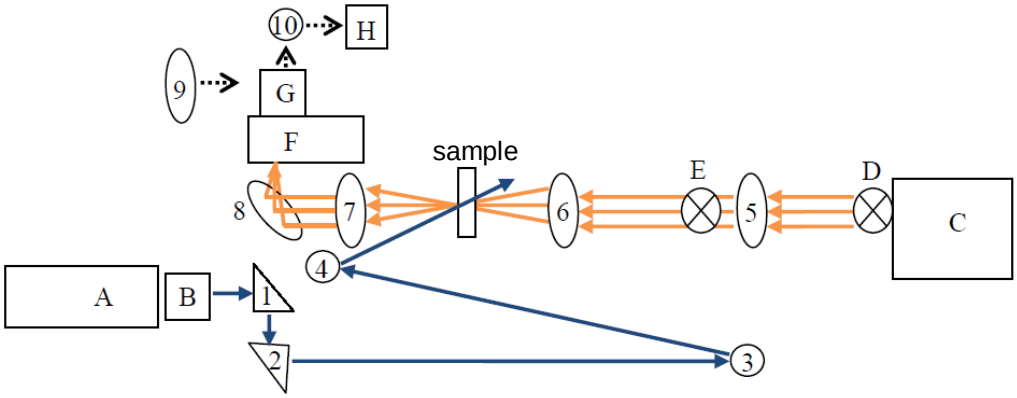

A few points on laser safety:

1. Never look directly into a laser beam. Be aware of reflections and scattered laser light. If you are unsure about where the laser path, do not turn on the laser!
2. Keep the beam at waist-level and contained within the blackouts around the laser table. Do not lean over the table putting your eye level to the laser beam.
3. For alignment, keep the laser power as low as possible (generally with a Q-Switch >400 μs). Wear proper eye protection when working with the laser.

Components:
A: Continuum Surelite I-10 Nd:YAG laser
B: Second and Third Harmonic Generator
C: Newport 250 W QTH Lamp
D: Slow Shutter
E: Fast Shutter
F: Cornerstone 130 Monochromator
G: Hamamatsu R928 PMT with in-house modified base
H: Thorlabs APD 110A

Optics:
1/2: 1" prisms
3/4/10: 1" mirrors
5: 10 cm focal length plano convex 2" lens
6: 10 cm focal length plano convex 2" lens
7: 10 cm focal length plano convex 2" lens
8: 10 cm focal length concave mirror
9: 5 cm focal length plano convex 2" lens
10: 5 cm focal length concave mirror

System Startup Routine:

1. Turn on the BNC 575 Pulse Generator.
2. Make sure the laser Q-Switch and Flashlamp BNC cables from the pulse generator are connected via a T-connector to the Film TA Q-Switch and Film TA Flashlamp BNC cables from the laser control box.
3. Turn on the laser.
    a. On the laser control box, turn the key a quarter-turn counterclockwise and allow the display to cycle through several groups of numbers.
    b. After the "Laser On" indicator lights up and the cooling pump is starts running, push the "Start/Stop" button and then the "Shutter" button. You will hear the shutter click open and the indicator lights on both buttons will be lit.
4. Turn on the Tektronix 3032B Oscilloscope. The oscilloscope will run a self-check. When it is finished, press any key to clear the screen.
5. Turn on the high voltage source for the PMT by flipping the orange switch. Set the dials to 730 V ("0" on the first dial, "700" on the second dial, "30" on the third dial, and "0" on the last dial).
6. Turn on the lamp by flipping the ON/OFF switch on the lamp power supply and pressing the "Lamp Start" button. The indicator should show 250 W. It

may fluctuate for a few minutes before it stabilizes. No warm-up time is required.

7. The default for this TA instrument is excitation with 355 nm laser and detection with the PMT detector. Please contact a lab manager to make the necessary changes to the system if necessary. Excitation at 532 nm and detection into the nIR is available.

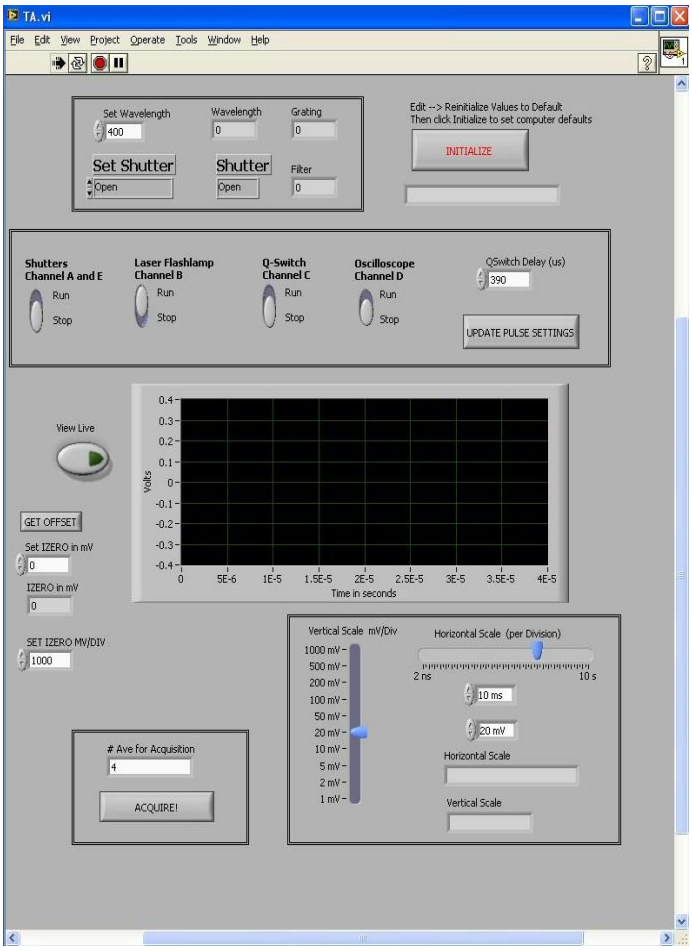

Program Start

1. On the computer, double click the "TA.vi" program on the desktop.
2. Click the white arrow to run the VI program continuously. The arrow will turn black when the program is running.
3. Click on the "Initialize" button at the top right hand corner. This opens communication to all the components and inputs the correct settings for the TA experiment. The indicator box below will indicate when the initialization is complete. The laser flashlamps will begin to fire.

Acquisition Setup

Optical Alignment

1. Make sure that Prism 1 (marked P1 on the optical table) is directed toward the Film TA system. If necessary, move the prism to the post closest to the laser output port and angled towards the Film TA.
2. Insert sample into the sample holder using a slitted business card.
3. Toggle on the "Shutters" switch and click "Update Settings".
   a. Make sure the sample slit is in the center of the lamp light beam. If necessary, adjust the vertical position of the sample holder or the horizontal position of the sample.
   b. Do not adjust the sample holder mount position or any of the surrounding optics.
4. Toggle off the "Shutters" switch and toggle on the "Laser Flashlamp" and "Q-Switch" switches. Make sure the Q-Switch delay is 380 μs or higher and click "Update Settings".
   a. Follow the laser beam path from the laser output port to the sample slit. Make sure that the laser hits in the center of all optics with no clipping of the beam.
   b. If necessary, adjust the horizontal or vertical knobs on the preceding optic to fix an offcenter or clipping beam on a prism or mirror.
   c. At this point, do not further adjust the sample holder.

Optimize Izero

1. Toggle off the "Laser Flashlamp" and "Q-Switch" switches and toggle on the "Shutters" and "Oscilloscope" switches and click "Update Settings".
2. At the top of the screen is the monochromator control. Choose a wavelength within your data acquisition and press Enter. The movement of the gratings should be audible and the wavelength indicator next to the control box should reflect the change in wavelength. A wavelength around 500-600 is a good wavelength at which to optimize IZero.
3. Move the filter wheel to an appropriate position for the wavelength.
4. At the lower right hand corner of the screen are the horizontal and vertical adjusters for the scope. Start with a 100 mV/div vertical setting and a 4 μs/div horizontal setting.
5. Observe the Izero level (the position of the baseline) directly on the scope screen. The PMT gives a negative signal. Increasing the magnitude of this negative signal will give a better signal to noise ratio. A good Izero should be over 2V. Maximize Izero using the following steps.

a. Adjust the large curved mirror before the monochromator using the horizontal and vertical adjuster knobs watching the scope to maximize the negative signal. If necessary, this mirror can be pivoted in its mount, but the mount should not be moved!Change the vertical setting on the scope using the software as needed to see the signal.
b. If Izero is still unsatisfactory (<1000 mV) after optimizing the position of the mirror, the monochromator slits can be adjusted. Note: The bandpass for this monochromator is 6-7 nm/mm. So a slit width of 0.5 mm gives a bandpass of ~3 nm. Adjust the entrance and exit slits as desired. For help in reading the micrometer, refer to the Cornerstone 130 motorized 1/8m Monochromator user manual.
    i. Apply a 10X multiplier to the micrometer markings to readout slit opening.
    ii. Each mark on the micrometer barrel corresponds to 10 μm of slit width. The "0" position is closed. One full turn of the barrel is equal to 250 μm of slit width. The default slit width is 500 μm.
    iii. Make sure both the entrance and exit slits are the same width.
c. If necessary, the PMT voltage can be adjusted up to 770 V to increase Izero. This will also slightly increase the noise level. The optimal PMT operating voltage is 730 V.

Acquisition Parameters

1. In the software, click "Get Offset". The program will compute Izero and return the value in the Izero indicator box. The oscilloscope will set the offset equal to Izero.
2. After a suitable Izero is computed, toggle on all 4 switches at the top of the screen, choose a QSwitch setting suitable for the acquisition (380 μs) and click "Update Settings".
3. Click the "View Live" button next to the waveform graph to view the TA signal on the computer or view the signal on the scope.
    a. Adjust the horizontal and vertical scale using the slide bars at the lower right-hand corner of the screen.
    b. The vertical scale should be such that the signal is fully on the screen and fills up as much of the screen as possible.
    c. The horizontal scale should be such that the signal decays all the way back to the baseline before the acquisition end.
    d. IMPORTANT: A vertical scale of less than 100 mV/div cannot be used!
    e. Note these settings.

4. Choose a few more wavelengths in the region of data acquisition and repeat steps 2-5.
    a. Make note of the Izero signal, and whether a larger mV/div setting is needed to compute Izero.
    b. Always use the largest needed Izero mV/div setting.
5. For data acquisition, the last inputted Izero mV/div setting will be used for EVERY wavelength. During data acquisition, this setting CANNOT be adjusted. Make sure to use an Izero mV/div setting large enough for all wavelengths of interest. Usually $Izero_{max}$ will be around 500 nm.

Acquiring TA Data:

1. At the bottom of the TA.vi screen, type in the number of waveforms to average for each acquisition and press Enter.
    a. The only available options are 4, 8, 16, 32, 64, 128, 512. If an unacceptable number is inputted, the scope will default to the closest option.
    b. Consider how sensitive the sample is to the laser pulse and how weak the signal might be. If sample damage is a concern, a lower number of averages potentially allows more acquisitions to be taken before a sample is damaged, but the baseline will be more noisy.
    c. 128 averages is a good choice for most samples.
2. Click "Acquire!" and the "Acquire!.vi" window will pop up.
3. On the top left of the screen enter in the "Wavelength Start", "Wavelength End", and the "Wavelength Step". Click "Update Scan Settings".
    a. If only one acquisition is needed, type the same wavelength into the starting and ending wavelength boxes and a 1 in the step wavelength box.
    b. On the right-hand top of the screen, the x of y indicator should update with the correct number of acquisitions.
4. In the center of the screen, type in a starting number filename for saving the data in the "Start at Temp File #" box.
    a. Data files will be saved to a "Temp Data Files" folder on the desktop.
    b. If the number in the "Start at Temp File #" box is 0, the first wavelength acquisition will be saved to file 0, the second to file 1, the third to file 2, etc.
    c. Data files saved to the same Temp File # will be overwritten!!
    d. If for any reason a run needs to be restarted, make sure the data temp file numbers remain continuous. This is important for the data processing program.

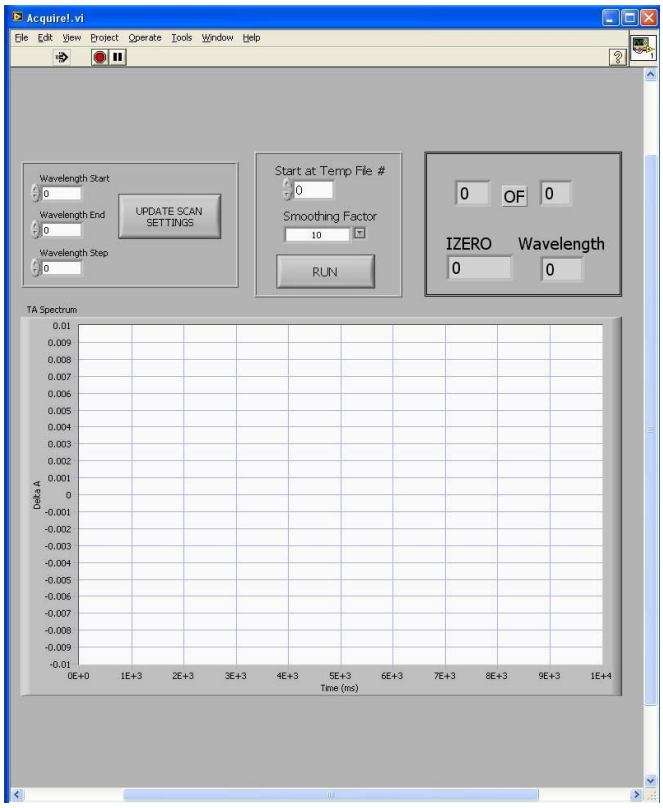

5. Choose a smoothing parameter. Smoothing results in a less noisy baseline and more manageable file size. See attached plots.
    a. A smoothing parameter of 1 is no smoothing.
    b. A smoothing parameter of 2 will average every 2 data points, reducing the 10,000 point data record to 5,000 points.
    c. A smoothing parameter of 10 will average every 10 data points, reducing the 10,000 point data record to 1,000 points.
6. The white graph at the bottom of the screen can be manually rescaled by double-clicking on the y-axis numbers and typing in the desired values. A good place to start is 0.001 and -0.001. The signal will appear for review after each iteration.
7. Click “Run”.
    a. The program will first compute Izero and then perform the TA acquisition for each wavelength using the settings specified on the “TA.vi” page 5.

    b. The indicator box on the top right of the screen will update with the wavelength being acquired, the Izero, and the x of y progress of the acquisition.

c. After acquisition at each specified wavelength, the TA signal will be displayed on the white graph in the middle of the screen and a pop-up box will appear: "Keep the same settings for the next iteration?"
    i. "Yes": The program will keep the horizontal and vertical scope settings the same for the next wavelength.
    ii. Select "No" to change settings. If you select "No", a new screen will pop up where settings can be changed for the next wavelength.
        1. IMPORTANT: There are default settings that appear on this screen, make sure to change ALL settings to your settings.
        2. After all settings are correct, click on "Save settings and return to acquisition" and the screen will close.
d. Select "End VI" and this will abort the VI. Any data already acquired will be in the Temp File folder on the desktop. To restart the acquisition, return to the TA window and click on the white arrow. Click on the "Acquire" button to return to the Acquisition window.

8. Repeat for all iterations.
9. After all data has been acquired, minimize the Acquisition and TA windows and transfer the temporary data files to your user folder on the server.
    a. Data is output in ΔA vs. Time (ms).
    b. NO PARAMETERS are saved in the data files.
        ii. Parameters that are important: wavelength start/stop/step, Izero, mV/div, time/div, # of averages, smoothing factor, scope termination.
        iii. Make note of these acquisition parameters in notebook or text file.

1. System Shutdown Routine:

1. Turn off the laser.
    a. Toggle off the "Flashlamp" and "Q-Switch" switches and click "Update Settings".
    b. Listen for the flashlamps to stop firing.
    c. On the Laser Control Box:
        i. push the "Shutter" button and then the "Start/Stop" button.
        ii. Turn the key to the off position. The LED on the laser PCU should read "OFF".
2. Turn off the Tektronix 3032B Oscilloscope.
2. On the high voltage source for the PMT, dial the first knob to "HV Off" and the other knobs to "0". Turn off the source by flipping the orange switch.

3. Turn off the BNC 575 Pulse Generator.
4. Turn off the lamp by pressing the "Lamp Off" button on the lamp power supply. Allow the lamp fans to run for a few minutes before turning off the power supply as the power supply also powers the cooling fan. Flip the orange ON/OFF switch once the fan stops.
5. If termination other than 1 kΩ was used, replace the 1 kΩ BNC terminator to the T on the channel 1 input of the scope.
6. If slits other than 0.70 mm were used, return the monochromator entrance and exit slits to 0.70 mm.
7. Cover all optics with bags.
8. Exit out of "TA.vi" and "Acquisition.vi" and double check that the acquired data has been transferred from the temporary file folder on the desktop to the appropriate non-temporary storage location.

Data Processing – TA Spectrum

1. To process the raw data and create a TA spectrum at various time values, double-click to open the Matlab program on the desktop.
2. In the Current Directory window, open the directory where your data files are stored. Note: The data files must have sequentially numeric filenames.
3. In the Command window, type "TAS" to begin the processing program.
4. Type in a filename to select T0 and press Enter. Ex: "5". Ideally, this should be a file in the middle of the run where the signal is strong.
5. A plot of the chosen data file will pop up in a separate window. Use the mouse cursor to mark the T0 point after the laser pulse. This is the maximum of the transient absorption signal.
6. Right click on the data point just created and select "Export Cursor Data to Workspace..". Press OK on the box that pops up to keep the variable name the default "cursor_info".
7. Close the Plot window and return to the Command window. Type in "y" and press Enter.
8. Enter another filename and make sure the data point created still marks a T0 that is correct for this data file. Next to the Plot window, a popup box will appear with three options. Choose the appropriate option. It is recommended to check at least one data file near the beginning, middle, and end of the run to make sure the T0 point is valid.
9. After it has been verified that T0 is good for all data files, choose the "Process Data" option.
10. Enter in the requested parameters.
    a. It is assumed that the signal fit nicely in the scope screen during acquisition: The signal decays all the way back to the baseline.

i. Smooth 1=10,000 data points
ii. Smooth 2=5,000 data points
iii. Smooth 5=2,000 data points
iv. Smooth 10=1,000 data points
v. Smooth 20=500 data points

11. The output file will contain all the requested time slices in the current directory with the filename "TA". This file can be imported into Excel.

Data Processing – TA Lifetimes

1. Raw data can be imported into Excel worksheets. The units are ΔA vs. Time (ms).
2. Delete ΔA values up to the peak of the TA decay (when the laser fires), but do not delete any time data points. Now Time=0 should be at the peak of the TA decay.
3. Fit this decay to the exponential decay function of your choice.

Troubleshooting

1. Laser does not fire. Make sure the BNC cables are connected to the Pulse Generator via a T-connector.
2. Program Freezes: Wait a few minutes and if nothing happens, click the red stop sign button at the top of the program. Wait a few seconds and click the white arrow to run the program again and pick up where you left off.
3. Program is not frozen, but "TA.vi" toggles do not do anything: Look at the BNC 575 Pulse Generator Display.
    a. If the circle on the pulse generator display screen is not flashing, press the RUN/STOP button on the front of the pulse generator. If the circle flashes, the problem should be solved.
    b. If the pulse generator display is frozen, turn off the laser (see Shutdown procedure above) and then turn off the BNC 575 Pulse Generator for 10 seconds, then turn it back on.
    c. If the pulse generator display is not frozen, exit the "TA.vi" program and check the GPIB connection. If the GPIB cable seems to be tight, open the "TA.vi" program again.
4. "TA.vi" program will not do anything after the "Acquire!.vi" window has been opened: This is normal. The "Acquire!" button should only be pressed when all the settings are correct to acquire data. Click the red stop sign button, and then the white arrow on the "TA.vi" window.
5. Laser PCU starts beeping: Stop the program, turn the laser key to off, and restart the laser following the startup procedure.

LIST OF REFERENCES

1. Huygens, C. *Traité de la Lumière*; Macmillan: London, 1912.

2. Fresnel, A. *Ann. Chem. Phys,* **1816**, *2*, 239-281.

3. Young, T. In *A Course of Lectures on Natural Philosophy and the Mechanical Arts*; Printed for J. Johnson: London, 1807; Vol. Volume 1, p 457-471.

4. Marion, J. B.; Heald, M. A. In *Classical Electromagnetic Radiation (Second Edition)*; Jerry, M., Ed.; Academic Press: 1980, p 1-33.

5. Maxwell, J. C. *A Treatise on Electricity and Magnetism*; Cambridge University Press: Cambridge, 2010; Vol. 1.

6. Planck, M. *Annalen Der Physik* **1901**, *4*, 553-561.

7. Einstein, A. *Annalen der Physik* **1905**, *322*, 132-148.

8. de Broglie, L. *Annalen Der Physik* **1925**, *(Paris), 3*, 22.

9. Davisson, C.; Germer, L. H. *Physical Review* **1927**, *30*, 705-740.

10. Thomson, G. P. C. W. *Theory and practice of electron diffraction*; Macmillan and co., limited: London, 1939.

11. Shankar, R. *Principles of quantum mechanics*; 2nd ed. ed.; Plenum Press: New York, 1994.

12. Rohatgi-Mukherjee, K. K. *Fundamentals of Photochemistry*; New Age International Ltd., Publishers: Sanjeev Offset, Delhi, 1986.

13. Smith, K. C. Stanford University School of Medicine; Vol. 2013.

14. Shriver, D. F.; Atkins, P. W. *Inorganic Chemistry*; 3rd ed. ed.; W. H. Freeman and Company: New York, 1999.

15. Turro, N. J. *Modern Molecular Photochemistry*; University Science Books: Sausalito, California, 1991.

16. Forster, T. *Annalen Der Physik* **1948**, *2*, 55-75.

17. Dexter, D. L. *J. Chem. Phys.* **1953**, *21*, 836-850.

18. Forster, T. *Angewandte Chemie-International Edition* **1969**, *8*, 333-&.

19. Birks, J. B. *Photophysics of Aromatic Molecules* **1970**, 704-704.

20. Birks, J. B. *Rep. Prog. Phys.* **1975**, *38*, 903-974.

21. Epple, R.; Forster, T. *Z Elektrochem* **1954**, *58*, 783-787.

22. Cohen, M. D. *Mol. Cryst. Liq. Cryst.* **1979**, *50*, 1-10.

23. Ferguson, J. *J. Chem. Phys.* **1965**, *43*, 306-&.

24. Avis, P.; Porter, G. *J. Chem. Soc., Faraday Trans.* **1974**, *8*, 1057-1065.

25. Winnik, F. M. *Macromolecules* **1990**, *23*, 233-242.

26. Winnik, F. M. *Chem. Rev.* **1993**, *93*, 587-614.

27. *Polymer Photophysics*; Phillips, D., Ed.; Chapman and Hall: New York, 1985.

28. Somersall, A. C.; Guillet, J. E. *J. Macromol. Sci.-Rev. Macromol. Chem. Phys.* **1975**, *C 13*, 135-187.

29. *Creation and Detection of the Excited State*; Lamola, A. A., Ed.; Marcel Dekker, Inc.: New York, 1971; Vol. Volume 1, Part A.

30. Marini, A.; Munoz-Losa, A.; Biancardi, A.; Mennucci, B. *J. Phys. Chem. B* **2010**, *114*, 17128-17135.

31. Williams, A. T. R.; Winfield, S. A.; Miller, J. N. *Analyst* **1983**, *108*, 1067-1071.

32. Dhami, S.; Demello, A. J.; Rumbles, G.; Bishop, S. M.; Phillips, D.; Beeby, A. *Photochem. Photobiol.* **1995**, *61*, 341-346.

33. Palsson, L., Monkman, A., Beeby, A.; Ltd., J. Y., Ed.

34. Norrish, R. G. W.; Porter, G. *Nature* **1949**, *164*, 658-658.

35. Lindqvist, L. *Hebd. Seances Acad. Sci., Ser. C* **1966**, *263*, 852-854.

36. Small, R. D.; Scaiano, J. C. *J. Am. Chem. Soc.* **1978**, *100*, 296-298.

37. Goppert-Mayer, M. *Annalen Der Physik* **1931**, *9*, 273-294.

38. Kaiser, W.; Garrett, C. G. B. *Phys. Rev. Lett.* **1961**, *7*, 229-231.

39. Franken, P. A.; Weinreich, G.; Peters, C. W.; Hill, A. E. *Phys. Rev. Lett.* **1961**, *7*, 118-120.

40. He, G. S.; Tan, L.-S.; Zheng, Q.; Prasad, P. N. *Chem. Rev.* **2008**, *108*, 1245-1330.

41. Ehrlich, J. E.; Wu, X. L.; Lee, I. Y. S.; Hu, Z. Y.; Rockel, H.; Marder, S. R.; Perry, J. W. *Opt. Lett.* **1997**, *22*, 1843-1845.

42. Sutherland, R.; Brant, M.; Heinrichs, J.; Rogers, J.; Slagle, J.; McLean, D.; Fleitz, P. *J. Opt. Soc. Am. B: Opt. Phys.* **2005**, *22*, 1939-1948.

43. Liao, C.; Shelton, A. H.; Kim, K. Y.; Schanze, K. S. *ACS Appl. Mater. Inter.* **2011**, *3*, 3225-3238.

44. Rao, S. V.; Rao, D. N.; Akkara, J. A.; DeCristofano, B. S.; Rao, D. *Chem. Phys. Lett.* **1998**, *297*, 491-498.

45. Paschotta, R. In *Field Guide to Laser Pulse Generation*; SPIE Press: Bellingham, WA, 2008.

46. Gaussian Beam. *Wikipedia, The Free Encyclopedia* [Online Early Access]. http://en.wikipedia.org/w/index.php?title=Gaussian_beam&oldid=560465837 (accessed July 4, 2013).

47. Wong, W. Y.; Harvey, P. D. *Macromol. Rapid Commun.* **2010**, *31*, 671-713.

48. Chawdhury, N.; Kohler, A.; Friend, R. H.; Younus, M.; Long, N. J.; Raithby, P. R.; Lewis, J. *Macromolecules* **1998**, *31*, 722-727.

49. Dray, A. E.; Wittmann, F.; Friend, R. H.; Donald, A. M.; Khan, M. S.; Lewis, J.; Johnson, B. F. G. *Synth. Met.* **1991**, *41*, 871-874.

50. Wittmann, H. F.; Fuhrmann, K.; Friend, R. H.; Khan, M. S.; Lewis, J. *Synth. Met.* **1993**, *55*, 56-61.

51. Daughton, W. J. G., F. L. *J. Electrochem. Soc.* **1982**, *129*, 173-179.

52. Lawrence, C. J. *Phys. Fluids* **1988**, *31*, 2786-2796.

53. Jaczewska, J. B., A.; Bernasik, A.; Moons, E.; Rysz, J. *Macromolecules* **2008**, *41*, 4802-4810.

54. Vella, J. Ph.D. Dissertation, University of Florida, 2009.

55. Glimsdal, E.; Carlsson, M.; Eliasson, B.; Minaev, B.; Lindgren, M. *J. Phys. Chem. A* **2007**, *111*, 244-250.

56. Gubler, U.; Bosshard, C. In *Polymers for Photonics Applications I*; Lee, K.-S., Ed.; Springer-Verlag Berlin Heidelberg: Germany, 2002; Vol. 158, p 123-191.

57. Chaumel, F.; Jiang, H. W.; Kakkar, A. *Chem. Mater.* **2001**, *13*, 3389-3395.

58. Cooper, T. M.; Krein, D. M.; Burke, A. R.; McLean, D. G.; Rogers, J. E.; Slagle, J. E.; Fleitz, P. A. *J. Phys. Chem. A* **2006**, *110*, 4369-4375.

59. Barkana, Y.; Belkin, M. *Surv. Ophthalmol.* **2000**, *44*, 459-478.

60. Hudson, S. J. *Aviat. Space Env. Med.* **1998**, *69*, 519-524.

61. Hollins, R. C. *Curr. Opin. Solid State Mater. Sci.* **1999**, *4*, 189-196.

62. Gvishi, R.; Narang, U.; Ruland, G.; Kumar, D. N.; Prasad, P. N. *Appl. Organomet. Chem.* **1997**, *11*, 107-127.

63. He, G. S.; Xu, G. C.; Prasad, P. N.; Reinhardt, B. A.; Bhatt, J. C.; Dillard, A. G. *Opt. Lett.* **1995**, *20*, 435-437.

64. Zhou, G. J.; Wong, W. Y. *Chem. Soc. Rev.* **2011**, *40*, 2541-2566.

65. McKay, T. J.; Bolger, J. A.; Staromlynska, J.; Davy, J. R. *J. Chem. Phys.* **1998**, *108*, 5537-5541.

66. Rogers, J. E.; Cooper, T. M.; Fleitz, P. A.; Glass, D. J.; McLean, D. G. *J. Phys. Chem. A* **2002**, *106*, 10108-10115.

67. Rogers, J. E.; Slagle, J. E.; Krein, D. M.; Burke, A. R.; Hall, B. C.; Fratini, A.; McLean, D. G.; Fleitz, P. A.; Cooper, T. M.; Drobizhev, M.; Makarov, N. S.; Rebane, A.; Kim, K. Y.; Farley, R.; Schanze, K. S. *Inorg. Chem.* **2007**, *46*, 6483-6494.

68. Kim, K.-Y.; Shelton, A. H.; Drobizhev, M.; Makarov, N.; Rebane, A.; Schanze, K. S. *J. Phys. Chem. A* **2010**, *114*, 7003.

69. Perry, J. W. *Nonlinear Optics of Organic Molecules and Polymers*; CRC Press: Boca Raton, FL, 1997.

70. Staromlynska, J.; McKay, T. J.; Bolger, J. A.; Davy, J. R. *J. Opt. Soc. Am. B: Opt. Phys.* **1998**, *15*, 1731-1736.

71. Chateau, D.; Chaput, F.; Lopes, C.; Lindgren, M.; Brannlund, C.; Ohgren, J.; Djourelov, N.; Nedelec, P.; Desroches, C.; Eliasson, B.; Kindahl, T.; Lerouge, F.; Andraud, C.; Parola, S. *ACS Appl. Mater. Inter.* **2012**, *4*, 2369-2377.

72. Zieba, R.; Desroches, C.; Chaput, F.; Carlsson, M.; Eliasson, B.; Lopes, C.; Lindgren, M.; Parola, S. *Adv. Funct. Mater.* **2009**, *19*, 235-241.

73. Westlund, R.; Malmstrom, E.; Lopes, C.; Ohgren, J.; Rodgers, T.; Saito, Y.; Kawata, S.; Glimsdal, E.; Lindgren, M. *Adv. Funct. Mater.* **2008**, *18*, 1939-1948.

74. Drobizhev, M.; Rebane, A.; Suo, Z.; Spangler, C. W. *J. Lumin.* **2005**, *111*, 291-305.

75. Albota, M.; Beljonne, D.; Bredas, J. L.; Ehrlich, J. E.; Fu, J. Y.; Heikal, A. A.; Hess, S. E.; Kogej, T.; Levin, M. D.; Marder, S. R.; McCord-Maughon, D.; Perry, J. W.; Rockel, H.; Rumi, M.; Subramaniam, C.; Webb, W. W.; Wu, X. L.; Xu, C. *Science* **1998**, *281*, 1653-1656.

76. McIlroy, S. P.; Clo, E.; Nikolajsen, L.; Frederiksen, P. K.; Nielsen, C. B.; Mikkelsen, K. V.; Gothelf, K. V.; Ogilby, P. R. *J. Org. Chem.* **2005**, *70*, 1134-1146.

77. Mardelli, M.; Olmsted, J. *J. Photochem.* **1977**, *7*, 277-285.

78. Carmichael, I.; Helman, W.; Hug, G. *J. Phys. Chem. Ref. Data* **1987**, *16*, 239-260.

79. Amand, B.; Bensasson, R. *Chem. Phys. Lett.* **1975**, *34*, 44-48.

80. Scaiano, J. C.; Redmond, R. W.; Mehta, B.; Arnason, J. T. *Photochem. Photobiol.* **1990**, *52*, 655-659.

81. Wilson, J. S.; Chawdhury, N.; Al-Mandhary, M. R. A.; Younus, M.; Khan, M. S.; Raithby, P. R.; Kohler, A.; Friend, R. H. *J. Am. Chem. Soc.* **2001**, *123*, 9412-9417.

82. Dubinina, G.; Price, R.; Abboud, K.; Wicks, G.; Wnuk, P.; Stepanenko, Y.; Drobizhev, M.; Rebane, A.; Schanze, K. *J. Am. Chem. Soc.* **2012**, *134*, 19346-19349.

83. Dubinina, G. G.; Price, R. S.; Wicks, G.; Drobizhev, M.; Wnuk, P.; Stepanenko, Y.; Rebane, A.; Schanze, K. S. *Proc. SPIE 8622* **2013**, *862218*.

84. Makarov, N. S.; Drobizhev, M.; Rebane, A. *Opt. Express* **2008**, *16*, 4029.

85. Bonneau, R.; Carmichael, I.; Hug, G. L. *Pure Appl. Chem.* **1991**, *63*, 290-299.

86. Porter, G.; Windsor, M. W. *J. Chem. Phys.* **1953**, *21*, 2088-2088.

87. Porter, G.; Windsor, M. W. *Proc. R. Soc. London, Ser. A* **1958**, *245*, 238-258.

88. Porter, G.; Windsor, M. W. *Discuss. Faraday Soc.* **1954**, 178-&.

89. Candeias, L. P.; Wildeman, J.; Hadziioannou, G.; Warman, J. M. *J. Phys. Chem. B* **2000**, *104*, 8366-8371.

90. Inigo, A. R.; Chiu, H. C.; Fann, W.; Huang, Y. S.; Jeng, U. S.; Lin, T. L.; Hsu, C. H.; Peng, K. Y.; Chen, S. A. *Phys. Rev. B: Condens. Matter* **2004**, *69*.

91. Jeng, U.; Hsu, C. H.; Sheu, H. S.; Lee, H. Y.; Inigo, A. R.; Chiu, H. C.; Fann, W. S.; Chen, S. H.; Su, A. C.; Lin, T. L.; Peng, K. Y.; Chen, S. A. *Macromolecules* **2005**, *38*, 6566-6574.

92. Tan, C. H.; Inigo, A. R.; Fann, W.; Wei, P. K.; Perng, G. Y.; Chen, S. A. *Org. Electron.* **2002**, *3*, 81-88.

93. Burroughes, J. H.; Bradley, D. D. C.; Brown, A. R.; Marks, R. N.; Mackay, K.; Friend, R. H.; Burns, P. L.; Holmes, A. B. *Nature* **1990**, *347*, 539-541.

94. Friend, R. H.; Gymer, R. W.; Holmes, A. B.; Burroughes, J. H.; Marks, R. N.; Taliani, C.; Bradley, D. D. C.; Dos Santos, D. A.; Bredas, J. L.; Logdlund, M.; Salaneck, W. R. *Nature* **1999**, *397*, 121-128.

95. Schwartz, B. J. *Annu. Rev. Phys. Chem.* **2003**, *54*, 141-172.

96. Sumpter, B. G.; Kumar, P.; Mehta, A.; Barnes, M. D.; Shelton, W. A.; Harrison, R. J. *J. Phys. Chem. B* **2005**, *109*, 7671-7685.

97. Traiphol, R.; Srikhirin, T.; Kerdcharoen, T.; Osotchan, T.; Scharnagl, N.; Willumeit, R. *Eur. Polym. J.* **2007**, *43*, 478-487.

98. Collison, C. J.; Rothberg, L. J.; Treemaneekarn, V.; Li, Y. *Macromolecules* **2001**, *34*, 2346-2352.

99. Hennebicq, E.; Deleener, C.; Bredas, J.-L.; Scholes, G. D.; Beljonne, D. *J. Chem. Phys.* **2006**, *125*.

100. Wang, P.; Collison, C. J.; Rothberg, L. J. *J. Photochem. Photobiol., A* **2001**, *144*, 63-68.

101. Yan, M.; Rothberg, L. J.; Kwock, E. W.; Miller, T. M. *Phys. Rev. Lett.* **1995**, *75*, 1992-1995.

102. Sherwood, G. A.; Cheng, R.; Smith, T. M.; Werner, J. H.; Shreve, A. P.; Peteanu, L. A.; Wildeman, J. *J. Phys. Chem. C* **2009**, *113*, 18851-18862.

103. Lim, S. H.; Bjorklund, T. G.; Bardeen, C. J. *Chem. Phys. Lett.* **2001**, *342*, 555-562.

104. Rolczynski, B. S.; Szarko, J. M.; Son, H. J.; Liang, Y. Y.; Yu, L. P.; Chen, L. X. *J. Am. Chem. Soc.* **2012**, *134*, 4142-4152.

105. Kodaira, T.; Watanabe, A.; Fujitsuka, M.; Ito, O. *Polymer* **1998**, *39*, 3793-3799.

106. Closs, G. L.; Piotrowiak, P.; Macinnis, J. M.; Fleming, G. R. *J. Am. Chem. Soc.* **1988**, *110*, 2652-2653.

107. Burrows, H. D.; de Melo, J. S.; Serpa, C.; Arnaut, L. G.; Miguel, M. D.; Monkman, A. P.; Hamblett, I.; Navaratnam, S. *Chem. Phys.* **2002**, *285*, 3-11.

108. Monkman, A. P.; Burrows, H. D.; Hamblett, I.; Navaratnam, S. *Chem. Phys. Lett.* **2001**, *340*, 467-472.

109. Samiullah, M.; Moghe, D.; Scherf, U.; Guha, S. *Phys. Rev. B: Condens. Matter* **2010**, *82*, 6.

110. Archer, S.; Weinstein, J. A. *Coord. Chem. Rev.* **2012**, *256*, 2530-2561.

111. Liu, S. J.; Chen, Y.; Xu, W. J.; Zhao, Q.; Huang, W. *Macromol. Rapid Commun.* **2012**, *33*, 461-480.

112. Shao, Y.; Yang, Y. *Adv. Mater.* **2005**, *17*, 2841-+.

113. Guo, F. Q.; Kim, Y. G.; Reynolds, J. R.; Schanze, K. S. *Chem. Commun.* **2006**, 1887-1889.

114. Wong, W. Y.; Wang, X. Z.; He, Z.; Chan, K. K.; Djurisic, A. B.; Cheung, K. Y.; Yip, C. T.; Ng, A. M. C.; Xi, Y. Y.; Mak, C. S. K.; Chan, W. K. *J. Am. Chem. Soc.* **2007**, *129*, 14372-14380.

115. Wong, W.-Y.; Chow, W.-C.; Cheung, K.-Y.; Fung, M.-K.; Djurisic, A. B.; Chan, W.-K. *J. Organomet. Chem.* **2009**, *694*, 2717-2726.

116. Schulz, G. L.; Holdcroft, S. *Chem. Mater.* **2008**, *20*, 5351-5355.

117. Cheng, K. W.; Mak, C. S. C.; Chan, W. K.; Ng, A. M. C.; Djurisic, A. B. *J. Polym. Sci., Part A: Polym. Chem.* **2008**, *46*, 1305-1317.

118. Padhy, H.; Sahu, D.; Chiang, I. H.; Patra, D.; Kekuda, D.; Chu, C.-W.; Lin, H.-C. *J. Mater. Chem.* **2011**, *21*, 1196-1205.

119. Yang, K.; Arif, M.; Foerster, M.; Scherf, U.; Guha, S. *Synth. Met.* **2009**, *159*, 2338-2341.

120. Haneline, M. R.; Tsunoda, M.; Gabbai, F. P. *J. Am. Chem. Soc.* **2002**, *124*, 3737-3742.

121. Gardinier, J. R.; Gabbai, F. P. *J. Chem. Soc., Dalton Trans.* **2000**, 2861-2865.

122. Tsunoda, M.; Gabbai, F. P. *J. Am. Chem. Soc.* **2000**, *122*, 8335-8336.

123. King, J. B.; Haneline, M. R.; Tsunoda, M.; Gabbai, F. P. *J. Am. Chem. Soc.* **2002**, *124*, 9350-9351.

124. Taylor, T. J.; Elbjeirami, O.; Burress, C. N.; Tsunoda, M.; Bodine, M. I.; Omary, M. A.; Gabbai, F. P. *J. Inorg. Organomet. Polym.* **2008**, *18*, 175-179.

125. Omary, M. A.; Kassab, R. M.; Haneline, M. R.; Elbjeirami, O.; Gabbai, F. P. *Inorg. Chem.* **2003**, *42*, 2176-2178.

126. Elbjeirami, O.; Burress, C. N.; Gabbai, F. P.; Omary, M. A. *J. Phys. Chem. C* **2007**, *111*, 9522-9529.

127. Burini, A.; Fackler, J. P.; Galassi, R.; Grant, T. A.; Omary, M. A.; Rawashdeh-Omary, M. A.; Pietroni, B. R.; Staples, R. J. *J. Am. Chem. Soc.* **2000**, *122*, 11264-11265.

128. Haneline, M. R.; Gabbai, F. P. *Inorg. Chem.* **2005**, *44*, 6248-6255.

129. Forero, S.; Nguyen, P. H.; Brutting, W.; Schwoerer, M. *PCCP* **1999**, *1*, 1769-1776.

130. Dai, L. M.; Winkler, B.; Dong, L. M.; Tong, L.; Mau, A. W. H. *Adv. Mater.* **2001**, *13*, 915-925.

131. Hoppe, H.; Arnold, N.; Sariciftci, N. S.; Meissner, D. *Sol. Energy Mater. Sol. Cells* **2003**, *80*, 105-113.

132. Sariciftci, N. S.; Braun, D.; Zhang, C.; Srdanov, V. I.; Heeger, A. J.; Stucky, G.; Wudl, F. *Appl. Phys. Lett.* **1993**, *62*, 585-587.

133. Yu, G.; Gao, J.; Hummelen, J. C.; Wudl, F.; Heeger, A. J. *Science* **1995**, *270*, 1789-1791.

134. Liu, Y. Q.; Liu, M. S.; Li, X. C.; Jen, A. K. Y. *Chem. Mater.* **1998**, *10*, 3301-3304.

135. Lee, T. W.; Park, O. O. *Adv. Mater.* **2000**, *12*, 801-804.

136. Nguyen, T. Q.; Martini, I. B.; Liu, J.; Schwartz, B. J. *J. Phys. Chem. B* **2000**, *104*, 237-255.

137. Koehler, A.; Hoffmann, S. T.; Baessler, H. *J. Am. Chem. Soc.* **2012**, *134*, 11594-11601.

138. Smilowitz, L.; Hays, A.; Heeger, A. J.; Wang, G.; Bowers, J. E. *J. Chem. Phys.* **1993**, *98*, 6504-6509.

139. Samuel, I. D. W.; Crystall, B.; Rumbles, G.; Burn, P. L.; Holmes, A. B.; Friend, R. H. *Chem. Phys. Lett.* **1993**, *213*, 472-478.

140. Monkman, A. P.; Burrows, H. D.; Miguel, M. D.; Hamblett, I.; Navaratnam, S. *Chem. Phys. Lett.* **1999**, *307*, 303-309.

141. Candeias, L. P.; Grozema, F. C.; Padmanaban, G.; Ramakrishnan, S.; Siebbeles, L. D. A.; Warman, J. M. *J. Phys. Chem. B* **2003**, *107*, 1554-1558.

142. Wachsmann-Hogiu, S.; Peteanu, L. A.; Liu, L. A.; Yaron, D. J.; Wildeman, J. *J. Phys. Chem. B* **2003**, *107*, 5133-5143.

143. Bjorklund, T. G.; Lim, S. H.; Bardeen, C. J. *J. Phys. Chem. B* **2001**, *105*, 11970-11977.

144. Cornil, J.; Beljonne, D.; Heller, C. M.; Campbell, I. H.; Laurich, B. K.; Smith, D. L.; Bradley, D. D. C.; Mullen, K.; Bredas, J. L. *Chem. Phys. Lett.* **1997**, *278*, 139-145.

145. Gierschner, J.; Mack, H. G.; Luer, L.; Oelkrug, D. *J. Chem. Phys.* **2002**, *116*, 8596-8609.

146. Rahman, M. H.; Chen, H.-L.; Chen, S.-A.; Chu, P. P. J. *J. Chin. Chem. Soc.* **2010**, *57*, 490-495.

147. Ou-Yang, W.-C.; Wu, T.-Y.; Lin, Y.-C. *Iran. Polym. J.* **2009**, *18*, 453-464.

148. Chen, S. H.; Su, A. C.; Huang, Y. F.; Su, C. H.; Peng, G. Y.; Chen, S. A. *Macromolecules* **2002**, *35*, 4229-4232.

149. Chen, S. H.; Su, A. C.; Chang, C. S.; Chen, H. L.; Ho, D. L.; Tsao, C. S.; Peng, K. Y.; Chen, S. A. *Langmuir* **2004**, *20*, 8909-8915.

150. Lobez, J. M.; Andrew, T. L.; Bulovic, V.; Swager, T. M. *ACS Nano* **2012**, *6*, 3044-3056.

151. Brabec, C. J.; Gowrisanker, S.; Halls, J. J. M.; Laird, D.; Jia, S.; Williams, S. P. *Adv. Mater.* **2010**, *22*, 3839-3856.

152. Chen, T. A.; Wu, X. M.; Rieke, R. D. *J. Am. Chem. Soc.* **1995**, *117*, 233-244.

153. Prosa, T. J.; Winokur, M. J.; McCullough, R. D. *Macromolecules* **1996**, *29*, 3654-3656.

154. Bao, Z.; Dodabalapur, A.; Lovinger, A. J. *Appl. Phys. Lett.* **1996**, *69*, 4108-4110.

155. Sirringhaus, H.; Tessler, N.; Friend, R. H. *Science* **1998**, *280*, 1741-1744.

156. Sirringhaus, H.; Brown, P. J.; Friend, R. H.; Nielsen, M. M.; Bechgaard, K.; Langeveld-Voss, B. M. W.; Spiering, A. J. H.; Janssen, R. A. J.; Meijer, E. W.; Herwig, P.; de Leeuw, D. M. *Nature* **1999**, *401*, 685-688.

157. Li, L. G.; Lu, G. H.; Yang, X. N. *J. Mater. Chem.* **2008**, *18*, 1984-1990.

158. Brown, P. J.; Thomas, D. S.; Kohler, A.; Wilson, J. S.; Kim, J. S.; Ramsdale, C. M.; Sirringhaus, H.; Friend, R. H. *Phys. Rev. B: Condens. Matter* **2003**, *67*.

159. Gurau, M. C.; Delongchamp, D. M.; Vogel, B. M.; Lin, E. K.; Fischer, D. A.; Sambasivan, S.; Richter, L. J. *Langmuir* **2007**, *23*, 834-842.

160. Guo, J.; Ohkita, H.; Benten, H.; Ito, S. *J. Am. Chem. Soc.* **2009**, *131*, 16869-16880.

161. Jiang, X. M.; Osterbacka, R.; An, C. P.; Vardeny, Z. V. *Synth. Met.* **2003**, *137*, 1465-1468.

162. Osterbacka, R.; An, C. P.; Jiang, X. M.; Vardeny, Z. V. *Science* **2000**, *287*, 839-842.

163. Sontag, S. K.; Marshall, N.; Locklin, J. *Chem. Commun.* **2009**, 3354-3356.

164. Corbitt, T. S.; Sommer, J. R.; Chemburu, S.; Ogawa, K.; Ista, L. K.; Lopez, G. P.; Whitten, D. G.; Schanze, K. S. *ACS Appl. Mater. Inter.* **2009**, *1*, 48-52.

165. Zhou, Z.; Corbitt, T. S.; Parthasarathy, A.; Tang, Y.; Ista, L. F.; Schanze, K. S.; Whitten, D. G. *J. Phys. Chem. Lett.* **2010**, *1*, 3207-3212.

166. Chemburu, S.; Corbitt, T. S.; Ista, L. K.; Ji, E.; Fulghum, J.; Lopez, G. P.; Ogawa, K.; Schanze, K. S.; Whitten, D. G. *Langmuir* **2008**, *24*, 11053-11062.

167. Lu, L. D.; Rininsland, F. H.; Wittenburg, S. K.; Achyuthan, K. E.; McBranch, D. W.; Whitten, D. G. *Langmuir* **2005**, *21*, 10154-10159.

168. Epe, B. *Chem. Biol. Interact.* **1991**, *80*, 239-260.

169. Bachowski, G. J.; Pintar, T. J.; Girotti, A. W. *Photochem. Photobiol.* **1991**, *53*, 481-491.

170. Triantaphylides, C.; Krischke, M.; Hoeberichts, F. A.; Ksas, B.; Gresser, G.; Havaux, M.; Van Breusegem, F.; Mueller, M. J. *Plant Physiol.* **2008**, *148*, 960-968.

171. Brezova, V.; Valko, M.; Breza, M.; Morris, H.; Telser, J.; Dvoranova, D.; Kaiserova, K.; Varecka, L.; Mazur, M.; Leibfritz, D. *J. Phys. Chem. B* **2003**, *107*, 2415-2425.

172. Kuimova, M. K.; Yahioglu, G.; Ogilby, P. R. *J. Am. Chem. Soc.* **2009**, *131*, 332-340.

173. Walsh, S. E.; Maillard, J. Y.; Russell, A. D.; Catrenich, C. E.; Charbonneau, D. L.; Bartolo, R. G. *Journal of Applied Microbiology* **2003**, *94*, 240-247.

174. Cen, L.; Neoh, K. G.; Kang, E. T. *Langmuir* **2003**, *19*, 10295-10303.

175. Andresen, M.; Stenstad, P.; Moretro, T.; Langsrud, S.; Syverud, K.; Johansson, L.-S.; Stenius, P. *Biomacromolecules* **2007**, *8*, 2149-2155.

176. Tiller, J. C.; Liao, C. J.; Lewis, K.; Klibanov, A. M. *Proc. Natl. Acad. Sci. U. S. A.* **2001**, *98*, 5981-5985.

177. McCluskey, D. M.; Smith, T. N.; Madasu, P. K.; Coumbe, C. E.; Mackey, M. A.; Fulmer, P. A.; Wynne, J. H.; Stevenson, S.; Phillips, J. P. *Acs Applied Materials & Interfaces* **2009**, *1*, 882-887.

178. Schulz-Ekloff, G.; Wohrle, D.; van Duffel, B.; Schoonheydt, R. A. *Microporous Mesoporous Mater.* **2002**, *51*, 91-138.

179. Ogawa, M.; Kuroda, K. *Chem. Rev.* **1995**, *95*, 399-438.

180. *Intercalation Chemistry*; Whittingham, M. S., Jacobson, A. J., Ed.; Academic Press: New York, 1982.

181. Jones, W. In *Photochemistry in Organized & Constrained Media*; Ramamurthy, V., Ed.; VCH Publishers, Inc.: New York, 1991.

182. Brinker, C. J. *Current Opinion in Colloid & Interface Science* **1998**, *3*, 166-173.

183. Decher, G.; Eckle, M.; Schmitt, J.; Struth, B. *Current Opinion in Colloid & Interface Science* **1998**, *3*, 32-39.

184. Winkler, B.; Dai, L.; Mau, A. W. H. *J. Mater. Sci. Lett.* **1999**, *18*, 1539-1541.

185. Cione, A. P. P.; Gessner, F.; Neumann, M. G. *J. Colloid Interface Sci.* **2001**, *240*, 539-543.

186. *Conjugated Polymers*; Bredas, J. L., Silbey, R., Ed.; Kluwer: Dordrecht, 1991.

187. Ray, S. S.; Okamoto, M. *Prog. Polym. Sci.* **2003**, *28*, 1539-1641.

188. Cornil, J.; Beljonne, D.; Calbert, J. P.; Bredas, J. L. *Adv. Mater.* **2001**, *13*, 1053-1067.

189. Tang, Y.; Zhou, Z.; Ogawa, K.; Lopez, G. P.; Schanze, K. S.; Whitten, D. G. *Langmuir* **2009**, *25*, 21-25.

190. Tozoni, J. R.; Guimaraes, F. E. G.; Atvars, T. D. Z.; Nowacki, B.; Marlleta, A.; Akcelrud, L.; Bonagamba, T. J. *Eur. Polym. J.* **2011**, *47*, 2259-2265.

191. Eguchi, M.; Takagi, S.; Tachibana, H.; Inoue, H. *J. Phys. Chem. Solids* **2004**, *65*, 403-407.

192. Takagi, K., Shichi, T. In *Solid State and Surface Photochemistry*; Ramamurthy, V., Schanze, K. S., Ed.; Marcel Dekker: New York, 2000; Vol. 5, p 31.

BIOGRAPHICAL SKETCH

Randi Sue Price grew up in LaPorte, Indiana with her parents Pamela and Dennis Price. In 2006, she graduated with her B.S. in chemistry from Purdue University in West Lafayette, Indiana. After graduation, she worked as an analytical chemist at the Office of Indiana State Chemist in West Lafayette, Indiana for two years analyzing commercially available pesticide formulations for label claim requirements set forth by state and local governments.

In 2008, she attended the University of Florida in Gainesville, FL to pursue her graduate degree under the advisement of Dr. Kirk Schanze in the study of the photophysics of organic and organometallic molecules, oligomers, and polymers including the development and instrumentation of a nanosecond transient absorption instrumentation system for analysis of solid-state materials and thin films. She received her Ph.D. from the University of Florida in the summer of 2013.